11

Data Analysis and Seismogram Interpretation

Peter Bormann, Klaus Klinge and Siegfried Wendt

11.1   Introduction

This Chapter deals with seismogram analysis and extraction of seismic parameter values for data exchange with national and international data centers, for use in research and last, but not least, with writing bulletins and informing the public about seismic events. It is written for training purposes and for use as a reference source for seismologists at observatories. It describes the basic requirements in analog and digital routine observatory practice i.e., to:

- recognize the occurrence of an earthquake in a record;
- identify and annotate the seismic phases;
- determine onset time and polarity correctly;
- measure the maximum ground amplitude and related period;
- calculate slowness and azimuth;
- determine source parameters such as the hypocenter, origin time, magnitude, source mechanism, etc..

In modern digital observatory practice these procedures are implemented in computer programs. Experience, a basic knowledge of elastic wave propagation (see Chapter 2), and the available software can guide a seismologist to analyze large amounts of data and interpret seismograms correctly. The aim of this Chapter is to introduce the basic knowledge, data, procedures and tools required for proper seismogram analysis and phase interpretation and to present selected seismogram examples.

Seismograms are the basic information about earthquakes, chemical and nuclear explosions, mining-induced earthquakes, rock bursts and other events generating seismic waves. Seismograms reflect the combined influence of the seismic source (see Chapter 3), the propagation path (see Chapter 2), the frequency response of the recording instrument (see 4.2 and 5.2), and the ambient noise at the recording site (e.g., Fig. 7.32). Fig. 11.1 summarizes these effects and their scientific usefulness. Accordingly, our knowledge of seismicity, Earth's structure, and the various types of seismic sources is mainly the result of analysis and interpretation of seismograms. The more completely we quantify and interpret the seismograms, the more fully we understand the Earth's structure, seismic sources and the underlying causing processes.
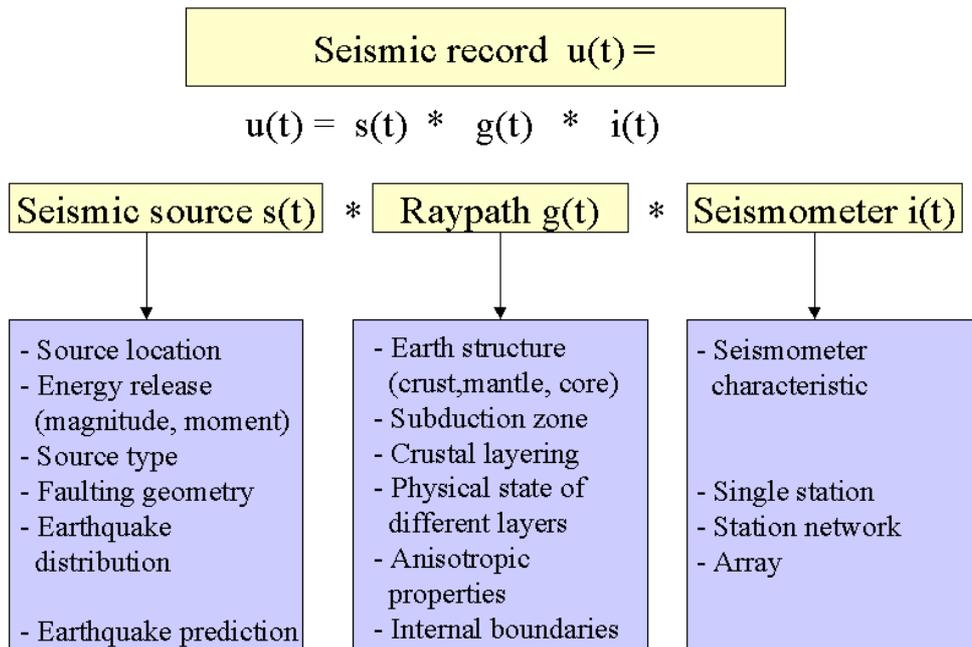
Fig. 11.1 Different factors/sub-systems (without seismic noise) which influence a seismic record (yellow boxes) and the information that can be derived from record analysis (blue boxes).

Seismological data analysis for single stations is nowadays increasingly replaced by network (see Chapter 8) and array analysis (see Chapter 9). Array-processing techniques have been developed for more than 20 years. Networks and arrays, in contrast to single stations, enable better signal detection and source location. Also, arrays can be used to estimate slowness and azimuth, which allow better phase identification. Further, more accurate magnitude values can be expected by averaging single station magnitudes and for distant sources the signal coherency can be used to determine onset times more reliably. Tab. 11.1 summarizes basic characteristics of single stations, station networks and arrays. In principle, an array can be used as a network and in special cases a network can be used as an array. The most important differences between networks and arrays are in the degree of signal coherence and the data analysis techniques used.

Like single stations, band-limited seismometer systems are now out-of-date and have a limited distribution and local importance only. Band-limited systems filter the ground motion. They distort the signal and may shift the onset time and reverse polarity (see 4.2). Most seismological observatories, and especially regional networks, are now equipped with broadband seismometers that are able to record signal frequencies between about 0.001 Hz and 50 Hz. The frequency and dynamic range covered by broadband recordings are shown in Fig. 11.2 and in Fig. 7.48 of Chapter 7 in comparison with classical band-limited analog recordings of the Worldwide Standard Seismograph Network (WWSSN).

Tab. 11.1 Short characteristic of single stations, station networks and arrays.

|	
Single station	Classical type of seismic station with its own data processing. Event location only possible by means of three-component records.
Station network	Local, regional or global distribution of stations that are as identical as possible with a common data center (see Chapter 8). Event location is one of the main tasks.
Seismic array	Cluster of seismic stations with a common time reference and uniform instrumentation. The stations are located close enough to each other in space for the signal waveforms to be correlated between adjacent sensors (see Chapter 9). Benefits are: • extraction of coherent signals from random noise; • determination of directional information of approaching wavefronts (determination of backazimuth of the source); • determination of local slowness and thus of epicentral distance of the source.
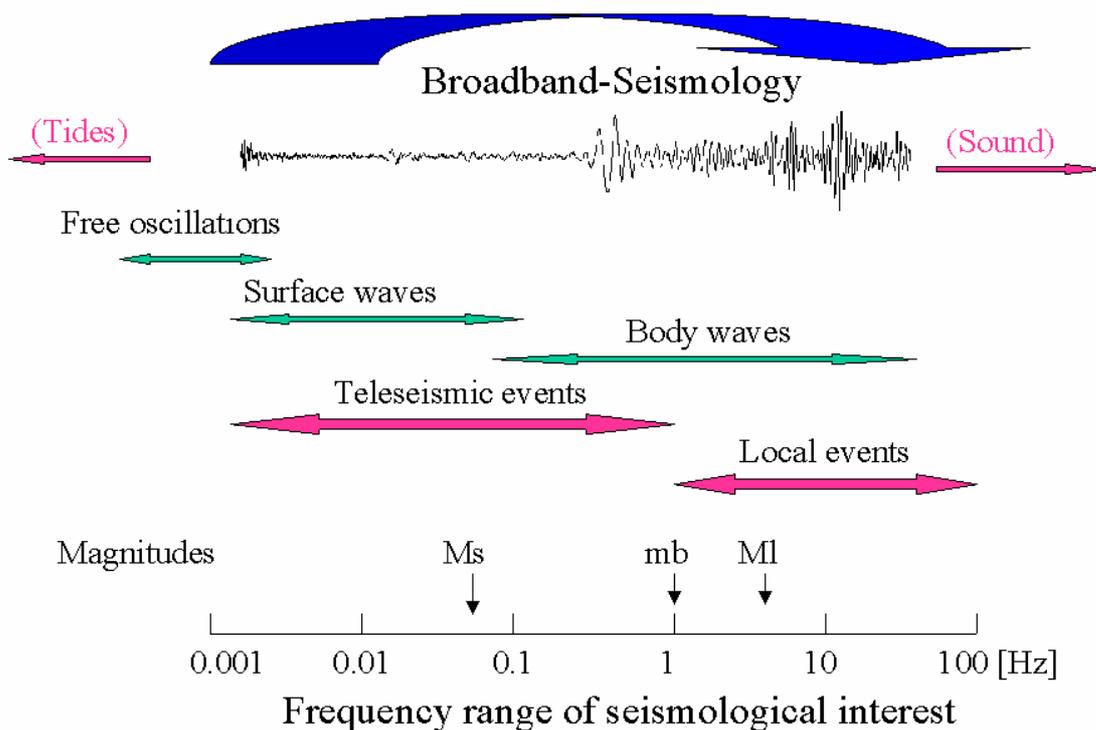
Fig. 11.2 Frequency range of seismological interest.

A number of these classical seismograph systems are still in operation at autonomous single stations in many developing countries and in the former Soviet Union. Also, archives are filled with analog recordings of these systems, which were collected over many decades.

These data constitute a wealth of information most of which has yet to be fully analyzed and scientifically exploited. Although digital data are superior in many respects, both for advanced routine analysis and even more for scientific research, it will be many years or even decades of digital data acquisition before one may consider the bulk of these old data as no longer needed. However, for the rare big and thus unique earthquakes, and for earthquakes in areas with low seismicity rates but significant seismic risk, the preservation and comprehensive analysis of these classical and historic seismograms will remain of the utmost importance for many years.

More and more old analog data will be reanalyzed only after being digitized and by using similar procedures and analysis programs as for recent original digital data. Nevertheless, station operators and analysts should still be in a position to handle, understand and properly analyze analog seismograms or plotted digital recordings without computer support and with only modest auxiliary means. Digital seismograms are analyzed in much the same way as classical seismograms (although with better and more flexible time and amplitude resolution) except that the digital analysis uses interactive software which makes the analysis quicker and easier, and their correct interpretation requires the same knowledge of the appearance of seismic records and individual seismic phases as for analog data. The analyst needs to know the typical features in seismic records as a function of distance, depth and source process of the seismic event, their dependence on the polarization of the different types of seismic waves and thus of the azimuth of the source and the orientation of sensor components with respect to it. He/she also needs to be aware of the influence of the seismograph response on the appearance of the record. Without this solid background knowledge, phase identifications and parameter readings may be rather incomplete, systematically biased or even wrong, no matter what kind of sophisticated computer programs for seismogram analysis are used.

Therefore, in this Chapter we will deal first with an introduction to the fundamentals of seismogram analysis at single stations and station networks, based on analog data and procedures. Even if there is now less and less operational need for this kind of instruction and training, from an educational point of view its importance can not be overemphasized. An analyst trained in comprehensive and competent analysis of traditional analog seismic recordings, when given access to advanced tools of computer-assisted analysis, will by far outperform any computer specialist without the required seismological background knowledge.

Automated phase identification and parameter determination is still inferior to the results achievable by well-trained man-power. Therefore, automated procedures are not discussed in this Manual although they are being used more and more at advanced seismological observatories as well as at station networks (see Chapter 8) and array centers (see Chapter 9). The Manual chiefly aims at providing competent guidance and advice to station operators and seismologists with limited experience and to those working in countries which lack many specialists in the fields which have to be covered by observatory personnel. On the other hand, specialists in program development and automation algorithms sometimes lack the required seismological knowledge or the practical experience to produce effective software for observatory applications. Such knowledge and experience, however, is an indispensable requirement for further improvement of computer procedures for automatic data analysis, parameter determination and source location in tune also with older data and established standards. In this sense, the Manual also addresses the needs of this advanced user community.

Accordingly, we first give a general introduction to routine seismogram interpretation of analog recordings at single stations and small seismic networks. Then we discuss both the similarities and the principal differences when processing digital data. The basic requirements for parameter extraction, bulletin production as well as parameter and waveform data exchange are also outlined. In the sub-Chapter on digital seismogram analysis we discuss in more detail problems of signal coherence, the related different procedures of data processing and analysis as well as available software for it. The majority of record examples from Germany has been processed with the program Seismic Handler (SHM) developed by K. Stammler which is used for seismic waveform retrieval and data analysis. This program and descriptions are available via http://www.szgrf.bgr.de/sh-doc/index.html. Reference is made, however, to other analysis software that is widely used internationally (see 11.4).

Typical examples of seismic records from different single stations, networks and arrays in different distance ranges (local, regional and teleseismic) and at different source depth are presented, mostly broadband data or filtered records derived therefrom. A special section is dedicated to the interpretation of seismic core phases (see 11.5.2.4 and 11.5.3). Since all Chapter authors come from Germany, the majority of records shown has unavoidably been collected at stations of the German Regional Seismic Network (GRSN) and of the Gräfenberg array (GRF). Since all these stations record originally only velocity-broadband (BB-velocity) data, all examples shown from GRSN/GRF stations of short-period (SP), long-period (LP) or BB-displacement seismograms corresponding to Wood-Anderson, WWSSN-SP, WWSSN-LP, SRO-LP or Kirnos SKD response characteristics, are **simulated records**. Since their appearance is identical with respective recordings of these classical analog seismographs this fact is not repeatedly stated throughout this Chapter and its annexes. The location and distribution of the GRSN and GRF stations is depicted in Fig. 11.3a. while Fig. 11.3b shows the location of the events for which records from these stations are presented. Users of this Chapter may feel that the seismograms presented by the authors are too biased towards Europe. Indeed, we may have overlooked some important aspects or typical seismic phases which are well observed in other parts of the world. Therefore, we invite anybody who can present valuable complementary data and explanations to submit them to the Editor of the Manual so that they can be integrated into future editions of the Manual.

For routine analysis and international data exchange a standard nomenclature of seismic phases is required. The newly elaborated draft of a IASPEI Standard Seismic Phase List is given in IS 2.1, together with ray diagrams for most phases. This new nomenclature partially modifies and completes the earlier one published in the last edition of the Manual of Seismological Observatory Practice (Willmore, 1979) and each issue of the seismic Bulletins of the International Seismological Centre (ISC). It is more in tune than the earlier versions with the phase definitions of modern Earth and travel-time models (see 2.7) and takes full advantage of the newly adopted, more flexible and versatile IASPEI Seismic Format (ISF; see 10.2.5) for data transmission, handling and archiving.

The scientific fundamentals of some of the essential subroutines in any analysis software are separately treated in Volume 2, Annexes (e.g., IS 11.1 or PD 11.1). More related Information Sheets and Program Descriptions may be added in the course of further development of this Manual.

a)
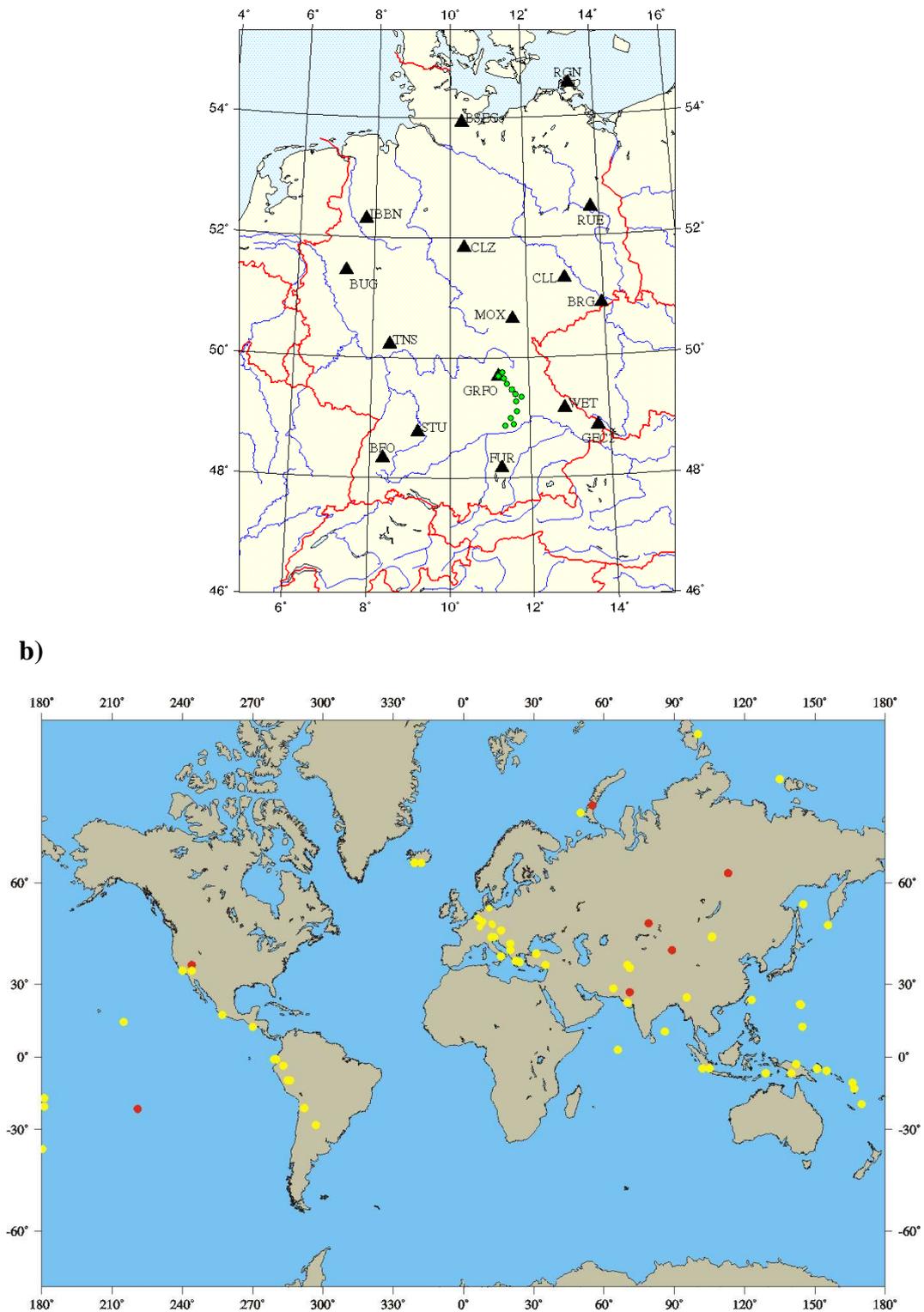
**Fig. 11.3** **a)** Stations of the German Regional Seismological Network (GRSN, black triangles) and the Graefenberg-Array (GRF, green dots); **b)** global distribution of epicenters of seismic events (red dots: underground nuclear explosions; yellow dots: earthquakes) for which records from the above stations will be presented in Chapter 11 and DS 11.1-11.4.

11.2   Criteria and parameters for routine seismogram analysis

11.2.1   Record duration and dispersion

The first thing one has to look for when assessing a seismic record is the duration of the signal. Due to the different nature and propagation velocity of seismic waves and the different propagation paths taken by them to a station, travel-time differences between the main wave groups usually grow with distance. Accordingly, the record spreads out in time. The various body-wave groups show no dispersion, so their individual duration remains more or less constant, only the time-difference between them changes with distance (see Fig. 2.48). The time difference between the main body-wave onsets is roughly < 3 minutes for events at distances D < 10°, < 16 min for D < 60°, < 30 min for D < 100° and < 45 min for D < 180° (see Fig. 1.2).

In contrast to body waves, velocity of surface waves is frequency dependent and thus surface waves are dispersed. Accordingly, depending on the crustal/mantle structure along the propagation path, the duration of Love- and Rayleigh-wave trains increases with distance. At D > 100° surface wave seismograms may last for an hour or more (see Fig. 1.2), and for really strong events, when surface waves may circle the Earth several times, their oscillations on sensitive long-period (LP) or broadband (BB) records may be recognizable over 6 to 12 hours (see Fig. 2.19). Even for reasonably strong regional earthquakes, e.g., $Ms \approx 6$ and $D \approx 10°$, the oscillations may last for about an hour although the time difference between the P and S onset is only about 2 min and between P and the maximum amplitude in the surface wave group only 5-6 min.

Finally, besides proper dispersion, scattering may also spread wave energy. This is particularly true for the more high-frequency waves traveling in the usually heterogeneous crust. This gives rise to signal-generated noise and coda waves. Coda waves follow the main generating phases with exponentially decaying amplitudes. The coda duration depends mainly on the event magnitude (see Figure 1b in DS 11.1) and only weakly on epicentral distance (see Figure 2 in EX 11.1). Thus, duration can be used for calculating magnitudes Md (see 3.2.4.3).

In summary, signal duration, the time difference between the Rayleigh-wave maximum and the first body-wave arrival (see Table 5 in DS 3.1) and in particular the time span between the first and the last recognized body-wave onsets before the arrival of surface waves allow a first rough estimate, whether the earthquake is a local, regional or teleseismic one. This rough classification is a great help in choosing the proper approach, criteria and tools for further more detailed seismogram analysis, source location, and magnitude determination.

11.2.2   Key parameters: Onset time, amplitude, period and polarity

Onset times of seismic wave groups, first and foremost of the P-wave first arrival, when determined at many seismic stations at different azimuth and at different distance, are the key input parameter for the location of seismic events (see IS 11.1). Travel times published in travel-time tables (such as Jeffreys and Bullen, 1940; Kennett, 1991) and travel-time curves, such as those shown in Figs. 2.40 and 2.50 or in the overlays to Figs. 2.47 and 2.48, have been derived either from observations or Earth models. They give, as a function of epicentral distance D and hypocentral depth h, the differences between *onset times* t_{ox} of the respective seismic phases x and the *origin time* OT of the seismic source. Onset times mark the first

energy arrival of a seismic wave group. The process of recognizing and marking a wave onset and of measuring its onset time is termed *onset time picking*. The recognition of a wave onset largely depends on the spectral signal-to-noise-ratio (SNR) for the given waveform as a whole and the steepness and amplitude of its leading edge. Both are controlled by the shape and bandwidth of the recording seismograph or filter (see Figs. 4.9 to 4.13). It is a classical convention in seismological practice to classify onsets, as a qualitative measure for the reliability of their time-picking, as either impulsive (i) or emergent (e). These lower case letters i or e are put in front of the phase symbol. Generally, it is easier to recognize and precisely pick the very first arrival (usually a P wave) on a seismogram than later phases that arrive within the signal-generated noise coda of earlier waves.

The relative precision with which an onset can be picked largely depends on the factors discussed above, but the absolute accuracy of onset-time measurement is controlled by the available time reference. Seismic body-wave phases travel rather fast. Their apparent velocities at the surface typically range between about 3 km/s and nearly 100 km/s (at the antipode the apparent velocity is effectively infinite). Therefore, an absolute accuracy of onset-time picking of less than a second and ideally less than 0.1 s is needed for estimating reliable epicenters (see IS 11.1) and determining good Earth models from travel-time data. This was difficult to achieve in earlier decades when only mechanical pendulum clocks or marine chronometers were available at most stations. They have unavoidable drifts and could rarely be checked by comparison with radio time signals more frequently than twice a day. Also, the time resolution of classical paper or film records is usually between 0.25 to 2 mm per second, thus hardly permitting an accuracy of time-picking better than a second. In combination with the limited timing accuracy, the reading errors at many stations of the classical world-wide network, depending also on distance and region, were often two to three seconds (Hwang and Clayton, 1991). However, this improved since the late 1970s with the availability of very-low frequency and widely received time signals, e.g., from the DCF and Omega time services, and recorders driven with exactly 50 Hz stabilized alternating current.

Yet, onset-time reading by human eye from analog records with minute marks led to sometimes even larger errors, a common one being the ± 1 min for the P-wave first arrival. This is clearly seen in Fig. 2.46 (left), which shows the travel-time picks collected by the ISC from the world-wide seismic station reports between 1964 and 1987. Nowadays, atomic clock time from the satellite-borne Global Positioning System (GPS) is readily available in nearly every corner of the globe. Low-cost GPS receivers are easy to install at both permanent and temporary seismic stations and generally affordable. Therefore the problem of unreliable absolute timing should no longer exist. Nevertheless, also with high resolution digital data and exact timing now being available it is difficult to decide on the real signal onset, even for sharp P from explosions. Douglas et al. (1997) showed that the reading errors have at best a standard deviation between 0.1 and 0.2 s. However, human reading errors no longer play a role when digital data are evaluated by means of seismogram analysis software which automatically records the time at the positions where onsets have been marked with a cursor. Moreover, the recognizability of onsets and the precision of time picks can be modified easily within the limits which are set by the sampling rate and the dynamic range of recording. Both the time and amplitude scales of a record can be compressed or expanded as needed, and task-dependent optimal filters for best phase recognition can be easily applied.

Fig. 11.4 shows such a digital record with the time scale expanded to 12 mm/s. The onset time can be reliably picked with an accuracy of a few tenths of a second. This P-wave first arrival has been classified as an impulsive (i) onset, although it looks emergent in this particular plot.

But by expanding the amplitude scale also, the leading edge of the wave arrival becomes steeper and so the onset appears impulsive. This ease with which digital records can be manipulated largely eliminates the value of qualitative characterization of onset sharpness by either i or e. Therefore, in the framework of the planned but not yet realized International Seismological Observing Period (ISOP), it is proposed instead to quantify the onset-time reliability. This could be done by reporting, besides the most probable or interpreter-preferred onset time, the estimated range of uncertainty by picking the earliest (t_{ox-}) and latest possible onset time (t_{ox+}) for each reported phase x, and of the first arrival in particular (see Fig. 11.6).
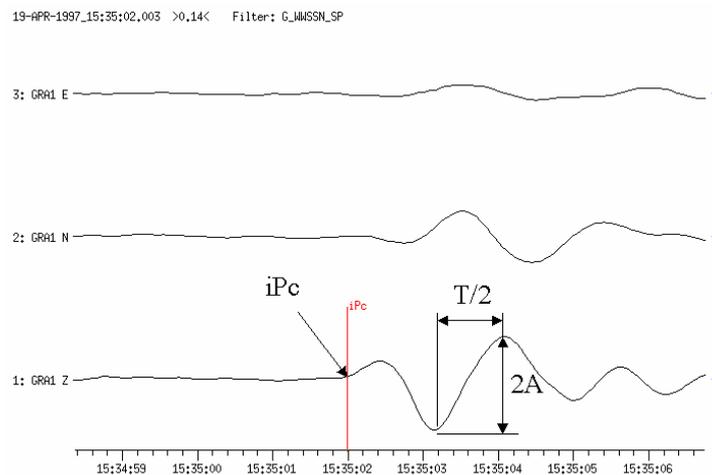

Fig. 11.4 First motion onset times, phase and polarity readings (c – compression; d – dilatation), maximum amplitude A and period T measurements for a sharp (i - impulsive) onset of a P wave from a Severnaya Zemlya event of April 19, 1997, recorded by a broadband three-component single station of the Gräfenberg Array, Germany.

Whereas the quality, quantity and spatial distribution of reported time picks largely controls the precision of source locations (see IS 11.1), the quality and quantity of amplitude readings for identified specific seismic phases determine the representativeness of classical event *magnitudes*. The latter are usually based on readings of maximum ground-displacement and related periods for body- and surface-wave groups (see 3.2). For symmetric oscillations amplitudes should be given as half peak-to-trough (double) amplitudes. The related periods should be measured as the time between neighboring peaks (or troughs) of the amplitude maximum or by doubling the time difference between the maximum peak and trough (see Fig. 11.4 and Fig. 3.9). Only for highly asymmetric wavelets should the measurement be made from the center line to the maximum peak or trough (see Fig. 3.9b). Some computer programs mark the record cycle from which the maximum amplitude A and the related T have been measured (see Figures 3 and 4 in EX 3.1).

Note that the measured maximum trace amplitudes in a seismic record have to be corrected for the frequency-dependent magnification of the seismograph to find the "true" ground-motion amplitude, usually given in nanometers (1 nm = 10^{-9}m) or micrometers (1 μm = 10^{-6}m), at the given period. Fig. 3.11 shows a few typical displacement amplification curves of standard seismographs used with paper or film records. For digital seismographs, instead of displacement magnification, the frequency dependent *resolution* is usually given in units of nm/counts, or in nm s^{-1}/count for ground velocity measurements. Note that both record amplitudes and related dominating periods do not only depend on the spectrum of the arriving

waves but are mainly controlled by the shape, center frequency and bandwidth of the seismograph or record filter response (see Fig. 4.13). Also, the magnifications given in the seismograph response curves are strictly valid only for steady-state harmonic oscillations without any transient response. The latter, however, might be significant when narrow-band seismographs record short wavelets of body waves. Signal shape, amplitudes and signal duration are then heavily distorted (see Figs. 4.10 and 4.17). Therefore, we have written "true" ground motion in quotation marks. Scherbaum (2001) gives a detailed discussion of signal distortion which is not taken into account in standard magnitude determinations from band-limited records. However, signal distortion must be corrected for in more advanced digital signal analysis for source parameter estimation. The distortions are largest for the very first oscillation(s) and they are stronger and longer lasting the narrower the recording bandwidth (see 4.2.1 and 4.2.2). The transient response decays with time, depending also on the damping of the seismometer. It is usually negligible for amplitude measurements on dispersed teleseismic surface wave trains.

To calculate ground motion amplitudes from record amplitudes, the frequency-dependent seismometer response and magnification have to be known from careful calibration (see 5.8). Analog seismograms should be clearly annotated and relate each record to a seismometer with known displacement magnification. For digital data, the instrument response is usually included in the header information of each seismogram file or given in a separate file that is automatically linked when analyzing data files. As soon as amplitudes and associated periods are picked in digital records, most software tools for seismogram analysis calculate instantaneously the ground displacement or ground velocity amplitudes and write them in related parameter files.

Another parameter which has to be determined (if the signal-to-noise-ratio permits) and reported routinely is the polarity of the P-wave first motion in vertical component records. Reliable observations of the first motion polarity at stations surrounding the seismic source in different directions allows the derivation of seismic fault-plane solutions (see 3.4 and EX 3.2). The wiring of seismometer components has to be carefully checked to assure that compressional first arrivals (c) appear on vertical-component records as an upward motion (+) while dilatational first arrivals (d) are recorded as a downward first half-cycle (-). The conventions for horizontal component recordings are + (up) for first motions towards N and E, and – (down) for motions towards S and W. These need to be taken into account when determining the backazimuth of the seismic source from amplitude and polarity readings on 3-component records (see EX 11.2, Figure 1). However, horizontal component polarities are not considered in polarity-based fault-plane solutions and therefore not routinely reported to data centers. Fig. 11.4 shows a compressional first arrival.

One should be aware, however, that narrow-band signal filtering may reduce the first-motion amplitude by such a degree that its polarity may no longer be reliably recognized or may even become lost completely in the noise (see Figs. 4.10 and 4.13). This may result in the wrong polarity being reported and hence erroneous fault-plane solutions. Since short-period (SP) records usually have a narrower bandwidth than medium- to long-period or even broadband records, one should differentiate between first-motion polarity readings from SP and LP/BB records. Also, long-period waves integrate over much of the detailed rupture process and so should show more clearly the overall direction of motion which may not be the same as the first-motion arrival in SP records which may be very small. Therefore, when reporting polarities to international data centers one should, according to recommendations in 1985 of the WG on Telegrafic Formats of the IASPEI Commission on Practice, unambiguously differentiate between such readings on SP (c and d) and those on LP and BB records,

respectively (u for "up" = compression and r for "rarefaction" = dilatation). Note, however, that reliable polarity readings are only possible on BB records!
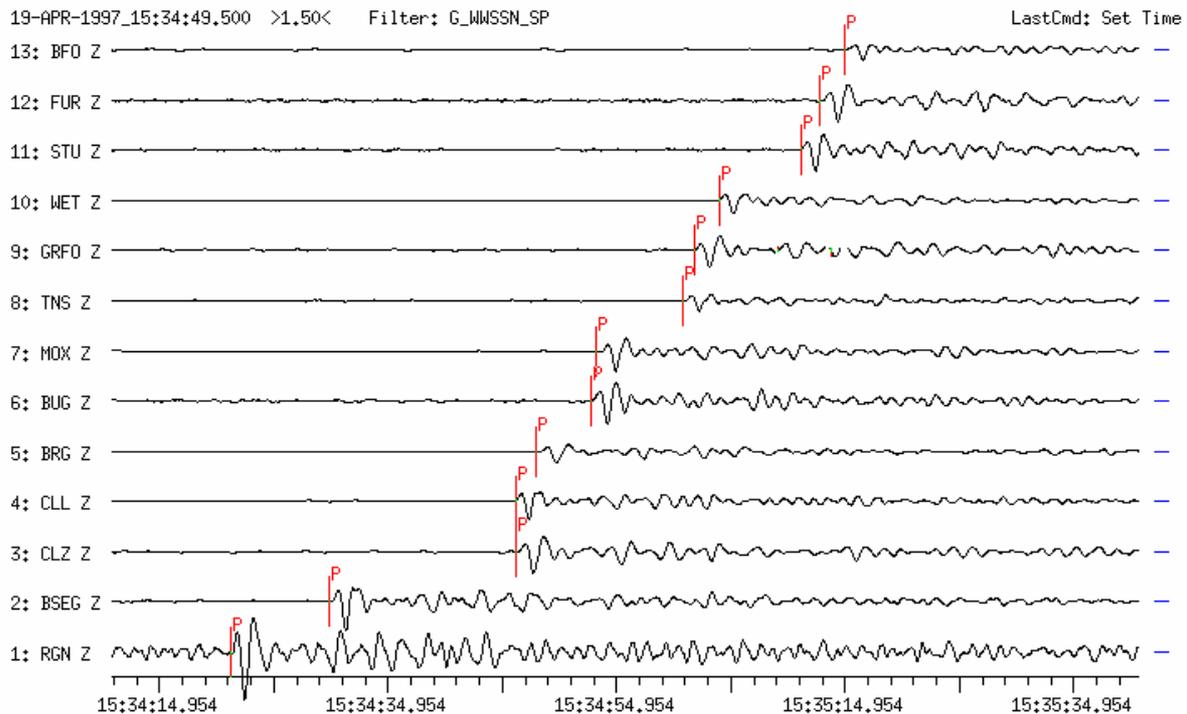

Fig. 11.5 WWSSN-SP vertical-component records of GRSN stations for the same event as in Fig. 11.4. While the P-wave amplitudes vary significantly within the network, the first-motion polarity remains the same.

11.2.3 Advanced wavelet parameter reporting from digital records

The parameters discussed in 11.2.1 have been routinely reported over the decades of analog recording. Digital records, however, allow versatile signal processing so that additional wavelet parameters can be measured routinely. Such parameters may provide a much deeper insight into the seismic source processes and the seismic moment release. Not only can onset times be picked but their range of uncertainty can also be marked. Further, for a given wave group, several amplitudes and related times may be quickly measured and these allow inferences to be drawn on how the rupture process may have developed in space and time. Moreover, the duration of a true ground displacement pulse t_w and the rise time t_r to its maximum amplitude contain information about size of the source, the stress drop and the attenuation of the pulse while propagating through the Earth. Integrating over the area underneath a displacement pulse allows to determine its signal moment m_s which is, depending on the bandwidth and corner period of the recording, related to the seismic moment M_0 (Seidl and Hellweg, 1988). Finally, inferences on the attenuation and scattering properties along the wave path can be drawn from the analysis of wavelet envelopes.

Fig. 11.6 depicts various parameters in relation to different seismic waveforms. One has to be aware, however, that each of these parameters can be severely affected by the properties of the seismic recording system (see Fig. 4.17 and Scherbaum, 1995 and 2001). Additionally, one may analyze the signal-to-noise ratio (SNR) and report it as a quantitative parameter for

characterizing signal strength and thus of the reliability of phase and parameter readings. This is routinely done when producing the Reviewed Event bulletin (RED) of the International Data Centre (IDC) in the framework of the CTBTO. The SNR may be either given as the ratio between the maximum amplitude of a considered seismic phase to that of the preceding ambient or signal-generated noise, or more comprehensively by determining the spectral SNR (see Fig. 11.47).
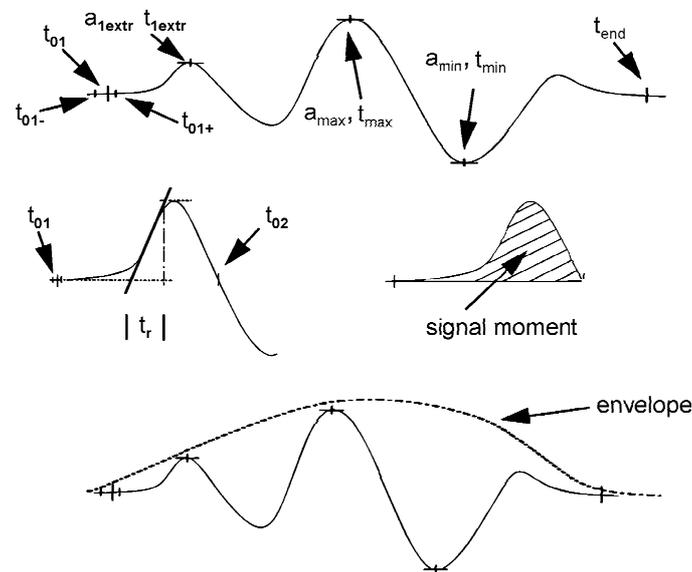

Fig. 11.6 Complementary signal parameters such as multiple wavelet amplitudes and related times, rise-time t_r of the displacement pulse, signal moment m_s and wavelet envelope (with modification from Scherbaum, Of Poles and Zeros, Fig. 1.9, p. 10, © 2001; with permission of Kluwer Academic Publishers).

Although these complementary signal parameters could be determined rather easily and quickly by using appropriate software for signal processing and seismogram analysis, their measurement and reporting to data centers is not yet common practice. It is expected, however, that the recently introduced more flexible formats for parameter reporting and storage (see ISF, 10.2.5), in conjunction with e-mail and internet data transfer, will pave the way for their routine reporting.

11.2.4 Criteria to be used for phase identification

11.2.4.1 Travel time and slowness

As outlined in Chapter 2, travel times of identified seismic waves are not only the key information for event location but also for the identification of seismic wave arrivals and the determination of the structure of the Earth along the paths which these waves have traveled. The same applies to the horizontal component s_x of the slowness vector s. The following relations hold:

$$s_x = dt/dD = p = 1/v_{app}$$

were v_{app} is the apparent horizontal velocity of wave propagation, dt/dD the gradient of the travel-time curve t(D) in the point of observation at distance D, and p is the ray parameter. Due to the given structure of the Earth, the travel-time differences between various types of seismic waves vary with distance in a systematic way. Therefore, differential travel-time curves with respect to the P-wave first arrival (see Figure 4 in EX 11.2) or absolute travel-time curves with respect to the origin time OT (see Figure 4 in EX 11.1 or overlay to Fig. 2.48) are the best tools to identify seismic waves on single station records. This is done by matching as many of the recognizable wave onsets in the record as possible with travel-time curves for various theoretically expected phases at epicentral distance D.

Make sure that the plotted t(D)-curves have the same time-resolution as your record and investigate the match at different distances. Relative travel-time curves thus allow not only the identification of best matching phases but also the distance of the station from the epicenter of the source to be estimated. Note, however, that from certain distance ranges the travel-time curves of different types of seismic waves (see Figure 4 in EX 11.2) are close to each other, or even overlap, for example for PP and PcP between about 40° and 50° (see Figure 6a in DS 11.2) and for S, SKS and ScS between 75° and 90° (see Fig. 11.7 and 11.54). Proper phase identification then requires additional criteria besides travel-time differences to be taken into account (see 11.2.4.2 to 11.2.4.4). Select the most probable distance by taking these additional criteria into account. Absolute travel-time curves allow also the origin time to be estimated (see exercises EX 11.1 and EX 11.2).
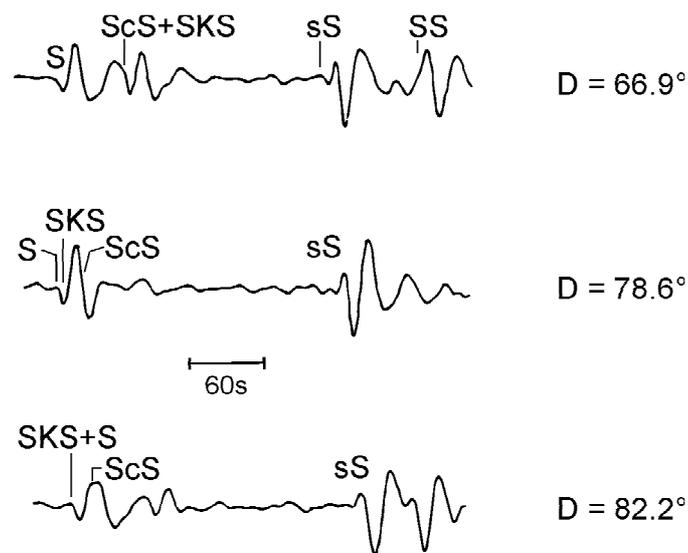

Fig. 11.7 Example of long-period horizontal component seismogram sections from a deep-focus earthquake in the Sea of Okhotsk (20.04.1984, mb = 5.9, h = 588 km), recorded at the stations RSSD, RSNY, and RSCP, respectively, in the critical distance range of overlapping travel-time branches of S, SKS and ScS. Because of the large focal depth the depth phase sS is clearly separated in time.

Note, however, that the travel-time curves shown in the overlays to Figs. 2.47 and 2.48, or those given in EX 11.1 and EX 11.2, are valid for near-surface sources only. Both absolute and (to a lesser extent) relative travel times change with source depth (see IASPEI 1991 Seismological Tables, Kennett, 1991) and, in addition, depth phases may appear (see Fig. 2.43 and Table 1 in EX 11.2). Note also that teleseismic travel-time curves (D > (17)20°) vary little from region to region. Typically, the theoretical travel times of the main seismic phases

deviate by less than 2 s from those observed (see Fig. 2.52). In contrast, local/regional travel-time curves for crustal and uppermost mantle phases may vary strongly from region to region. This is due to the pronounced lateral variations of crustal thickness and structure (see Fig. 2.10), age, and seismic wave velocities in continental and oceanic areas. This means local/regional travel-time curves have to be derived for each region in order to improve phase identification and estimates of source distance and depth.

Often, rapid epicentre and/or source depth estimates are already available from data centers prior to detailed record analysis at a given station. Then modern seismogram analysis software such as SEISAN (Havskov, 1996; Havskov and Ottemöller, 1999), SEIS89 (Baumbach, 1999), GIANT (Rietbrock and Scherbaum, 1998) or Seismic Handler (SH and SHM) (Stammler, http://www.szgrf.bgr.de/sh-doc/index.html) allow the theoretically expected travel times for all main seismic phases to be marked on the record. This eases phase identification. An example is shown in Fig. 11.13 for a record analyzed with Seismic Handler.

However, **theoretically calculated onset-times based on a global average model should only guide the phase identification but not the picking of onsets!** Be aware that one of the major challenges for modern global seismology is 3-D tomography of the Earth. What are required are the location and the size of anomalies in wave velocity with respect to the global 1-D reference model. Only then will material flows in the mantle and core (which drive plate tectonics, the generation of the Earth's magnetic field and other processes) be better understood. Station analysts should never trust the computer generated theoretical onset times more than the ones that they can recognize in the record itself. For Hilbert transformed phases (see 2.5.4.3) onset times are best read after filtering to correct for the transforming. Without unbiased analyst readings we will never be able to derive improved models of the inhomogeneous Earth. Moreover, the first rapid epicenters, depths and origin-times published by the data centers are only preliminary estimates and are usually based on first arrivals only. Their improvement, especially with respect to source depth, requires more reliable onset-time picks, and the identification of secondary (later) arrivals (see Figure 7 in IS 11.1).

At a local array or regional seismic network center both the task of phase identification and of source location is easier than at a single station because local or regional slowness can be measured from the time differences of the respective wave arrivals at the various stations (see 9.4, 9.5, 11.3.4 and 11.3.5). But even then, determining D from travel-time differences between P or PKP and later arrivals can significantly improve the location accuracy. This is best done by using three-component broadband recordings from at least one station in the array or network. The reason this is recommended is that travel-time differences between first and later arrivals vary much more rapidly with distance than the slowness of first arrivals. On the other hand, arrays and regional networks usually give better control of the backazimuth of the source than 3-component recordings (see 11.2.4.3), especially for low-magnitude events.

11.2.4.2 Amplitudes, dominating periods and waveforms

Amplitudes of seismic waves vary with distance due to geometric spreading, focusing and defocusing caused by variations in wave speed and attenuation. To correctly identify body-wave phases one has first to be able to differentiate between body- and surface-wave groups and then estimate at least roughly, whether the source is at shallow, intermediate or rather large depth. At long range, surface waves are only seen on LP and BB seismograms. Because of their 2D propagation, geometrical spreading for surface waves is less than for body waves

that propagate 3-D. Also, because of their usually longer wavelength, surface waves are less attenuated and affected less by small-scale structural inhomogeneities than body waves. Therefore, on records of shallow seismic events, surface-wave amplitudes dominate over body-wave amplitudes (see Figs. 11.8 and 11.9) and show less variability with distance (see Fig. 3.13). This is also obvious when comparing the magnitude calibration functions for body and surface waves (see figures and tables in DS 3.1).
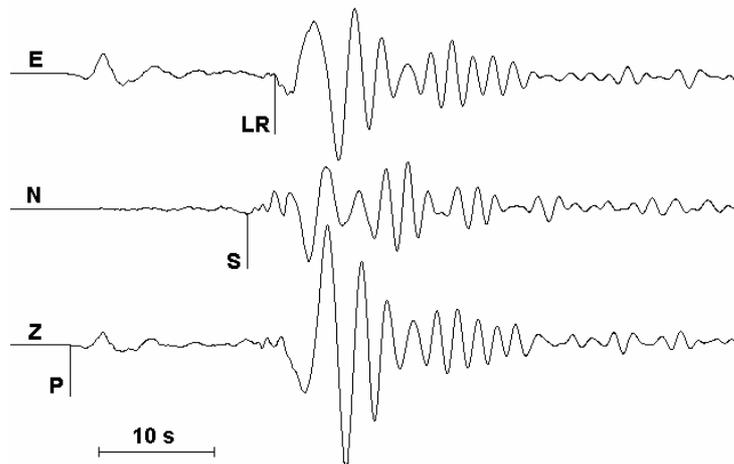
Fig. 11.8 Three-component BB-velocity record at station MOX of a mine collapse in Germany; (13 March 1989; Ml = 5.5) at a distance of 112 km and with a backazimuth of 273°. Note the Rayleigh surface-wave arrival LR with subsequent normal dispersion.
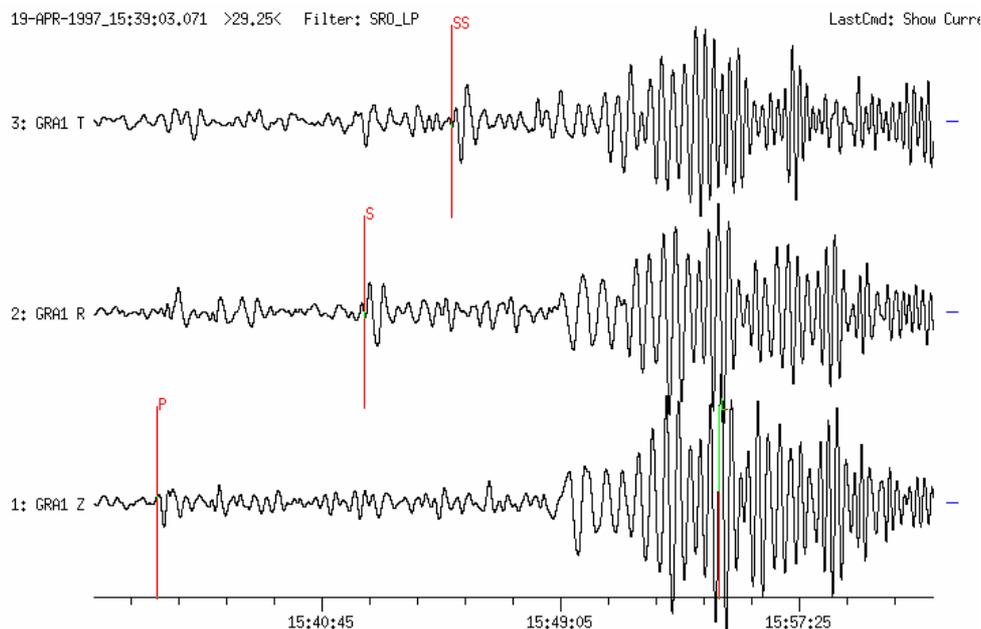
**Fig. 11.9** T-R-Z rotated three-component seismogram (SRO-LP filter) from an earthquake east of Severnaya Zemlya (19 April 1997, D = 46.4°, mb = 5.8, Ms = 5.0). The record shows P, S, SS and strong Rayleigh surface waves with clear normal dispersion. The surface wave maximum has periods of about 20 s. It is called an Airy-phase and corresponds to a minimum in the dispersion curve for continental Rayleigh waves (see Fig. 2.9).

However, as source depth increases, surface-wave amplitudes decrease relative to those of body waves, the decrease being strongest for shorter wavelengths. Thus, the surface waves from earthquakes at intermediate (> 70 km) or great depth (> 300 km) may have amplitudes smaller than those of body waves or may not even be detected on seismic records (see Figure 2 in EX 11.2). This should alert seismogram analysts to look for depth phases, which are then usually well separated from their primary waves and so are easily recognized (see Fig. 11.7 above and Figure 6a and b in DS 11.2).

Another feature that helps in phase identification is the waveform. Most striking is the difference in waveforms between body and surface waves. Dispersion in surface waves results in long wave trains of slowly increasing and then decreasing amplitudes, whereas non-dispersive body waves form short duration wavelets. Usually, the longer period waves arrive first ("normal" or "positive" dispersion) (see Figs. 11.8 and 11.9). However, the very long-period waves (T > 60 s) , that penetrate into the mantle down to the asthenosphere (a zone of low wave speeds), may show inverse dispersion. The longest waves then arrive later in the wave train (see Fig. 2.18).

For an earthquake of a given seismic moment, the maximum amplitude of the S wave is about five-times larger at source than that of the P waves (see Figs. 2.3, 2.23, and 2.41). This is a consequence of the different propagation velocities of P and S waves (see Eq. (3.2). Also the spectrum is different for each wave type. Thus, P-wave source spectra have corner frequencies about $\sqrt{3}$ times higher than those of S. In high-frequency filtered records this may increase P-wave amplitudes with respect to S-wave amplitudes (see Fig. 11.10 right). Additionally, the frequency-dependent attenuation of S waves is significantly larger than for P waves.
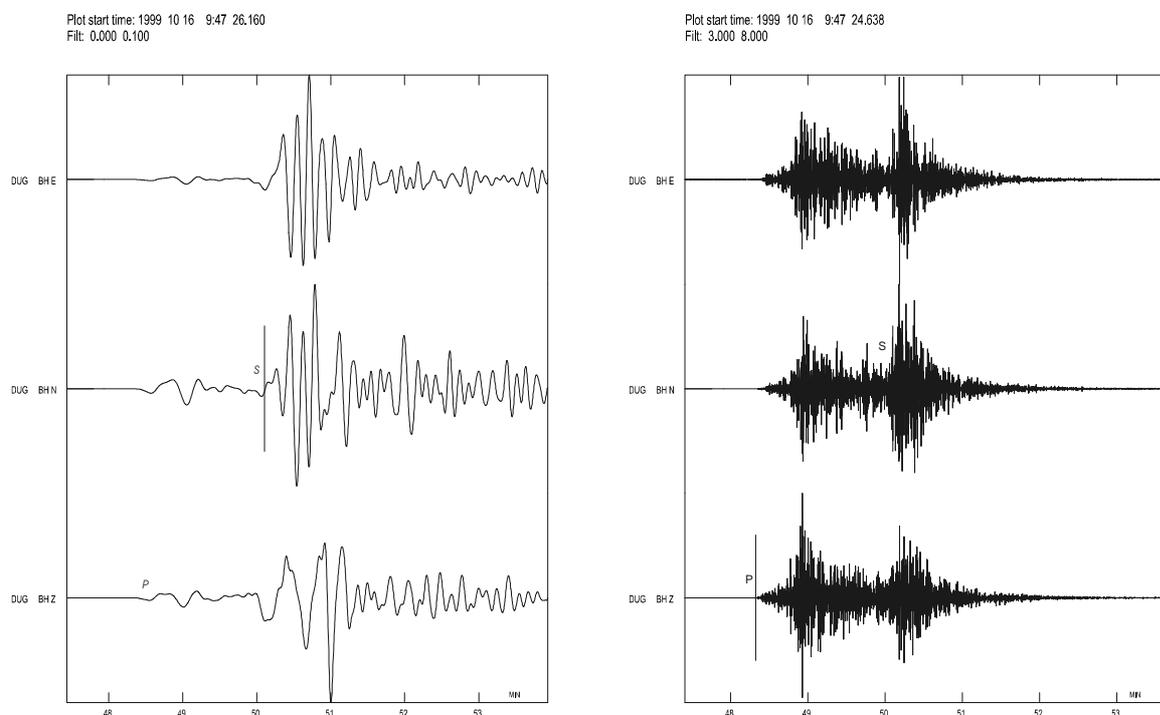

Fig. 11.10 Left: Low-pass filtered (< 0.1 Hz) and right: band-pass filtered (3.0-8.0 Hz) seismograms of the Oct. 16, 1999, earthquake in California (mb = 6.6, Ms = 7.9) as recorded at the broadband station DUG at D = 6° (courtesy of L. Ottemöller).

Due to both effects, S waves and their multiple reflections and conversions are – within the teleseismic distance range – mainly observed on LP or BB records. On the other hand, the different P-wave phases, such as P, PcP, PKP, and PKKP, are well recorded, up to the largest epicentral distances, by SP seismographs with maximum magnification typically around 1 Hz.

Generally, the rupture duration of earthquakes is longer than the source process of explosions. It ranges from less than a second for small microearthquakes up to several minutes for the largest shallow crustal shocks with a source which is usually a complex multiple rupture process (see Fig. 11.11, Fig. 3.7 and Figure 5b in DS 11.2).
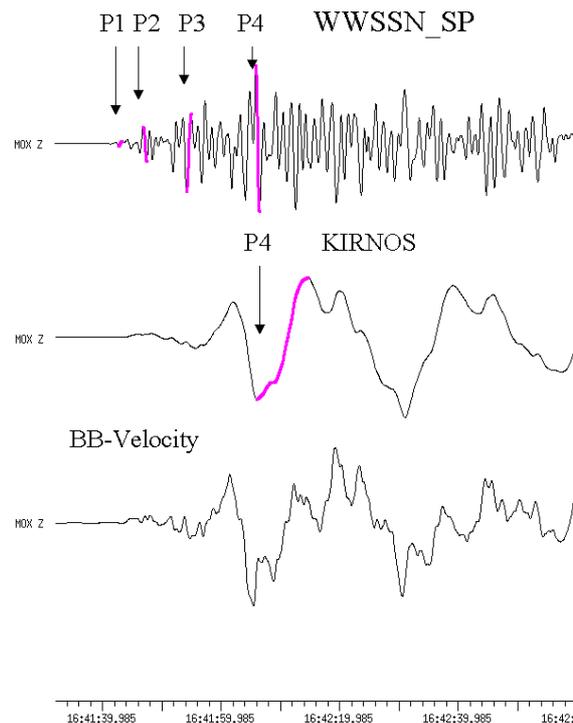

Fig. 11.11   Vertical component records of the P-wave group from a crustal earthquake in Sumatra (04 June 2000; mb = 6.8, Ms = 8.0) at the GRSN station MOX at D = 93.8°. **Top:** WWSSN-SP (type A); **middle:** medium-period Kirnos SKD BB-displacement record (type C), and **bottom:** original BB-velocity record. Clearly recognizable is the multiple rupture process with P4 = P_{max} arriving 25 s after the first arrival P1. The short-period magnitude mb determined from P1 would be only 5.4, mb = 6.3 from P2 and mb = 6.9 when calculated from P4. When determining the medium-period body-wave magnitude from P4 on the Kirnos record then mB = 7.4.

As compared to shallow crustal earthquakes, deep earthquakes of comparable magnitude are often associated with higher stress drop and smaller source dimension. This results in the strong excitation of higher frequencies and thus simple and impulse-like waveforms (see Fig. 4.13 and Figures 6a and b in DS 11.2). Therefore S waves from deep earthquakes may be recognizable in short-period records even at teleseismic distances. The same applies to waveforms from explosions. As compared to shallow earthquakes, when scaled to the same magnitude, their source dimension is usually smaller, their source process simpler and their source duration much shorter (typically in the range of milliseconds). Accordingly, explosions generate significantly more high-frequency energy than earthquakes and usually produce shorter and simpler waveforms. Examples are given in Figures 1 to 5 of DS 11.4. Note,

however, that production explosions in large quarries or open cast mines, with yields ranging from several hundred to more than one kiloton TNT, are usually fired in sequences of time-delayed sub-explosions, which are spread out over a large area. Such explosions may generate rather complex wave fields, waveforms and unusual spectra, sometimes further complicated by the local geology and topography, and thus not easy to discriminate from local earthquakes.

At some particular distances, body waves may have relatively large amplitudes, especially near caustics (see Fig. 2.29 for P waves in the distance range between 15° and 30°; or around D = 145° for PKP phases). In contrast, amplitudes decay rapidly in shadow zones (such as for P waves beyond 100°; see Fig. 11.63). The double triplication of the P-wave travel-time curve between 15° and 30° results in closely spaced successive onsets and consequently rather complex waveforms (Fig. 11.49). At distances between about 30° and 100°, however, waveforms of P may be simple (see Figs. 11.52 and 11.53). Beyond the PKP caustic, between 145° < D < 160°, longitudinal core phases split into three travel-time branches with typical amplitude-distance patterns. This, together with their systematic relative travel-time differences, permits rather reliable phase identification and distance estimates, often better than 1° (see Figs. 11.62 and 11.63 as well as exercise EX 11.3).

Fig. 11.12 is a simplified diagram showing the relative frequency of later body-wave arrivals with respect to the first arrival P or the number n of analyzed earthquakes, as a function of epicentral distance D between 36° and 166°. They are based on observations in standard records (see Fig. 3.11) of types A4 (SP - short-period, < 1.5 s), B3 (LP – long-period, between 20 s and 80 s) and C (BB - broadband displacement between 0.1 s and 20 s) at station MOX in Germany (Bormann, 1972a). These diagrams show that in the teleseismic distance range one can mainly expect to observe in SP records the following longitudinal phases: P, PcP, ScP, PP, PKP (of branches ab, bc and df), P'P' (= PKPPKP), PKKP, PcPPKP, SKP and the depth phases of P, PP and PKP. In LP and BB records, however, additionally S, ScS, SS, SSS, SKS, SKSP, SKKS, SKKP, SKKKS, PS, PPS, SSP and their depth phases are frequently recorded. This early finding based on the visual analysis of traditional analog film recordings has recently been confirmed by stacking SP and LP filtered broadband records of the Global Digital Seismic Network (GDSN) (Astiz et al., 1996; see Figs. 2.47 and 2.48 with overlays).

Since these diagrams and stacked seismogram sections reflect, in a condensed form, some systematic differences in waveforms, amplitudes, dominating periods and relative frequency of occurrence of seismic waves in different distance ranges, they may, when used in addition to travel-time curves, give some guidance to seismogram analysts as to what kind of phases they may expect at which epicentral distances and in which kind of seismic records. Note, however, that the appearance of these phases is not "obligatory", rather, it may vary from region to region, depending also on the source mechanisms and the radiation pattern with respect to the recording station, the source depth, the area of reflection (e.g., underneath oceans, continental shield regions, young mountain ranges), and the distance of the given station from zones with frequent deep earthquakes. Therefore, no rigid rules for phase identification can be given. Also, Fig. 11.12 considers only teleseismic earthquakes. Local and regional earthquakes, however, are mainly recorded by SP short-period seismographs of type A or with Wood-Anderson response. There are several reasons for this. Firstly, SP seismographs have usually the largest amplification and so are able to record (at distances smaller than a few hundred kilometers) sources with magnitudes of zero or even less. Secondly, as follows from Fig. 3.5, the corner frequency of source displacement spectra for

events with magnitudes < 4 is usually > 1 Hz, i.e., small events radiate relatively more high-frequency energy. Thirdly, in the near range the high frequencies have not yet been reduced so much by attenuation and scattering, as they usually are for f > 1 Hz in the teleseismic range. Therefore, most local recordings show no waves with periods longer than 2 s. However, as Ml increases above 4, more and more long-period waves with large amplitudes are generated and these dominate in BB records of local events, as illustrated with the records in Figs. 11.8 and 11.10.
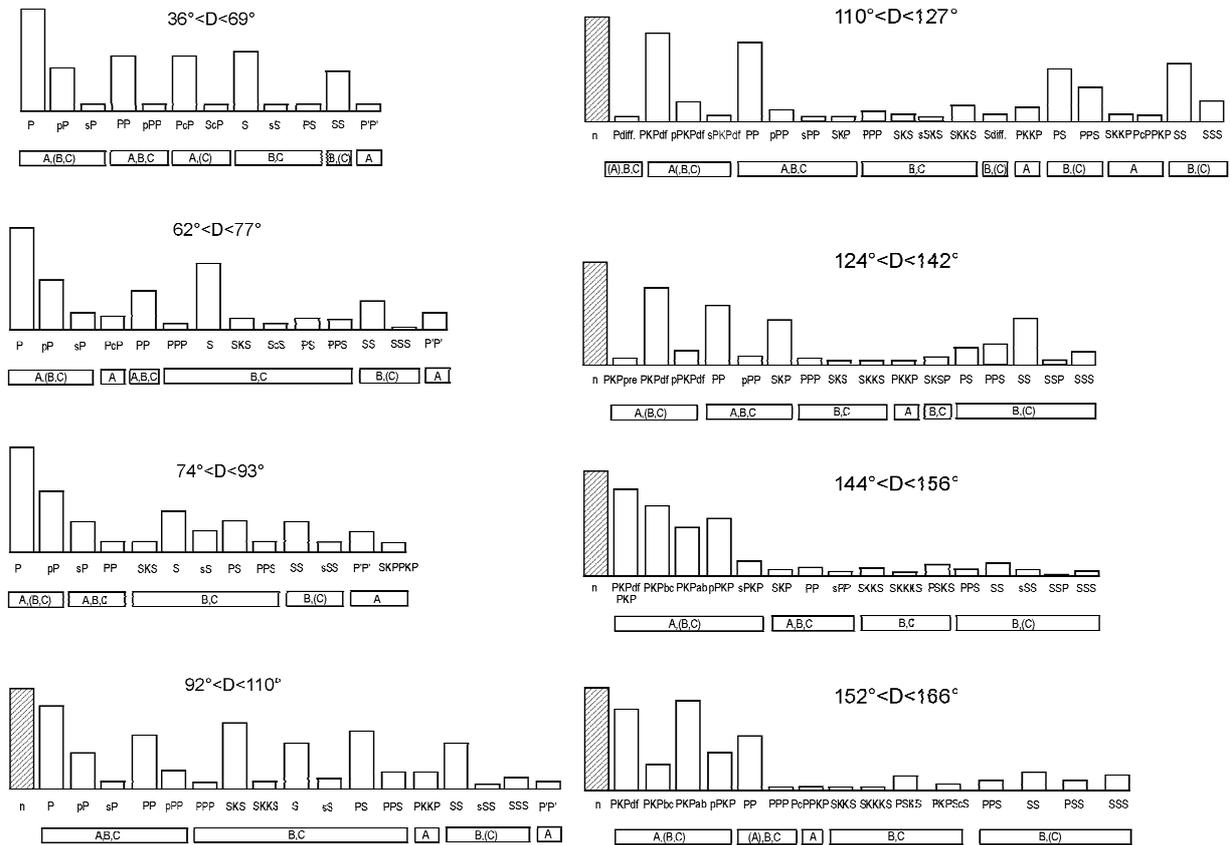
Fig. 11.12 Relative frequency of occurrence of secondary phases in standard analog records at station MOX, Germany, within the teleseismic distance range 36° to 166°. The first column relates to 100% of analyzed P-wave first arrivals or of analyzed events (hatched column), respectively. In the boxes beneath the phase columns the type of standard records is indicated in which these phases have been observed best or less frequently/clear (then record symbols in brackets). A – short-period; B – long-period LP, C – Kirnos SKD BB-displacement.

11.2.4.3 Polarization

As outlined in 2.2 and 2.3, P and S waves are linearly polarized, with slight deviations from this ideal in the inhomogeneous and partially anisotropic real Earth (see Figs. 2.6 and 2.7). In contrast, surface waves may either be linearly polarized in the horizontal plane perpendicular to the direction of wave propagation (transverse polarization; T direction; e.g., Love waves) or elliptically polarized in the vertical plane oriented in the radial (R) direction of wave propagation (see Figs. 2.8, 2.13 and 2.14). P-wave particle motion is dominatingly back and forth, parallel to the seismic ray, whereas S-wave motion is perpendicular to the ray direction.

Accordingly, a P-wave motion can be split into two main components, one vertical (Z) and one horizontal (R) component. The same applies to Rayleigh waves, but with a 90° phase shift between the Z and R components of motion. S waves, on the other hand, may show purely transverse motion, oscillating in the horizontal plane (SH; i.e., pure T component, as Love waves) or motion in the vertical propagation plane, at right angles to the ray direction (SV), or in any other combination of SH and SV. In the latter case S-wave particle motion has Z, R and T components, with SV wave split into a Z and an R component.

Thus, when 3-component records are available, the particle motion of seismic waves in space can be reconstructed and used for the identification of seismic wave types. However, usually the horizontal seismometers are oriented in geographic east (E) and north (N) direction. Then, first the backazimuth of the source has to be computed (see EX 11.2) and then the horizontal components have to be rotated into the horizontal R direction and the perpendicular T direction, respectively. This *axis rotation* is easily performed when digital 3-component data and suitable analysis software are available. It may even be carried one step further by rotating the R component once more into the direction of the incident seismic ray (longitudinal L direction). The T component then remains unchanged but the Z component is rotated into the Q direction of the SV component. Such a *ray-oriented co-ordinate system* separates and plots P, SH and SV waves in 3 different components L, T and Q, respectively. These axes transformations are easily made given digital data from arbitrarily oriented orthogonal 3-component sensors such as the widely used triaxial sensors STS2 (see Fig. 5.13 and DS 5.1). However, the principle types of polarization can often be quickly assessed with manual measurement and elementary calculation from analog 3-component records and the backazimuth from the station to the source be estimated (see EX 11.2).

Note that all direct, reflected and refracted P waves and their multiples, as well as conversions from P to S and vice versa, have their dominant motion confined to the Z and R (or L and Q) plane. This applies to all core phases, also to SKS and its multiples, because K stands for a P-wave leg in the outer core. In contrast, S waves may have both SV and SH energy, depending on the source type and rupture orientation. However, discontinuities along the propagation path of S waves act as selective SV/SH filters. Therefore, when an S wave arrives at the free surface, part of its SV energy may be converted into P, thus forming an SP phase. Consequently, the energy reflected as S has a larger SH component as compared to the incoming S. So the more often a mixed SH/SV type of S wave is reflected at the surface, the more it becomes of SH type. Accordingly, SSS, SSSS etc. will show up most clearly or even exclusively on the T component (e.g., Fig. 11.37) unless the primary S wave is dominantly of SV-type (e.g., Fig. 11.13). As a matter of fact, Love waves are formed through constructive interference of repeated reflections of SH at the free surface. Similarly, when an S wave hits the core-mantle boundary, part of its SV energy is converted into P which is either refracted into the core (as K) or reflected back into the mantle as P, thus forming the ScP phase. Consequently, multiple ScS is also usually best developed on the T component.

Fig. 11.13 shows an example of the good separation of several main seismic phases on an Z-R-T-component plot. At such a large epicentral distance (D = 86.5°) the incidence angle of P is small (about 15°; see EX 3.3). Therefore, the P-wave amplitude is largest on the Z component whereas for PP, which has a significantly larger incidence angle, the amplitude on the R component is almost as large as Z. For both P and PP no T component is recognizable above the noise. SKS is strong in R and has only a small T component (effect of anisotropy, see Fig. 2.7). The phase SP has both a strong Z and R component. Love waves (LQ) appear as the first surface waves in T with very small amplitudes in R and Z. In contrast, Rayleigh

waves (LR) are strongest in R and Z. SS in this example is also largest in R. From this one can conclude, that the S waves generated by this earthquake are almost purely of SV type. In other cases, however, it is only the difference in the R-T polarization which allows S to be distinguished from SKS in this distance range of around 80° where these two phases arrive closely to each other (see Fig. 11.14 and Figure 13e in DS 11.2).
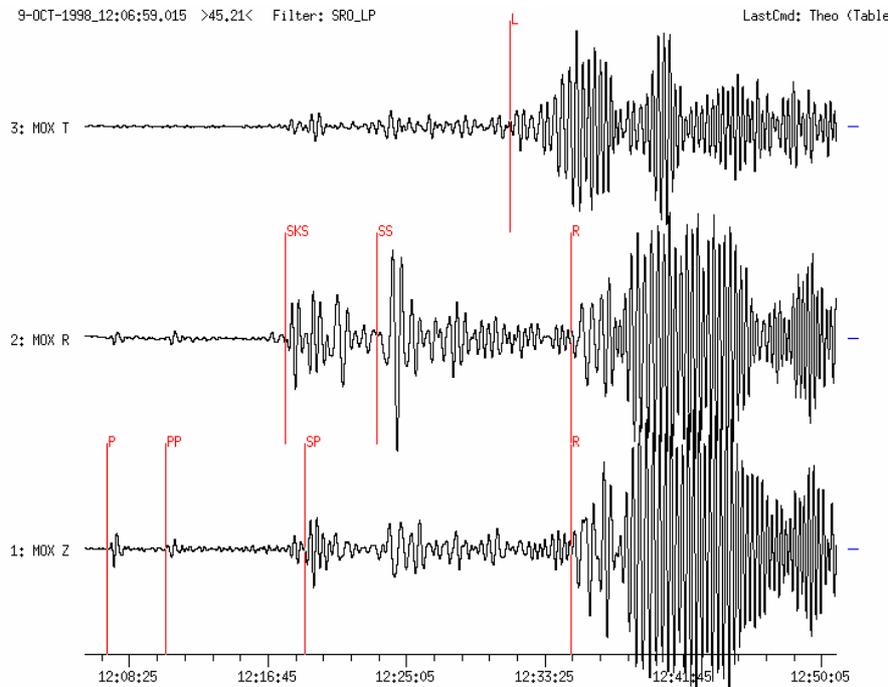

Fig. 11.13 Time-compressed long-period filtered three-component seismogram (SRO-LP simulation filter) of the Nicaragua earthquake recorded at station MOX (D = 86.5°). Horizontal components have been rotated (ZRT) with R (radial component) in source direction. The seismogram shows long-period phases P, PP, SKS, SP, SS and surface waves L (or LQ for Love wave) and R (or LR for Rayleigh wave).
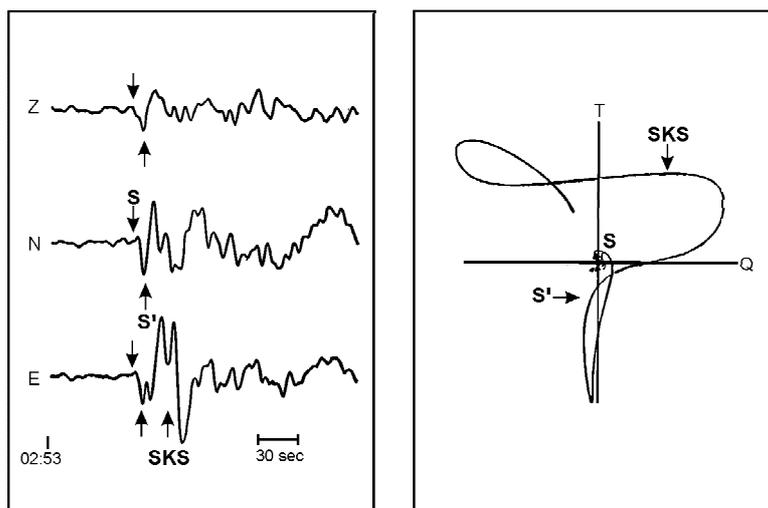
Fig. 11.14 Ray-oriented broadband records (left: Z-N-E components; right: particle motion in the Q-T plane) of the S and SKS wave group from a Hokkaido Ms = 6.5 earthquake on 21 March 1982, at station Kasperske Hory (KHC) at an epicentral distance of D = 78.5°.

The empirical travel-time curves in Fig. 2.49 (from Astiz et al., 1996) summarize rather well, which phases (according to the overlay of Fig. 2.48) are expected to dominate the vertical, radial or transverse ground motion in rotated three-component records.

If we supplement the use of travel-time curves with seismic recordings in different frequency bands, and take into account systematic differences in amplitude, frequency content and polarization for P, S and surface waves, and when we know the distances, where caustics and shadow zones occur, then the identification of later seismic wave arrivals is entertaining and like a detective inquiry into the seismic record.

11.2.4.4 Example for documenting and reporting of seismogram parameter readings

Fig. 11.15 shows a plot of the early part of a teleseismic earthquake recorded at stations of the GRSN. At all stations the first arriving P wave is clearly recognizable although the P-wave amplitudes vary strongly throughout the network. This is not a distance effect (the network aperture is less than 10% of the epicentral distance) but rather an effect of different local site conditions related to underground geology and crustal heterogeneity. As demonstrated with Figs. 4.35 and 4.36, the effect is not a constant for each station but depends both on azimuth and distance of the source. It is important to document this. Also, Fig. 11.15 shows for most stations a clear later arrival about 12 s after P. For the given epicentral distance, no other main phase such as PP, PPP or PcP can occur at such a time (see differential travel-time curves in Figure 4 of EX 11.2). It is important to pick such later (so-called secondary) onsets which might be "depth phases" (see 11.2.5.1) as these allow a much better determination of source depth than from P-wave first arrivals alone (see Figure 7 in IS 11.1).
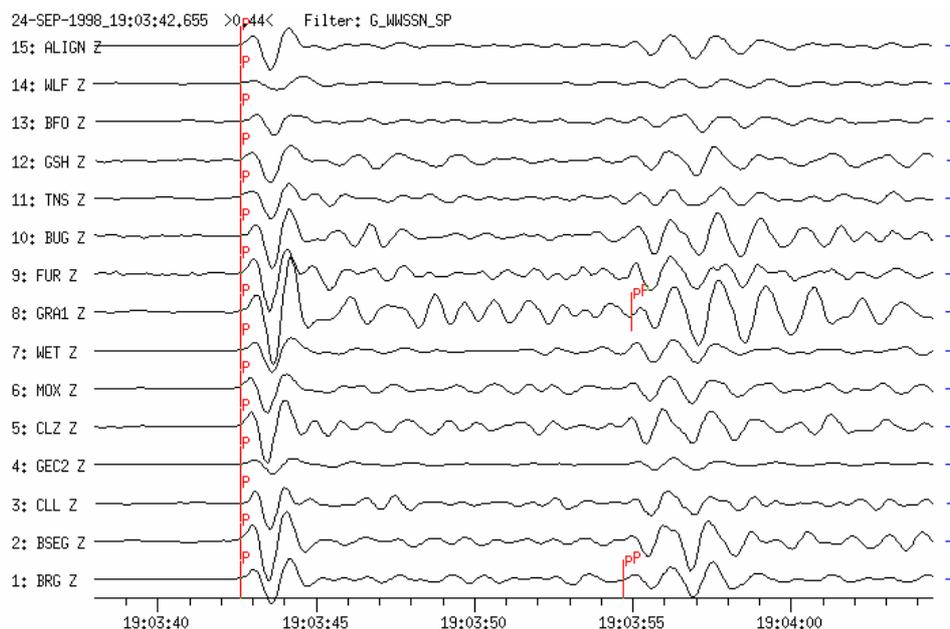
Fig. 11.15 WWSSN-SP filtered seismograms at 14 GRSN, GRF, GERESS and GEOFON stations from an earthquake in Mongolia (24 Sept. 1998; depth (NEIC-QED) = 33 km; mb = 5.3, Ms = 5.4). Coherent traces have been time-shifted, aligned and sorted according to epicentral distance (D = 58.3° to BRG, 60.4° to GRA1 and 63.0° to WLF). Note the strong variation in P-wave signal amplitudes and clear depth phases pP arriving about 12 s after P.

Tab. 11.2 gives for the Mongolia earthquake shown in Fig. 11.15 the whole set of parameter readings made at the analysis center of the Central Seismological Observatory Gräfenberg (SZGRF) in Erlangen, Germany:

- first line: date, event identifier, analyst;
- second and following lines: station, onset time, onset character (e or i), phase name (P, S, etc.), direction of first particle motion (c or d), analyzed component, period [s], amplitude [nm], magnitude (mb or Ms), epicentral distance [°]; and
- last two lines: source parameters as determined by the SZGRF (origin time OT, epicentre, average values of mb and Ms, source depth and name of Flinn-Engdahl-region).

Generally, these parameters are stored in a database, used for data exchange and published in lists, bulletins and the Internet (see IS 11.2). The onset characters i (impulsive) should be used only if the time accuracy is better than a few tens of a second, otherwise the onset will be described as e (emergent). Also, when the signal-to-noise-ratio (SNR) of onsets is small and especially, when narrow-band filters are used, the first particle motion should not be given because it might be distorted or lost in the noise. Broadband records are better suited for polarity readings (see Fig. 4.10). Their polarities, however, should be reported as u (for "up" = compression) and r (for "rarefaction" = dilatation) so as to differentiate them from short-period polarity readings (c and d, respectively).

Tab. 11.2 Parameter readings at the SZGRF analysis center for the Mongolia earthquake shown in Fig. 11.15 from records of the GRSN.

```
                                          ev_id 980924007      KLI
        1998-09-24
          BRG    19:03:27.2   e  P       Z  T 1.2  A 135.5    mb 5.9 D 58.3
          ALIGN  19:03:27.2   e  P       Z  T 1.1  A 124.1    mb 5.8
          BSEG   19:03:28.2   e  P       Z  T 1.1  A 198.3    mb 6.0 D 58.4
          CLL    19:03:28.6   e  P       Z  T 0.9  A 98.9     mb 5.8 D 58.5
          GEC2   19:03:36.3   i  P     c Z  T 1.2  A 46.9     mb 5.4 D 59.6
          CLZ    19:03:36.6   e  P       Z  T 1.1  A 177.7    mb 6.0 D 59.6
          MOX    19:03:36.9   e  P       Z  T 1.2  A 122.4    mb 5.8 D 59.6
          WET    19:03:38.5   e  P       Z  T 1.2  A 107.2    mb 5.7 D 59.9
          BRG    19:03:39.3   e  pP      Z
          GRA1   19:03:42.6   i  P     c Z  T 1.1  A 286.5    mb 6.2 D 60.4
                                           b_slo 6.8 b_az   54
          BUG    19:03:48.5   e  P       Z  T 1.1  A 162.4    mb 5.8 D 61.4
          FUR    19:03:48.6   e  P       Z  T 1.1  A 174.3    mb 5.8 D 61.3
          TNS    19:03:49.9   e  P       Z  T 1.1  A 103.0    mb 6.0 D 61.5
          GSH    19:03:54.5   e  P       Z  T 1.3  A 132.3    mb 6.0 D 62.3
          GRA1   19:03:55.0   e  pP      Z
          BFO    19:03:57.4   e  P       Z  T 1.1  A 55.2     mb 5.6 D 62.8
          WLF    19:04:00.1   e  P       Z  T 1.7  A 80.3     mb 5.6 D 63.0
          GRA1   19:11:52.2   e  S       E                           D 60.4
          GEC2   19:30:36.0   e  L       Z  T 19.9 A 3895.8   MS 5.5
          GRA1   19:31:03.6   e  L       Z  T 20.6 A 3398.7   MS 5.5

        SZGRF  OT 18:53:39.3  45.30N  106.84E    mb_av 5.8 MS_av 5.5
        DEP   44km ▲ MONGOLIA
```

Note that for this event the international data center NEIC had "set" the source depth to 33 km because of the absence of reported depth phases. The depth-phase picks at the GRSN, however, with an average time difference of pP-P of about 12 s, give a focal depth of 44 km. Also note in Tab. 11.2 the large differences in amplitudes (A) determined from the records of individual stations. The resulting magnitudes mb vary between 5.4 (GEC2) and 6.2 (GRA1)!

11.2.5 Criteria to be used in event identification and discrimination

11.2.5.1 Discrimination between shallow and deep earthquakes

Earthquakes are often classified on depth as: shallow focus (depth between 0 and 70 km), intermediate focus (depth between 70 and 300 km) and deep focus (depth between 300 and 700 km). However, the term "deep-focus earthquakes" is also often applied to all sub-crustal earthquakes deeper than 70 km. They are generally located in slabs of the lithosphere which are subducted into the mantle. As noted above, the most obvious indication on a seismogram that a large earthquake has a deep focus is the small amplitude of the surface waves with respect to the body-wave amplitudes and the rather simple character of the P and S waveforms, which often have impulsive onsets (see Fig. 4.13). In contrast to shallow-focus earthquakes, S phases from deep earthquakes may sometimes be recognizable even in teleseismic short-period records. The body-wave/surface-wave ratio and the type of generated surface waves are also key criteria for discriminating between natural earthquakes, which mostly occur at depth larger than 5 km, and quarry blasts, underground explosions or rockbursts in mines, which occur at shallower depth (see 11.2.5.2).

A more precise determination of the depth h of a seismic source, however, requires either the availability of a seismic network with at least one station being very near to the source, e.g., at an epicentral distance D < h (because only in the near range the travel time t(D, h) of the direct P wave varies strongly with source depth h), or the identification of seismic *depth phases* on the seismic record. The most accurate method of determining the focal depth of an earthquake in routine seismogram analysis, particularly when only single station or network records at teleseismic distances are available, is to identify and read the onset times of depth phases. A depth phase is a characteristic phase of a wave reflected from the surface of the Earth at a point relatively near the hypocenter (see Fig. 2.43). At distant seismograph stations, the depth phases pP or sP follow the direct P wave by a time interval that changes only slowly with distance but rapidly with depth. The time difference between P and other primary seismic phases, however, such as PcP, PP, S, SS etc. changes much more with distance. When records of stations at different distances are available, the different travel-time behavior of primary and depth phases makes it easier to recognize and identify such phases. Because of the more or less fixed ratio between the velocities of P and S waves with $v_P/v_s \approx \sqrt{3}$, pP and sP follow P with a more or less fixed ratio of travel-time difference t(sP-P) ≈ 1.5 t(pP-P) (see Figs. 11.16 and 11.17). Animations of seismic ray propagation and phase recordings from deep earthquakes are given in files 3 and 5 of IS 11.3 and related CD-ROM.

The time difference between pP and sP and other direct or multiple reflected P waves such as pPP, sPP, pPKP, sPKP, pPdif, sPdif, etc. are all roughly the same. S waves also generate depth phases, e.g., sS, sSKS, sSP etc. The time difference sS-S is only slightly larger than sP-P (see Figs. 1.4 and 11.17). The difference grows with distance to a maximum of 1.2 times the sP-P time. These additional depth phases may also be well recorded and can be used in a similar way for depth determination as pP and sP.

Given the rough distance between the epicenter and the station, the hypocenter depth (h) can be estimated within $\Delta h \approx \pm 10$ km from travel-time curves or determined by using time-difference tables for depth-phases (e.g., from $\Delta t(pP-P)$ or $\Delta t(sP-P)$; see Kennett, 1991 or Table 1 in EX 11.2) or the "rule-of-thumb" in Eq. (11.4). An example is given in Fig. 11.18. It depicts broadband records of the GRSN from a deep earthquake (h = 119 km) in the

Volcano Islands, West Pacific. The distance range is 93° to 99°. The depth phases pP and pPP are marked. From the time difference pP-P of 31.5 s and an average distance of 96°, it follows from Table 1 in EX 11.2 that the source depth is 122 km. When using Eq. (11.4) instead, we get h = 120 km. This is very close to the source depth of h = 119 km determined by NEIC from data of the global network.

Note that on the records in Fig. 11.18 the depth phases pP and pPP have larger amplitudes than the primary P wave. This may be the case also for sP, sS etc., if the given source mechanism radiates more energy in the direction of the upgoing rays (p or s; see Fig. 2.43) than in the direction of the downgoing rays for the related primary phases P, PP or S. Also, in Fig. 11.18, pP, PP and pPP have also longer periods than P. Accordingly, they are more coherent throughout the network than the shorter P waves. Fig. 11.37 shows for the same earthquake the LP-filtered and rotated 3-component record at station RUE, Germany, with all identified major later arrivals being marked on the record traces. This figure is an example of the search for and comprehensive analysis of secondary phases.
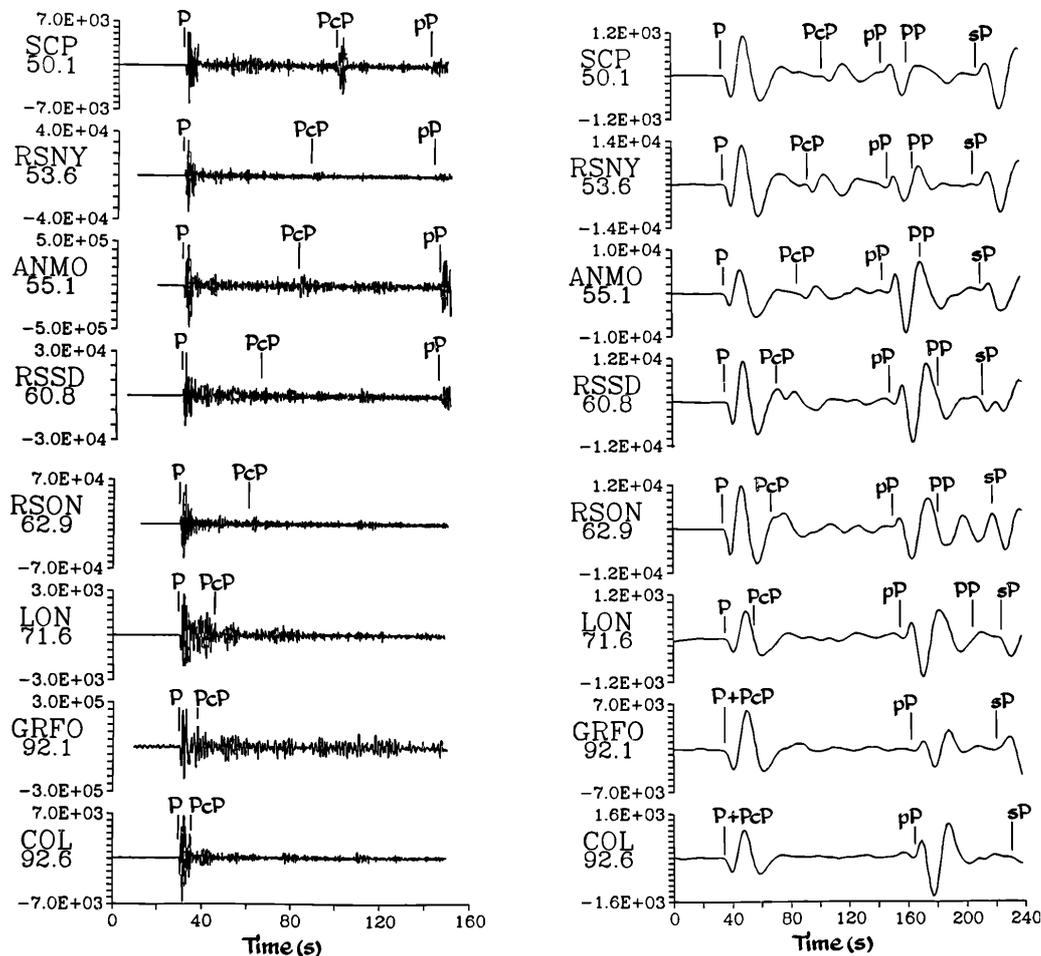
Fig. 11.16 Short-period (left) and long-period (right) seismograms from a deep-focus Peru-Brazil border region earthquake on May 1, 1986 (mb = 6.0, h = 600 km) recorded by stations in the distance range 50.1° to 92.2°. Note that the travel-time difference between P and its depth phases pP and sP, respectively, remains nearly unchanged. In contrast PcP comes closer to P with increasing distance and after merging with P at joint grazing incidence on the core-mantle boundary form the diffracted wave Pdif (reprinted from Anatomy of Seismograms, Kulhánek, Plate 41, p. 139-140; © 1990; with permission from Elsevier Science).
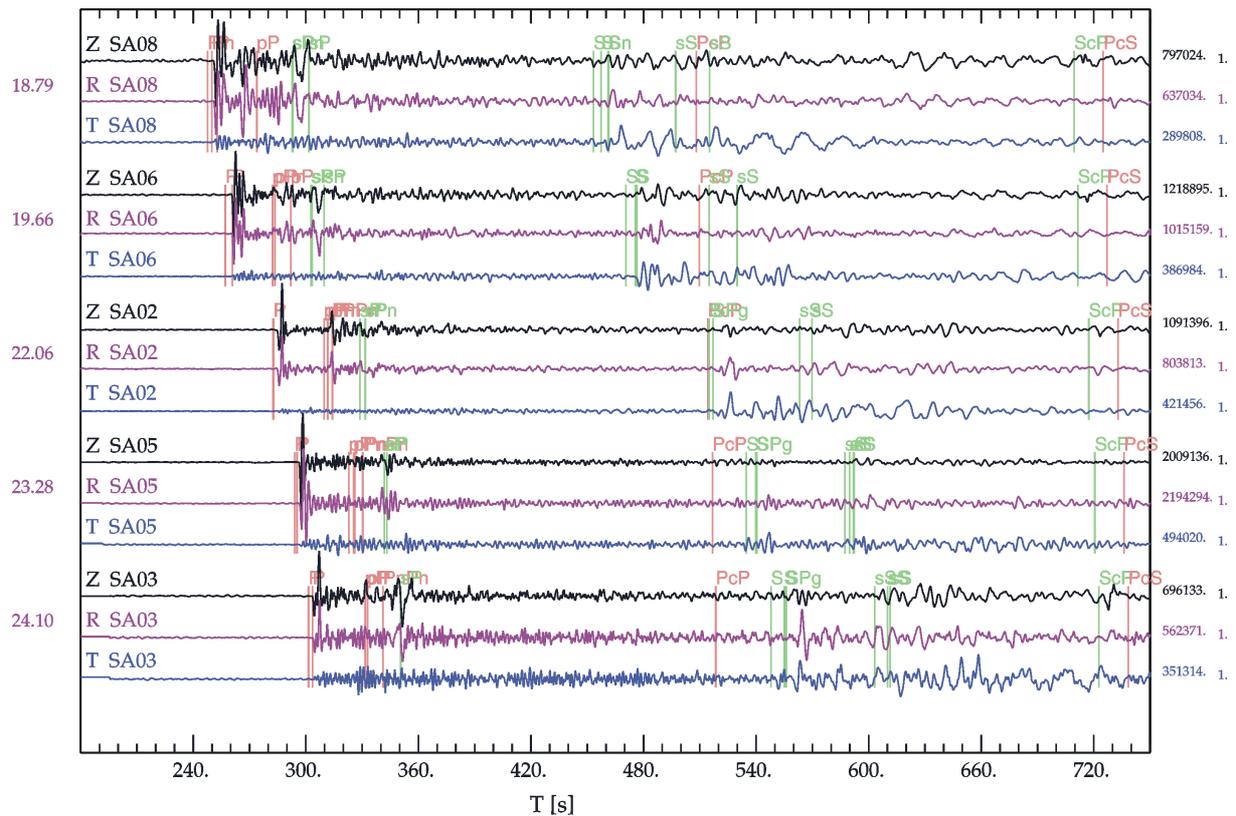
Fig. 11.17 3-component recordings in the distance range 18.8° to 24.1° from a regional network of portable BB instruments deployed in Queensland, Australia (seismometers CMG3ESP; unfiltered velocity response; see DS 5.1). The event occurred in the New Hebrides at 152 km depth. On each set of records the predicted phase arrival times for the AK135 model (see Fig. 2.53) are shown as faint lines. The depth phases pP, sP and sS are well developed but their waveforms are complex because several of the arrivals have almost the same travel time (courtesy of B. Kennett).

Crustal earthquakes usually have a source depth of less than 30 km, so the depth phases may follow their primary phases so closely that their waveforms overlap (see Fig. 11.19). Identification and onset-time picking of depth phases is then usually no longer possible by simple visual inspection of the record. Therefore, in the absence of depth phases reported by seismic stations, international data centers such as NEIC in its Monthly Listings of Preliminary (or Quick) Determination of Epicenters often fix the source depth of (presumed) crustal events at 0 km, 10 km or 33 km, as has been the case for the event shown in Fig. 11.15. This is often further specified by adding the capital letter N (for "normal depth" = 33 km) of G (for depth fixed by a geophysicist/analyst). Waveform modeling, however (see 2.8 and Figs. 2.57 to 2.59), may enable good depth estimates for shallow earthquakes to be obtained from the best fit of the observed waveforms to synthetic waveforms calculated for different source depth. Although this is not yet routine practice at individual stations, the NEIC has, since 1996, supplemented depth determinations from pP-P and sP-P by synthetic modeling of BB-seismograms. The depth determination is done simultaneously with the

determination of fault-plane solutions. This has reduced significantly the number of earthquakes in the PDE listings with arbitrarily assigned source depth 10G or 33N.
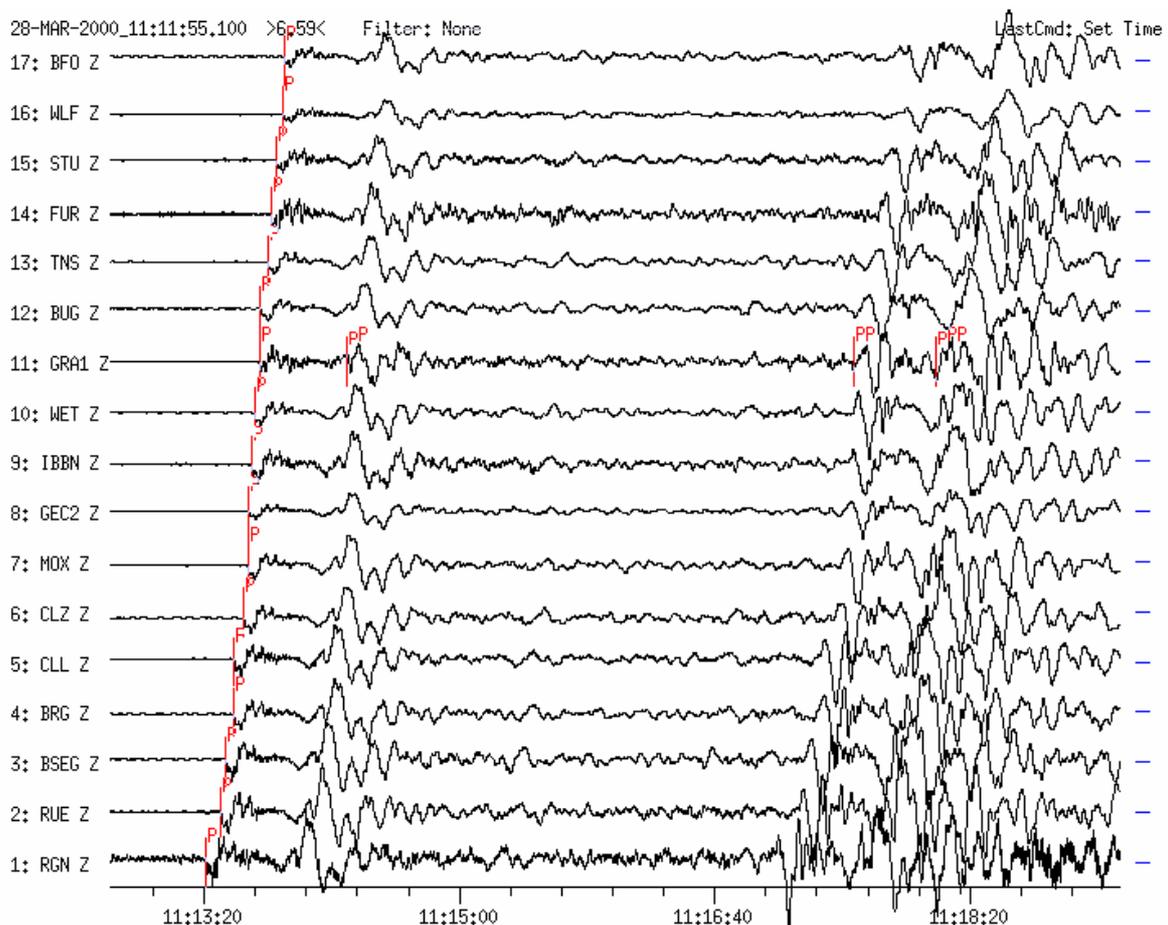
Fig. 11.18 Broadband vertical-component seismograms of a deep (h = 119 km) earthquake from Volcano Islands region recorded at 17 GRSN, GRF and GEOFON stations. (Source data by NEIC: 2000-03-28 OT 11:00:21.7 UT; 22.362°N, 143.680°E; depth 119 km; mb 6.8; D = 96.8° and BAZ = 43.5° from GRA1). Traces are sorted according to distance. Amplitudes of P are smaller than pP. Phases with longer periods PP, pP and pPP are much more coherent than P.

Note, however, that often there is no clear evidence of near-source surface reflections in seismic records, or they show apparent pP and sP but with times that are inconsistent from station to station. Douglas et al. (1974 and 1984) have looked into these complexities, particularly in short-period records. Some of these difficulties are avoided in BB and LP recordings. Also, for shallow sources, surface-wave spectra may give the best indication of depth but this method is not easy to apply routinely. In summary, observational seismologists should be aware that depth phases are vital for improving source locations and making progress in understanding earthquakes in relation to the rheological properties and stress conditions in the lithosphere and upper mantle. Therefore, they should do their utmost to recognize depth phases in seismograms despite the fact that they are not always present and that it may be difficult to identify them reliably.

More examples of different kinds of depth phases are given in Figs. 11.34 and 11.35d as well as in Figure 6b of DS 11.2 and Figures 1b, 2b, 5b and 7a +b in DS 11.3.

SK1: 1993.232.05.r7
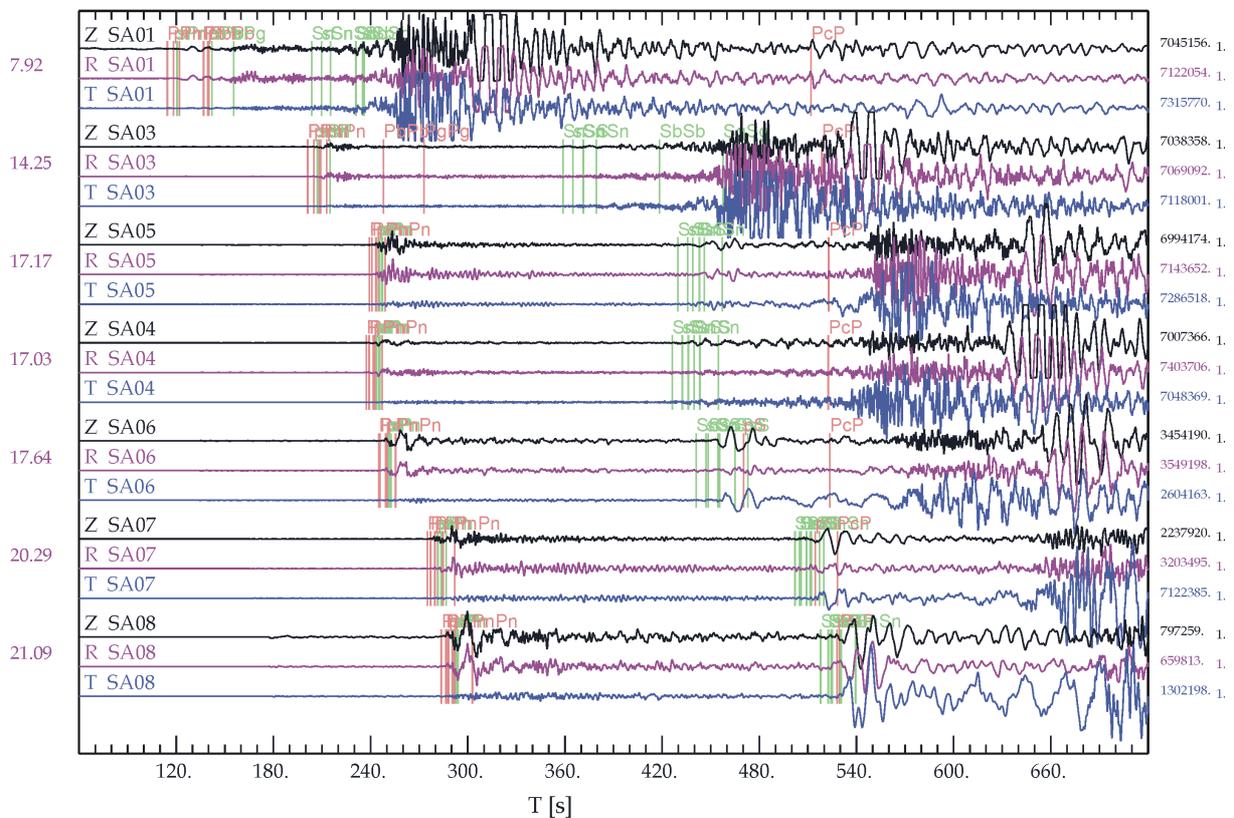
Fig. 11.19 3-component records in the distance range between 7.9° and 21.1° by a regional network of portable broadband instruments deployed in Queensland, Australia (seismometers CMG3ESP; unfiltered velocity response). The event occurred in Papua New Guinea at 15 km depth. As in Fig. 11.17 the predicted phase arrival times for the AK135 model are depicted. Primary, depth and other secondary arrivals (such as PnPn in the P-wave group and SbSb as well as SgSg in the S-wave group) superpose to complex wavelets. Also note that several of the theoretically expected phases have such weak energy that they can not be recognized on the records at the marked predicted arrival times above the noise level or the signal level of other phases (e.g., PcP at most stations) (courtesy of B. Kennett).

11.2.5.2 Discrimination between natural earthquakes and man-made seismic events

Quarry and mining blasts, besides dedicated explosion charges in controlled-sources seismology, may excite strong seismic waves. The largest of these events may have local magnitudes in the range 2 to 4 and may be recorded over distances of several hundred kilometers. Rock bursts or collapses of large open galleries in underground mines may also generate seismic waves (see Figure 3 in EX 11.1). The magnitude of these induced seismic events may range from around 2 to 5.5 and their waves may be recorded world-wide (as it was the case with the mining collapse shown in Fig. 11.8). In some countries with low to moderate natural seismicity but a lot of blasting and mining, anthropogenic (so-called "man-made" or "man-induced") events may form a major fraction of all recorded seismic sources,

3and may even outnumber recordings of earthquakes. Then a major seismological challenge is the reliable discrimination of different source types. Fig. 11. 39 shows a comparison of seismograms from: (a) a mining-induced earthquake; (b) a quarry blast; (c) a local earthquake; (d) a regional earthquake; and (e) a teleseismic earthquake. Seismograms (a) and (b) show that the high-frequency body-wave arrivals are followed, after Sg, by well developed lower-frequency and clearly dispersed Rayleigh surface waves (Rg; strong vertical components). This is not so for the two earthquake records (c) and (d) because sources more than a few kilometers deep do not generate short-period fundamental Rayleigh waves of Rg type. For even deeper (sub-crustal) earthquakes (e.g., Fig. 2.41) only the two high-frequency P- and S-wave phases are recorded within a few hundred kilometers from the epicenter.

Based on these systematic differences in frequency content and polarization, some observatories that record many quarry blasts and mining events, such as GRFO, have developed automatic discrimination filters to separate them routinely from tectonic earthquakes. Chernobay and Gabsatarova (1999) give references to many other algorithms for (semi-) automatic source classification. These authors tested the efficiency of the spectrogram and the Pg/Lg spectral ratio method for routine discrimination between regional earthquakes with magnitudes smaller than 4.5 and chemical (quarry) explosions of comparable magnitudes based on digital records obtained by a seismic network in the Northern Caucasus area of Russia. They showed that no single method can yet assure reliable discrimination between seismic signals from earthquakes and explosions in this region. However, by applying a self-training algorithm, based on hierarchical multi-parameter cluster analysis, almost 98% of the investigated events could be correctly classified and separated into 19 groups of different sources. However, local geology and topography as well as earthquake source mechanisms and applied explosion technologies may vary significantly from region to region (see page 18 of this Chapter). Therefore, there exists no straightforward and globally applicable set of criteria for reliable discrimination between man-made and natural earthquakes.

In this context one should also discuss the discrimination between natural earthquakes (EQ) and underground nuclear explosions (UNE). The Comprehensive Nuclear-Test-Ban Treaty (CTBT) has been negotiated for decades as a matter of high political priority. A Preparatory Commission for the CTBT Organization (CTBTO) has been established with its headquarters in Vienna (http://www.ctbto.org) which is operating an International Monitoring System (IMS; see http://www.nemre.nn.doe.gov/nemre/introduction/ims_descript.html, Fig. 8.12 and Barrientos et al., 2001). In the framework of the CTBTO, initially a Prototype International Data Centre (PIDC; http://www.pidc.org/) was established in Arlington, USA, which is replaced since 2001 by the International Data Centre in Vienna. Agreement was reached only after many years of demonstrating the potential of seismic methods to discriminate underground explosions from earthquakes, down to rather small magnitudes mb ≈ 3.5 to 4. Thus, by complementing seismic event detection and monitoring with hydroacoustic, infrasound and radionuclide measurements it is now highly probable that test ban violations can be detected and verified.

The source process of UNEs is simpler and much shorter than for earthquake shear ruptures (see Figs. 3.3 – 3.5 and related discussions). Accordingly, P waves from explosions have higher predominant frequencies and are more like impulses than earthquakes and have compressional first motions in all directions. Also, UNEs generate lower amplitude S and surface waves than earthquakes of the same body-wave magnitude (see Fig. 11.20).
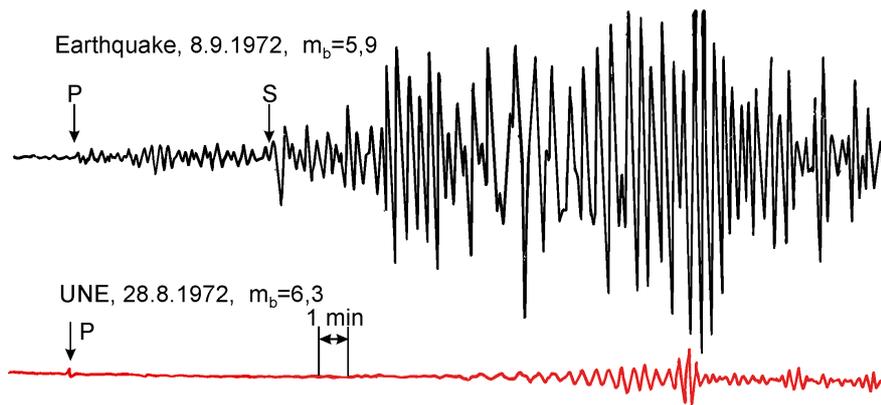
Fig. 11.20 Broadband displacement records of an earthquake and an underground nuclear explosion (UNE) of comparable magnitude and at nearly the same distance (about 40°).
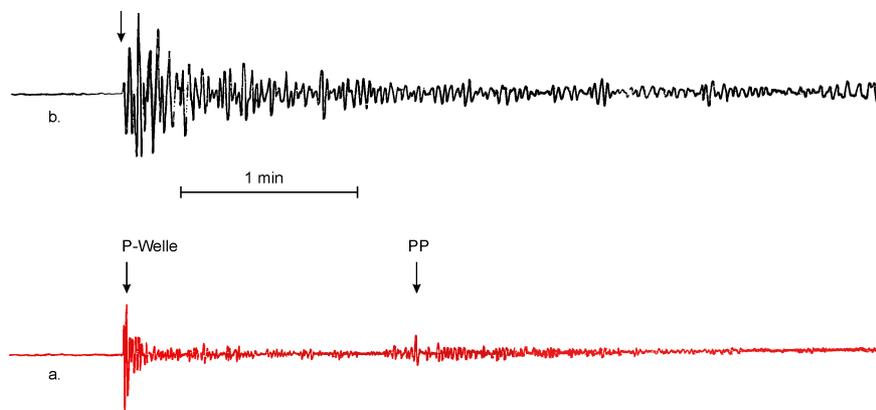

Fig. 11.21 Short-period records at station MOX a) of an underground nuclear explosion at the Semipalatinsk (SPT) test site in Kazakhstan (D = 41°) and b) of an earthquake with comparable magnitude and at similar distance.

In short-period records of higher time resolution the difference in frequency content, complexity and duration of the P-wave group between underground nuclear explosions and earthquakes is often clear. Fig. 11.21 gives an example. As early as 1971 Weichert developed an advanced short-period spectral criterion for discriminating between earthquakes and explosions and Bormann (1972c) combined in a single complexity factor K differences in frequency content, signal complexity and duration to a powerful heuristic discriminant.

Another powerful discriminant is the ratio between short-period P-wave magnitude mb and long-period surface-wave magnitude Ms. The former samples energy around 1 Hz while the latter samples long-period energy around 0.05 Hz. Accordingly, much smaller Ms/mb ratios are observed for explosions than for earthquakes (see Fig. 11.20). Whereas for a global sample of EQs and UNEs the two population overlap in an Ms/mb diagram, the separation is good when earthquakes and explosions in the same region are considered (Bormann, 1972c). Early studies have shown that with data of mb ≥ 5 from only one teleseismic station 100% of the observed UNEs with magnitudes from the SPT test site could be separated from 95% of the EQs in Middle Asia, whereas for the more distant test site in Nevada (D = 81°) 95% of the UNEs could be discriminated from 90% of the EQs in the Western USA and Middle America (see Fig. 11.22).
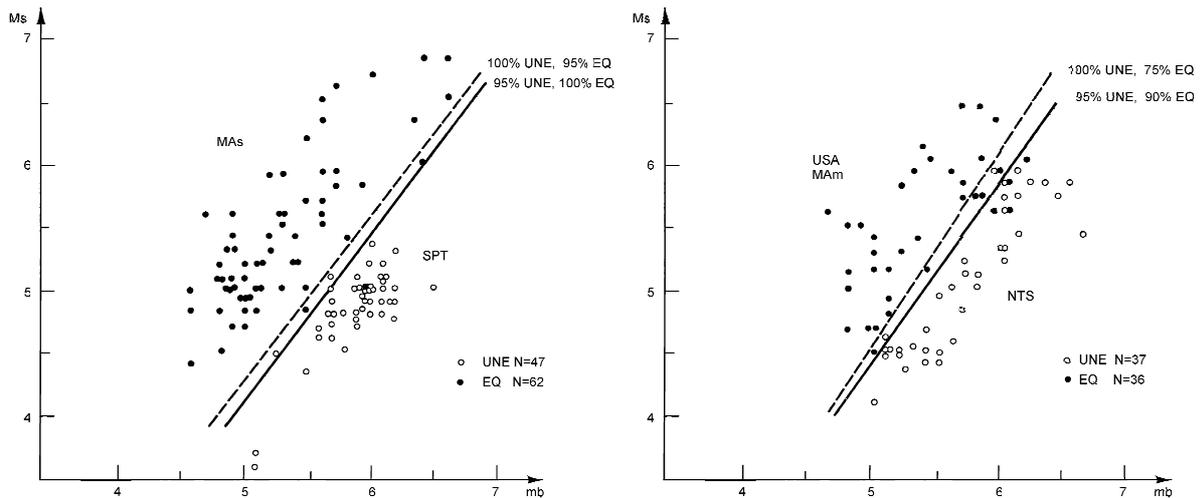
Fig. 11.22 Separation of EQs and UNEs by the Ms/mb criterion according to data collected at station MOX, Germany. Left: for Middle Asia and the test site in Semipalatinsk (SPT), right: for USA/Middle America and the Nevada test site (NTS).

Other potential discrimination criteria, such as the different azimuthal distribution of P-wave first-motion polarities expected from UNEs (always +) and EQs (mixed + and -), have not proved to be reliable. One reason is, that due to the narrowband filtering, which is applied to reach the lowest possible detection threshold, the P waveform, and particularly the first half cycle, is often so much distorted, that the real first-motion polarity is no longer recognizable in the presence of noise (see Fig. 4.10). Detailed investigations also revealed that simplified initial model assumptions about the difference between explosion and earthquake sources do not hold true. Surprisingly, the explosion source is poorly understood and source dimensions around magnitude mb seem to be the same for earthquakes and explosions. Also, many explosions do not approximate to a point-like expansion source in a half-space: significant Love waves are generated (e.g., by Novaya Zemlya tests) and many P seismograms show arrivals that can not be explained (see, e.g., Douglas and Rivers, 1988). Further, it has become clear that much of the differences observed between records of UNEs and EQs are not due to source differences but rather to differences in the geology, topography and seismotectonics of the wider area around the test sites, and that this necessitates the calibration of individual regions (e.g., Douglas et al., 1974).

In summary, one can say that the key criteria to separate EQs and explosions usually work well for large events, however, difficulties come with trying to identify every EQ down to magnitudes around mb = 4 with about 8000 earthquakes of this size per year. It is beyond the scope of this section to go into more detail on this issue. Rather, the Editor has invited experts from the CTBTO community to write for Volume 2 of the Manual a complementary information sheet on advanced event detection and discrimination routines. This still forthcoming information sheet will catalog the most important criteria, which have been developed so far for discrimination and show more examples about their application to and efficiency in different regions.

11.2.6 Quick event identification and location by means of single-station three-component recordings

11.2.6.1 What is the best way of analyzing three-component seismograms?

Increasingly seismograms are being analyzed at laboratories that receive the data in (near) real time from networks or arrays of seismometers (see Chapters 8 and 9). The seismograms can then be analyzed jointly. Nevertheless, there remain many single, autonomous stations operating around the world, in countries of the former Soviet Union and developing countries in particular. Some of these single stations still record only with analog techniques. Yet much can be done even under these "old-fashioned" conditions by the station personnel, provided that at least some form of 3-component recording, either BB or both SP and LP, is available. With such recordings it will be possible to assess quickly the source type, estimate its rough location and magnitude, and identify in some detail later seismic phases, without waiting for rapid epicenter determinations by international data centers before record analysis can begin. Rather, there would be advantages if, in future, readings of secondary phases, particularly depth phases, were reported as early as possible to regional and global data centers. Such readings are indispensable for more accurate hypocenter location (see Figure 7 in IS 11.1). Only recently both NEIC and the ISC began considering the introduction of more flexible and sophisticated algorithms that can best make use of secondary phase readings for more reliable (and rapid) hypocenter locations.

It has also been realized that accurate epicentral distances estimated from three-component broadband readings of secondary phases can significantly improve location estimates by array stations based purely on measurements of the P-wave vector slowness (originally by using solely vertical-component SP sensors). Now, since modern software for digital seismogram analysis has made it much simpler and faster than in the "analog past" to evaluate three-component broadband data, we focus on such data here. Other procedures of modern multi-station (but usually single-component) data analysis are dealt with later *en passant*. Array analysis is discussed in detail in Chapter 9.

How then to proceed best in analyzing analog presentations of seismograms? The most important rules, taking the discussion under 11.2.4 and 11.2.5 into account, are:

Take interest!	**Be curious!**	**Ask questions!**
	to your seismic record	

1. Are you **NEAR** (D < 20°) **or TELESEISMIC** (D > 20°)?

Criteria:

• **Frequencies**	on SP records $f \geq 1$ Hz	$f \leq 1$ Hz
• **Amplitudes**	on LP records **not or weaker**	**large, also for later phases**
• **Record duration**	**< 20 min**	**> 20 min**
	(for magnitudes < 5; may be longer for strong earthquakes; see Fig. 1.2)	

2. Is your **D < 100°** **or** **D > 100° ?**

Criteria:

• **Surface wave max.**	after P arrival **< 45 ± 5 min** or	**> 45 ± 5 min** (Table 5 in DS 3.1)
• **Record duration**	on LP records **< 1.5 hours** or	**> 1.5 hours**
	(may be larger for very strong earthquakes; see Fig. 1.2)	

3.   Are you   **SHALLOW   or   DEEP** (> 70 km)?
Criteria:
• **Surface waves**   on LP records **strong**   **weak or none**
• **Depth phases**   usually   **not clear**   **well separated and often clear**
• **Waveforms**   usually   **more complex**   **more impulsive**

4. Is the first strong horizontal arrival   **S   or   SKS ?**
Criteria:
• **Time difference to P**   **< 10 ± 0.5 min**   **≈ 10 ± 0.5 min**
• **Polarization**   large horiz. A **in R and/or T**   **in R only**
Warning ! If the first strong horizontal arrival follows P after ≈ 10 ± 0.5 min it may be SKS. Check polarization! (see Fig. 11.14). Misinterpreting SKS as S may yield D estimates up to 20° too short. Look also for later multiple S arrivals (SP, SS, SSS) with better D control.

5.   What are the first longitudinal and transverse onsets for D > 100° ?
Beyond 100° epicentral distance first arrivals may still be P, which may be seen particularly in LP records of large earthquakes up to about almost 150° (see Fig. 11.63). This P, however, has been diffracted around the core-mantle boundary and is termed Pdif (old Pdiff; see Figs. 11.59 and 11.63). First onsets in SP records are usually PKiKP and PKPdf (see Fig. 11.59), or, somewhat later PP, which is often the first strong longitudinal Z-component arrival in both SP, LP and BB records (see Figs. 11.60 and 11.63). The first strong arrivals on horizontal (R) components are PKS or SKS. Misinterpretation of the first P-wave and S-wave arrivals as direct P and S, respectively, may result in epicentral distance estimates up to more than 70° too short! This can be avoided by taking the criteria under **2.** into account. Also note, that the travel-time difference between PKPdf and PKS or SKS is (almost) independent of distance. The first arriving P and S waves do not then allow distance to be estimated. Therefore look for later arriving multiple reflected S waves such as SS, SSS, etc., which are usually well developed in this distance range on horizontal LP records and so allow D to to be estimated with an error of usually < 2°.

Additionally, one might look for criteria discussed in sub-section 11.2.5.2 for discriminating between explosions and earthquakes.

If only very broadband digital records are available, which are usually proportional to ground velocity, it is best to filter them to produce standard analog WWSSN-SP and -LP seismograms before starting a reconnaissance analysis. One may also simulate Kirnos SKD BB-displacement and Wood-Anderson (WA) SP-displacement seismograms (for response characteristics see Fig. 3.11), because all these responses are required for proper magnitude estimation according to established standards. Only after these seismograms have been produced should one begin with the detailed analysis. The analysis might include phase identification, picking of onset times, amplitudes and periods, and the application, if required, of special filters, such as the ones for inverse Hilbert transformation of phases, which have been distorted by traveling through internal caustics (see 2.5.4.3), or for separating phases on their polarization to improve phase discrimination.

Of course, in countries with many seismic sources recorded every day it will not be possible, particularly for untrained interpreters, to apply all these criteria to every seismic signal. On the other hand, this kind of checking takes only a few seconds, minutes at most, for an experienced interpreter who has already trained himself/herself in recognizing immediately

the different record patterns on seismograms from systems with standard responses. In addition, many data centers specialize in analyzing only seismograms from local, regional or teleseismic sources. Accordingly, either the number of questions to be asked to the record or the number of signals to be analyzed will be reduced significantly. Also, the task might be significantly eased at observatories or analysis centers which have advanced routines available for digital seismogram analysis such as SEISAN or Seismic Handler. Provided that first hypocenter estimates are already available from international data centers or from analysis of array or network recordings, these computer programs allow the theoretical onset times of expected seismic phases to be displayed on the seismogram. However, these theoretical times should not be followed blindly but considered only as assistance. The additional information on amplitudes, frequency content, and polarization has to be taken into account before giving a name to a recognizable onset! (see 11.2.4 and 11.2.5).

On the other hand, it is meaningless to list more detailed and strict criteria and rules about the appearance and identification of seismic phases in different distance ranges, because they vary from event to event and from source region to source region. They also depend on the specific conditions of the given propagation paths and the local environment at the receiving station. Therefore, every station operator or network analyst has to develop, through experience and systematic data analysis, his/her own criteria for improved seismogram analysis, source identification, and location. In any event, however, the general approach to record analysis given above should be followed to avoid the analysis becoming thoughtless, boring and routine, which will inevitably result in the reporting of inhomogeneous and incomplete low-quality data of little value for research or to the general user.

11.2.6.2 Hypocenter location

If well calibrated 3-component broadband and/or long-period recordings are available then it is possible to locate sufficiently strong local events (Ml > 3) and teleseismic sources (mb > 5) with an accuracy comparable to or even better than those for un-calibrated arrays or station networks. This was demonstrated more than 30 years ago (Bormann, 1971a and b) by using standard film records of type A, B and C (responses see Fig. 3.11). Amplitudes and onset times were at that time still measured by using an ordinary ruler or a sub-millimeter scaled magnification lens. Nevertheless, the mean square error of epicenters thus located within the distance range 20° < D < 145° was less than 300 km when compared with the epicenter coordinates published by the seismological World Data Centers A and B. Fig. 11.23 shows the statistical distribution of errors in azimuth and distance based on several hundred 3-component event locations.

Note that the errors in distance estimated from readings of P and later secondary phases within the distance range 80° < D < 120° are mostly less than about ±1° and rarely greater than ±2° . The mean errors seldom differ significantly from zero, and where they do it is usually for specific regions (distance/azimuth ranges). Taking such systematic errors into account, the location accuracy can be improved. Many seismic arrays and networks now use routinely multi-phase epicentral distance determinations for improving their slowness-based source locations. Some advanced software for seismogram analysis like SHM (see 11.4.1) includes this complementary interactive analysis feature.

Backazimuth derived from SP 3-component recordings may have large systematic errors up to several tens of degrees. This is not so if LP or BB records are used. Whereas individual

determinations of backazimuth from SP records might deviate up to about 40° from the true source azimuth, the errors are rarely (except at low SNR) larger than 10° when BAZ is determined from BB records (provided that the magnification of the horizontal components is known with high accuracy or identical!). The reason for this is obvious from Fig. 2.6 and the related discussion. The particle motion in SP records is complicated and random due to wave scattering and diffraction by small-scale heterogeneities in the crust and by rough surface topography at or near the station site (see Buchbinder and Haddon, 1990). In contrast, LP or BB records, which are dominated by longer wavelength signals, usually show simpler P waveforms with clearer first-motion polarity than do SP records. In addition, later phase arrivals, which are crucial for accurate distance determination from single station records, stand out more clearly or are recognizable only in BB or LP records (see Fig. 11.24).
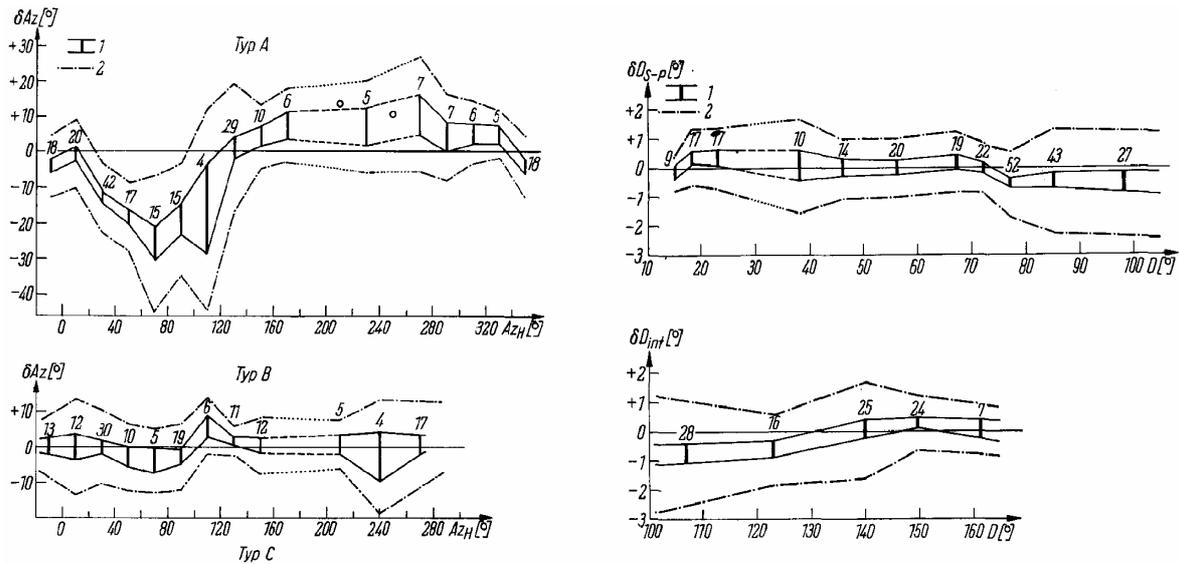
Fig. 11.23 Left: Errors in backazimuth Az (or BAZ) at station MOX estimated using 3-component records of type A (SP) and of type C (Kirnos SKD BB-displacement). Right: Errors in estimating the epicentral distance D at station MOX from records of type C using travel-time difference S-P in the distance range 10° < D < 100° or travel-time differences between other seismic phases for D > 100°. The solid lines give the 90% confidence interval for the mean error with number of the observations; the dash-dot lines are the 90% confidence interval for a single observation.

Simple 3-component event locations based solely on readings of onset times of identified phases, polarity of P-wave first motions and horizontal component amplitude ratio should proceed as follows:

- general event classification (near/far; shallow/deep; D < 100°/> 100° etc.);
- picking and identifying the most pronounced phases by comparing the 3-component record traces and related polarization characteristics (Fig. 11.24);
- determination of D by a) matching the identified body-wave phases with either overlays of differential travel-time curves of equal time scale (see Figures 2 to 4 in EX 11.2), b) by measuring their onset-time differences and comparing them with respective distance-dependent differential travel-time tables or c) by computer calculation of D based on digital time picks for identified phases and local, regional and/or global travel-time models integrated into the analysis program;

- determination of source depth h on the basis of identified depth phases (see 11.2.5.1) and following correction of D, again by using either travel-time curves, differential t-D tables or computer assisted time-picks and comparison with travel-time models;

- determination of the backazimuth (against North) from the station to the source from the first-motion directions in the original Z, N and E component records and from the amplitude ratio A_E/A_N. For details see Figure 1 and explanations given in EX 11.2;

- determination of the epicenter location and coordinates by using appropriate map projections with isolines of equal azimuth and distance from the station (see Figure 5 in EX 11.2) or by means of suitable computer map projections.
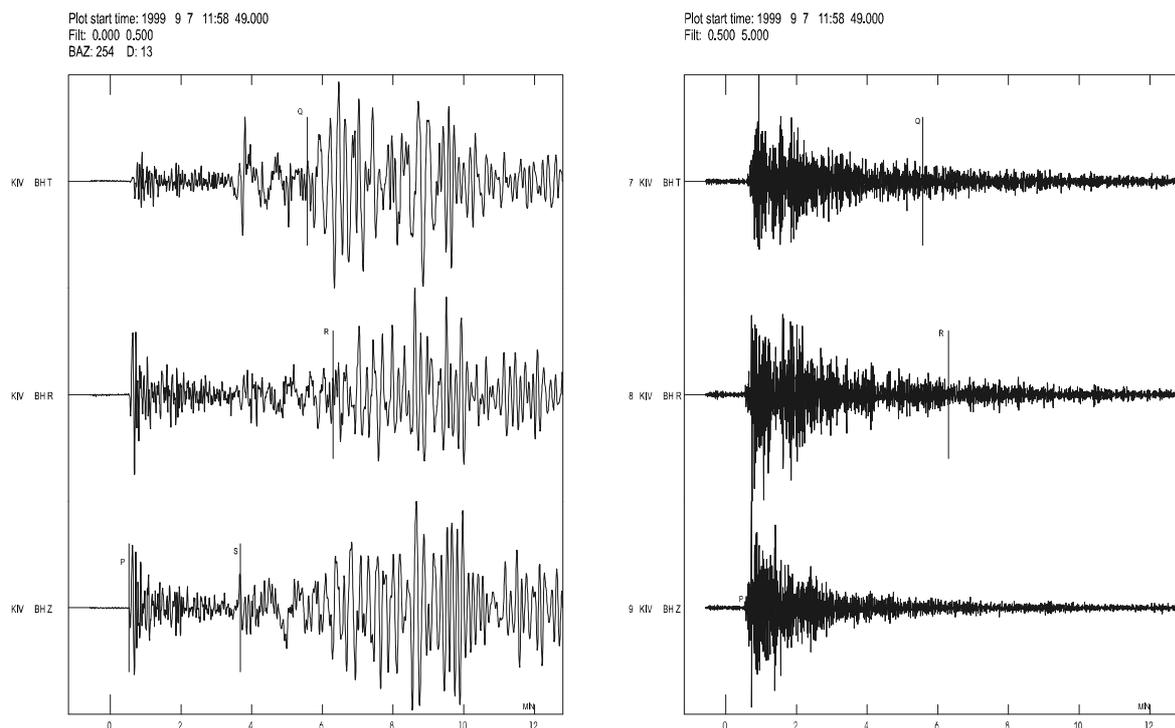
Fig. 11.24 Left: Low-pass filtered digital broadband record of the Global Seismograph Network (GSN) station KIV from the shallow (h = 10 km) Greece earthquake of 07 Sept. 1999 (mb = 5.8) at a distance of D = 13°. Note the clearly recognizable polarity of the first P-wave half-cycle! The record components have been rotated into the directions Z, R and T after determination of the backazimuth from first-motion polarities in Z, N and E (BAZ = 134°). Accordingly, P and Rayleigh waves are strongest in Z and R while S and Love wave are strongest in T. **Right:** The recordings after SP bandpass filtering (0.5-5.0 Hz). The SNR for the P-wave first-motion amplitude is much smaller and their polarity less clear. Also later arrivals required for distance determination are no longer recognizable (signal processing done with SEISAN; courtesy of L. Ottemöller).

Rough estimates of D may be made - in the absence of travel-time tables or curves or related computer programs – using the following "rules-of- thumb":

hypocenter distance   d [in km] $\approx \Delta$t(Sg-Pg) [in s] $\times$ 8 (near range only)   (11.1)

epicentral distance   D [in km] $\approx \Delta t$(Sn-Pn) [in s] $\times$ 10 (in Pn-Sn range < 15°)   (11.2)

epicentral distance   D [in °] $\approx \{\Delta t$(S-P) [in min] - 2$\} \times$ 10 (for 20°< D <100°)   (11.3)

In the absence of travel-time curves or tables for depth phases one may use another "rule-of-thumb" for a rough estimate of source depth from the travel-time difference Δt(pP-P):

source depth   h [in km] $\approx = \Delta t$(pP-P)/2 [in s] $\times$ 7 (for h < 100 km)   (11.4)
                          or $\times$ 8 (for 100 km < h < 300 km)
                          or $\times$ 9 (for h > 300 km)

Bormann (1971a) showed that in the absence of a sufficiently strong P-wave arrival, the backazimuth can be determined from horizontal components of any later seismic phase which is polarized in the vertical propagation plane, such as PP, PS, PKP or SKS. These phases are often much stronger in BB or LP records than P. However, because of phase shifts on internal caustics (PP, PS, SP, PKPab) for most of these phases the 180° ambiguity in azimuth determined from the ratio A_E/A_N can not be resolved as it can for P by taking into account the first-motion polarity in the Z component. However, by considering the inhomogeneous global distribution of earthquake belts, this problem can usually be solved.

Modern computer programs for seismogram analysis include subroutines that allow quick determination of both azimuth and incidence angle from particle motion analysis over the whole waveform of P or other appropriate phases. This is done by determining the direction of the principal components of the particle motion, using, as a measure of reliability of the calculated azimuth and incidence angle, the degree of particle motion linearity/ellipticity. Such algorithms are available in the SEIS89 software (Baumbach, 1999). Christoffersson et al. (1988) describe a maximum-likelihood estimator for analyzing the covariance matrix for a single three-component seismogram (see also Roberts and Christoffersson, 1990). The procedure allows joint estimation of the azimuth of approach, and for P and SV waves the apparent angle of incidence and, hence, information on apparent surface velocity and thus on epicentral distance. This was been implemented in the SEISAN software (Havskov and Ottemöller, 1999). Fig. 11.25 shows an example of the application of the software to a portion of the BB recording at Kongsberg (KONO) in Norway for the 12 November 1999, Turkey earthquake (Mw = 7.1). The program finds a high correlation (0.9) between the particle motions in the three components, gives the estimate of the backazimuth as 134°, an apparent velocity of 9.6 km/s and the corresponding location of this earthquake at 40.54°N and 30.86° E. This was only about 50 km off the true epicenter.

Applying similar algorithms to digital 3-component data from short-period P waves recorded at regional distances, Walck and Chael (1991) show that more than 75% of the records yielded backazimuth within 20° of the correct values. They found, however, a strong dependence on the geological structure. Whereas stations located on Precambrian terranes produced accurate backazimuth for SNR > 5 dB, stations on sedimentary rocks with complicated structure had much larger errors. Excluding these stations, the RMS backazimuth error is only about 6° for recordings with SNR > 10 dB.

Ruud et al. (1988) found that three-component locations for epicenters at distances up to about 1000 km seldom deviated more than 50 km from network solutions, such deviations being mainly due to errors in azimuth estimates. For short-period teleseismic P waves, however, location errors occasionally exceeded 800 km, mainly because of poor distance

estimates derived from incidence angles (slowness) alone. For stronger sources, where BB records can be used, distance can be determined using travel-time differences. The location errors are then reduced to about 1°. Thus, three-component digital broadband data allow reliable epicenters to be determined quickly with just single station records, and even data from stations that still use analog recording may provide rapid and reliable epicenter estimates. For combined single station and network location see Cassidy et al. (1990).
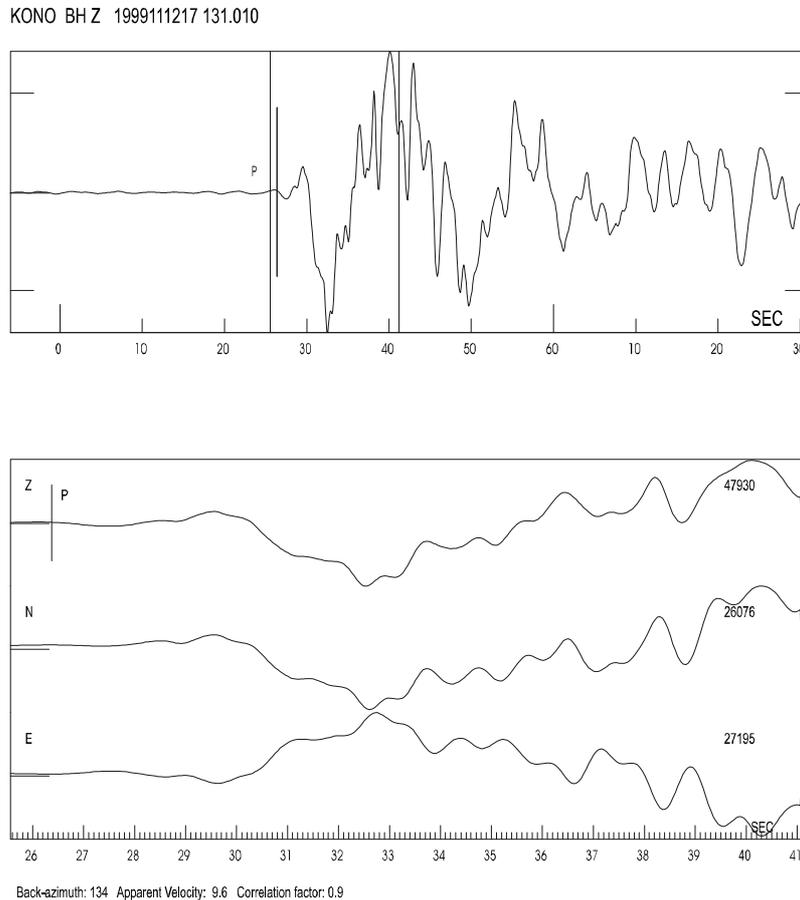
Fig. 11.25 Example of azimuth determination and epicenter location of the 12 Nov. 1999 Turkey earthquake by correlation analysis of three-component digital BB records at station KONO, Norway. Backazimuth, apparent velocity, and correlation factor are determined from the P-wave record section marked in the upper figure. For more details see text (signal processing done with SEISAN; courtesy of L. Ottemöller).

11.2.7 Magnitude determination

When epicentral distance and depth of a seismic source are (at least roughly) known the magnitude of the event can be estimated. The general procedures to be followed in magnitude determination (and the measurement of amplitudes, periods or record duration) as well as the specifics of different magnitude scales to be used for local, regional or teleseismic recordings are dealt with in detail in section 3.2. DS 3.1 gives the magnitude calibration functions, both for the teleseismic standard magnitudes (mb and Ms) and several other magnitude scales for local, regional and teleseismic magnitudes. The various procedures can be learnt from an exercise given in EX 3.1, which also gives solutions for the different tasks.

11.2.8 Hypocenter location by means of network and array recordings

Hypocenter location is simplified if records from at least 3 stations are available. The more uniformly the stations are distributed around the source in azimuth and distance (with distances ranging from close-in to long range) and the more seismic phases are used for location, the lower the uncertainty in the estimates. The procedures in both manual and computer assisted multi-station hypocenter location are outlined in IS 11.1, which gives the underlying algorithms and error calculations, as well as standard and advanced methods for both absolute and relative location. Also discussed is the influence of deviations from the assumed Earth models on the locations. The improvements in hypocenter relocation achievable with better Earth models are also demonstrated.

EX 11.1 aims at epicenter location by a simple circle and chord method using seismograms from local stations both inside and outside the network. The epicentral distances have to be determined first for each station by identifying on its records the phases Pg, Sg, Pn and/or Sn and matching them to a local travel-time curve.

With digital multi-station data and advanced seismogram analysis software, source location becomes almost a trivial task. One just picks a sufficient number of first arrival times (see Fig. 11.5), activates the relevant location program for local, regional and/or teleseismic sources and gets the result, including a map showing the epicenter if required, in an instant. The accuracy of location, particularly source depth, can be significantly improved by picking not only P-wave first arrivals but later arrivals too, which give a much better distance and depth control than slowness data alone. Examples for both local and teleseismic event locations based on seismic network and array data are given in the following sections. Location using array data is described in Chapter 9, together with the underlying theory.

11.3   Routine signal processing of digital seismograms

Standard analysis includes all data pre-processing and processing operations for the interpretation and inversion of broadband seismograms. Important time-domain processes are signal detection, signal filtering, restitution and simulation, phase picking, polarization analysis as well as beamforming and vespagram analysis for arrays. In the frequency domain the main procedures are frequency-wavenumber (f-k) and spectral analysis. Array-techniques as f-k and vespagram analysis, slowness and azimuth determination for plane waves, and beamforming are discussed in detail in Chapter 9 but a few examples are also shown below. Spectral analysis can be used for the estimation of the frequency content of a seismic wave, and of seismic noise (see 4.1 and 7.2, respectively).

11.3.1 Signal detection

The first task of routine data analysis is the detection of a seismic signal. A signal is distinguishable from the seismic background noise either on the basis of its larger amplitudes or its differences in shape and frequency. Various methods are used for signal detection. Threshold detectors and frequency-wavenumber analysis are applied to the continuous stream of data. In practice, the threshold is not constant but varies with the season and the time of the day. For this reason, the threshold detectors determine the average signal power in two

moving time windows: one long term (LTA) and one short term (STA). The ratio of the STA to LTA corresponds to the signal-to-noise-ratio (SNR). For details on the STA/LTA trigger and its optimal parameter setting see IS 8.1.

In practice, BB records are filtered before detectors are used. Useful filters are Butterworth high-pass filters with corner frequencies $f_c > 0.5$ Hz or standard band-pass types with center frequency $f = 1$ Hz for teleseismic P waves and high-pass filter with $f_c > 1$ Hz for local sources. Fig. 11.26 demonstrates detection and onset-time measurement for a weak, short-period P wave. In the lowermost 30 s segment of a BB-velocity seismogram the oceanic microseisms dominate in the period band 4-7 s. The two other traces are short-period seismograms after narrow band-pass (BP) filtering with: (1) a filter to simulate a WWSSN-SP seismogram; and (2) a two step Butterworth BP filter of 2nd-order with cut-off frequencies of 0.7 and 2 Hz, respectively. The latter filter produces, for the noise conditions at the GRF-array, the best SNR for teleseismic signals. Seismic networks designed to detect mainly local seismic events may require other filter parameters that take account of local noise conditions, for optimal detection (see IS 8.1).

Generally, a seismic signal is declared when the SNR exceeds a pre-set threshold. Various procedures, some analytical and some based on personal experience, are used to differentiate between natural earthquakes, mining-induced earthquakes and different kinds of explosions. Usually, the detected signals are analyzed for routine parameter extraction and data exchange.
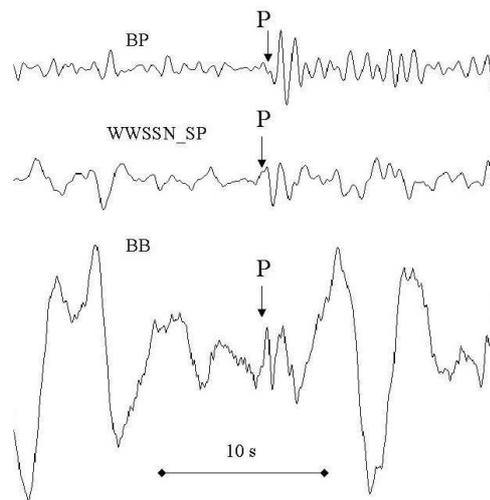
Fig 11.26 Bandwidth and SNR: A small short-period P-wave arrival which is within the noise level on a BB-velocity record (lower trace) may be detected by using a WWSSN-SP simulation filter (middle trace) or a Butterworth band-pass filter (BP; uppermost trace). The SNR is 0.2 on the original BB record, about 1 on the WWSSN-SP filter and about 2 on the BP-filtered trace. The seismogram is of an earthquake in the Kurile Islands on 25 March 2002, 6:18:13 UT, recorded at station GRA1, Germany.

11.3.2 Signal filtering, restitution and simulation

Classical broadband seismographs, such as the Russian Kirnos SKD, record ground displacement with constant magnification over a bandwidth of 2.5 decades or about 8 octaves. The IDA-system (International Deployment of Accelerometers) deployed in the 1970s, used originally LaCoste-Romberg gravimeters for recording long-period waves from strong earthquakes proportional to ground acceleration over the band from DC to about 0.1 Hz

(nowadays replaced by STS1). Modern strong-motion sensors such as the Kinemetrics Inc. Episensor ES-T have a flat response to ground acceleration in an even broader frequency band from DC to 200 Hz. In contrast, feedback-controlled BB sensors for recording weak-motion usually have a response proportional to the ground velocity (see Fig. 11.27 right). Such BB recordings, however, are often not suitable for direct visual record analysis and parameter extraction in the time domain. Low-frequency signals and surface waves of weak earthquakes are not or only poorly seen. Therefore, BB data must be transformed by applying digital filters in a way that yields optimal seismograms for specific investigations and analysis.

For some research tasks and ordinary routine analysis of BB seismograms the application of high-pass, low-pass and band-pass filters is usually sufficient. However, simultaneous multi-channel data processing or the determination of source parameters according to internationally agreed standards (such as body- and surface-wave magnitudes, which are defined on the basis of former analog band-limited recordings) often require simulation of a specific response, including those of classical analog seismograph systems (Seidl, 1980). Another special problem of simulation is "restitution". Restitution is the realization of a seismograph system whose transfer function is directly proportional to ground displacement, velocity or acceleration in the broadest possible frequency range. The restitution of the true ground displacement down to (near) zero frequencies is a precondition for seismic moment-tensor determinations both in the spectral and the time domain (e.g., signal moment; see Fig. 11.6). It is achieved by extending the lowermost corner frequency of the seismometer computationally far beyond that of the physical sensor system. Both the simulation of arbitrary band-limited seismograph systems as well as the extreme broadband "restitution" of the true ground motion is therefore a necessary step in pre-processing of digital BB data.

Simulation is the mapping of a given seismogram into the seismogram of another type of seismograph, e.g., those of classical analog recordings such as WWSSN-SP, WWSSN-LP, Kirnos SKD, SRO-LP, and Wood-Anderson (WA). Up to now, amplitudes and periods for the determination of body- and surface-wave magnitudes mb and Ms are measured on simulated WWSSN-SP and WWSSN-LP or SRO-LP seismograms, respectively, and the maximum amplitude for the original local Richter magnitude is measured on Wood-Anderson simulated seismograms. Fig. 11.27 (left) depicts the displacement response of these seismographs.

The possibility of carrying out these simulations with high accuracy and stability defines the characteristics that have to be met by modern digital broadband seismograph:

- large bandwidth;
- large dynamic range;
- high resolution;
- low instrumental seismometer self-noise (see 5.6.2);
- low noise induced by variations in air pressure and temperature (see 5.3.4, 5.3.5, and 7.4.4);
- analytically exactly known transfer function (see 5.2).

Fig. 11.27 (right) depicts the displacement responses of a few common BB-velocity sensors such as:

- the original Wielandt-Streckeisen STS1 with a bandwidth of 2 decades between the 3-db roll-off points at frequencies of 0.05 Hz and 5 Hz (anti-aliasing filter). These seismographs are deployed in the world's first broadband array (GRF) around Gräfenberg/Erlangen in Germany (see Fig. 11.3a);

- the advanced STS1 that is generally used at the global IRIS network of very broadband (VBB) stations (velocity bandwidth of about 3.3 decades between 5 Hz and 360 s; see also DS 5.1);
- the STS2 seismographs (see DS 5.1) that are usually operated in the frequency range between 0.00827 Hz and 40 Hz (velocity bandwidth of 3.7 decades or about 12 octaves, respectively). They are used at the stations of the GRSN (see Fig. 11.3a) but also deployed world-wide at stations of the GEOFON network and at many others.

All these seismographs can be considered to be linear systems within the range of their usual operation. The transfer function H(s) of a linear system can be calculated from its poles and zeros by using the following general equation:

$$H(s) = N * \Pi\,(s - z_i) / \Pi\,(s - p_k) \qquad (11.5)$$

where N is the gain factor, $s = j\omega$ with $\omega = 2\pi f$ and j the complex number $\sqrt{-1}$, z_i are the zeros numbering from $i = 1$ to m and p_k the poles with $k = 1$ to n. Zeros are those values for which the numerator in Eq. (11.5) becomes zero while the poles are the values for which the denominator becomes zero.

Tab. 11.3 summarizes the poles and zeros of the classical standard responses WWSSN-SP, WWSSN-LP, WA (Wood-Anderson), Kirnos SKD and SRO-LP which control the shape of the response curves. Tab. 11.4 gives the same for the three broadband responses shown in Fig. 11.27 on the right. Not given are the gain factors because they depend on the specific data acquisition system and its sensitivity.
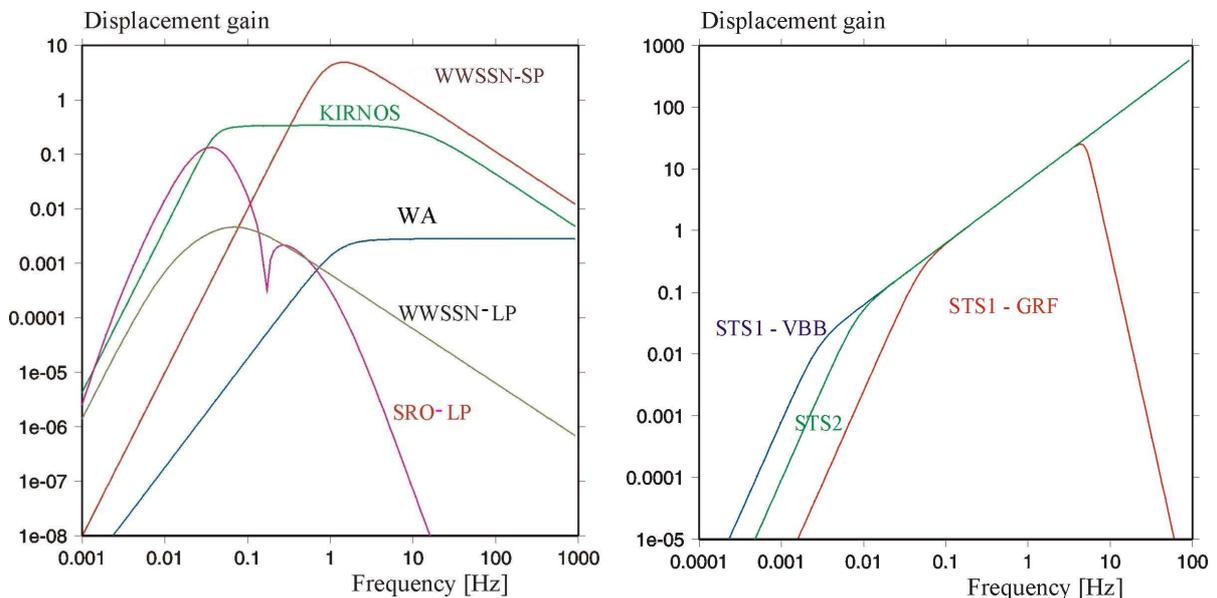
Fig. 11.27 Left: Displacement amplitude response characteristics of classical seismographs; **right:** The same for broadband seismographs STS1(GRF) (old version as used at the Gräfenberg array), STS1 (VBB) (advanced version as used in the IRIS global network) and STS2. For STS1 (VBB) and STS2 no anti-aliasing filter is shown. The classical responses shown on the left can be simulated with digital data from these broadband systems (see text).

Tab. 11.3 Zeros and poles corresponding to the displacement transfer functions depicted in Fig. 11.27 left for the classical analog standard seismographs WWSSN-SP, WWSSN-LP, WA, Kirnos SKD and SRO-LP.

Seismograph	Zeros	Poles
WWSSN-SP	(0.0, 0.0)	(-3.3678, -3.7315) (=p_1)
	(0.0, 0.0)	(-3.3678, 3.7315) (=p_2)
	(0.0, 0.0)	(-7.0372, -4.5456) (=p_3)
		(-7.0372, 4.5456) (=p_4)
WWSSN-LP	(0.0, 0.0)	(-0.4189, 0.0)
	(0.0, 0.0)	(-0.4189, 0.0)
	(0.0, 0.0)	(-6.2832E-02, 0.0)
		(-6.2832E-02, 0.0)
WA	(0.0, 0.0)	(-6.2832, -4.7124)
	(0.0, 0.0)	(-6.2832, 4.7124)
Kirnos SKD	(0.0, 0.0)	(-0.1257, -0.2177)
	(0.0, 0.0)	(-0.1257, 0.2177)
	(0.0 0.0)	(-80.1093, 0.0)
		(-0.31540, 0.0)
SRO-LP	(0.0, 0.0)	(-1.3000E-01, 0.0)
	(0.0, 0.0)	(-6.0200, 0.0)
	(0.0, 0.0)	(-8.6588, 0.0)
	(-5.0100E+01, 0.0)	(-3.5200E+01, 0.0)
	(-0.0, 1.0500)	(-2.8200E-01, 0.0)
	(-0.0, -1.0500)	(-3.9300, 0.0)
	(0.0, 0.0)	(-2.0101E-01, 2.3999E-01)
	(0.0, 0.0)	(-2.0101E-01, -2.3999E-01)
		(-1.3400E-01, 1.0022E-01)
		(-1.3400E-01, -1.0022E-01)
		(-2.5100E-02, 0.0)
		(-9.4200E-03, 0.0)

Tab. 11.4 Zeros and poles corresponding to the displacement transfer functions of the velocity-proportional broadband seismographs STS1(GRF), STS1-VBB(IRIS) and STS2 as depicted in Fig. 11.27 right. From their output data seismograms according to the classical analog standard seismographs WWSSN-SP, WWSSN-LP, WA, Kirnos SKD and SRO-LP are routinely simulated at the SZGRF in Erlangen, Germany.

Seismograph	Zeros	Poles
STS2	(0.0, 0.0)	(-3.674E-2, -3.675E-3)
	(0.0, 0.0)	(-3.674E-2, 3.675E-3)
	(0.0, 0.0)	
STS1(GRF)	(0.0, 0.0)	(-0.2221, -0.2222)
	(0.0, 0.0)	(-0.2221, 0.2222)
	(0.0, 0.0)	(-31.416, 0.0)
		(-19.572, 4.574)
		(-19.572, -24.574)
		(-7.006, 30.625)
		(-7.006, -30.625)
		(-28.306, 13.629)
		(-28.306, -13.629)
STS1(VBB))	(0.0, 0.0)	(-1.2341E-02, 1.2341E-02)
	(0.0, 0.0)	(-1.2341E-02, -1.2341E-02)
	(0.0, 0.0)	

Using the data given in these tables, the exact responses of the respective seismographs can be easily found. As an example, we calculate the response curve of the WWSSN-SP. According to Tab. 11.3 it has three zeros and four poles. Thus we can write Eq. (11.5) as

$$H(s) = N * s^3 / (s-p_1)(s-p_2)(s-p_3)(s-p_4) \qquad (11.6)$$

with

$p_1 = -3.3678 – 3.7315j$
$p_2 = -3.3678 + 3.7315j$
$p_3 = -7.0372 – 4.5456j$
$p_4 = -7.0372 + 4.5456j.$

Taking into account the discussions in section 5.2.7, the squared lower angular corner frequency of the response (that is in the given case the eigenfrequency of the WWSSN-SP seismometer) is $\omega_l^2 = p_1 \cdot p_2$ whereas the squared upper angular eigenfrequency (which used to be in the classical SP records that of the galvanometer) is $\omega_u^2 = p_3 \cdot p_4$. Since the product of conjugate complex numbers $(a + bj)(a – bj) = a^2 + b^2$ it follows for the poles:

$\omega_l^2 = 25.27$ with $f_l = 0.80$ Hz and
$\omega_u^2 = 70.18$ with $f_u = 1.33$ Hz.

When comparing these values for the corner frequencies of the displacement response of WWSSN-SP in Fig. 11.27 (left) one recognizes that the maximum displacement magnification (slope approximately zero) lies indeed between these two values. Further, as outlined in 5.2.7, a conjugate pair of poles such as p_1 and p_2 or p_3 and p_4 correspond to a second order corner of the amplitude response, i.e., to a change in the slope of the asymptote to the response curve by 2 orders. Further, the number of zeros controls the slope of the response curve at the low-frequency end, which is three in the case of the WWSSN-SP (see Eq. (11.6) and Tab. 11.3). Thus, at its low-frequency end, the WWSSN-SP response has according to its three zeros a slope of 3. This changes at the first pair of poles, i.e., at $f_l = 0.8$ Hz, by 2 orders from 3 to 1 (i.e., to velocity proportional!), and again at $f_u = 1.33$ Hz by two orders from 1 to –1. This is clearly to be seen in Fig. 11.27. In the same manner, the general shape of all the responses given in that figure can be assessed or precisely calculated according to Eq. (11.5) by using the values for the poles and zeros given in Tabs. 11.3 and 11.4. Doing the same with the values given in Tab. 11.3 for WWSSN-LP one gets for $f_l = 0.06667$ Hz, corresponding to the 15 s seismometer and $f_u = 0.009998$ Hz corresponding to the 100 s galvanometer, used in original WWSS-LP seismographs. The aim of the exercise in EX 5.5 is to calculate and construct with the method shown above the responses of seismographs operating at several seismic stations of the global network from the data given in their SEED header information.

Note that the poles and zeros given in Tabs. 11.3 and 11.4 are valid only if the input signal to the considered seismographs is ground displacement (amplitude A_d). Consequently, the values in Tab. 11.3 are not suitable for simulating the responses of the classical seismographs if the input signal to the filter is not displacement. From the output of the STS2, any simulation filter gets as an input a signal, which is velocity-proportional within the frequency range between 0.00827 Hz and 40 Hz. Its amplitude is $A_v = \omega A_d$. Accordingly, the transfer function of the simulation filter $H_{fs}(s)$ has to be the convolution product of the inverse of the transfer function $H_r(s)$ of the recording instrument and the transfer function $H_s(s)$ of the seismograph that is to be simulated:

$$H_{fs}(s) = H_r^{-1}(s) * H_s(s). \tag{11.7}$$

Thus, even for the same $H_s(s)$ to be simulated, the poles and zeros of the simulation filter differ depending on those of the recording seismograph. Tab. 11.5 gives, as an example from the SZGRF, the poles and zeros of the displacement filters for simulating the responses shown in Fig. 11.27 (left), and the poles and zeros given in Tab. 11.3, from output data of the STS2.

Tab. 11.5 Poles and zeros of the simulation filters required for simulating standard seismograms of WWSSN-SP, WWSSN-LP, WA, Kirnos SKD and SRO-LP, respectively from STS2 BB-velocity records.

Simulation-filter for	Zeros	Poles
WWSSN-SP	(-3.6743E-02, -3.6754E-02) (-3.6743E-02, 3.6754E-02)	(-3.3678, -3.7316) (-3.3678, 3.7315) (-7.0372, -4.5456) (-7.0372, 4.5456)
WWSSN-LP	(-3.6743E-02, -3.6754E-02) (-3.6743E-02, 3.6754E-02)	(-0.4189, 0.0) (-0.4189, 0.0) (-6.2832E-02, 0.0) (-6.2832E-02, 0.0)
WA	(-3.6743E-02, -3.6754E-02) (-3.6743E-02, 3.6754E-02)	(-6.2832, -4.7124) (-6.2832, 4.7124) (0.0, 0.0)
Kirnos SKD	(-3.6743E-02, -3.6754E-02) (-3.6743E-02, 3.6754E-02)	(-0.12566, -0.2177) (-0.1257, 0.2177) (-80.1094, 0.0) (-0.3154, 0.0)
SRO-LP	(-3.6744E-02, -3.6754E-02) (-3.6743E-02, 3.6754e-02) (-5.0100E+01, 0) (-0, 1.0500) (-0, -1.0500) (0.0, 0.0) (0.0, 0.0)	(-1.3000E-01, 0.0) (-6.0200, 0.0 (-8.6588, 0.0) (-3.5200E+01, 0.0) (-2.8200E-01, 0.0) (-3.9301E+00, 0.0) (-2.0101E-01, 2.3999E-01) (-2.0101E-01, -2.3999E-01) (-1.3400E-01, 1.0022E-01) (-1.3400E-01, -1.0022E-01) (-2.5100E-02,0.0) (-9.4200E-03,0.0)

Fig. 11.28 shows a comparison of the original three-component BB-velocity record of an STS2 at station WET from a local earthquake in Germany with the respective seismograms of a simulated Wood-Anderson (WA) seismograph. For a teleseismic earthquake Fig. 11.29 gives the STS2 BB-velocity record together with the respective simulated records for WWSSN-SP and LP. Figs. 11.30 and 11.31 give two more examples of both record simulation and the restitution of very broadband (VBB) true ground displacement. VBB restitution of ground displacement is achieved by convolving the given displacement response of the recording seismometer with its own inverse, i.e.,:

$$H_{rest}(s) = H_s^{-1}(s) * H_s(s). \tag{11.8}$$

However, Eq. (11.8) works well only for frequencies smaller than the upper corner frequency (anti-alias filter!) and for signal amplitudes that are well above the level of ambient, internal (instrumental), and digitization noise.
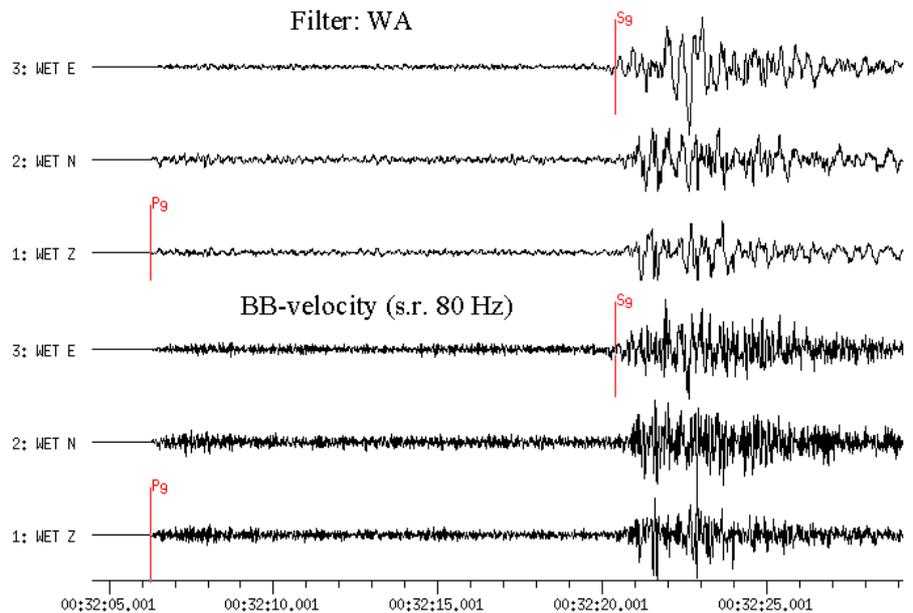
Fig. 11.28 3-component recordings at station WET (Wettzell) of a local earthquake at an epicentral distance of D = 116 km. Lower traces: original STS2 records with sampling rate of 80 Hz; upper traces: simulated Wood-Anderson (WA) recordings. Note that the displacement-proportional WA record contains less high frequency oscillations than the velocity-proportional STS2 record (compare responses shown in Fig. 11.27).
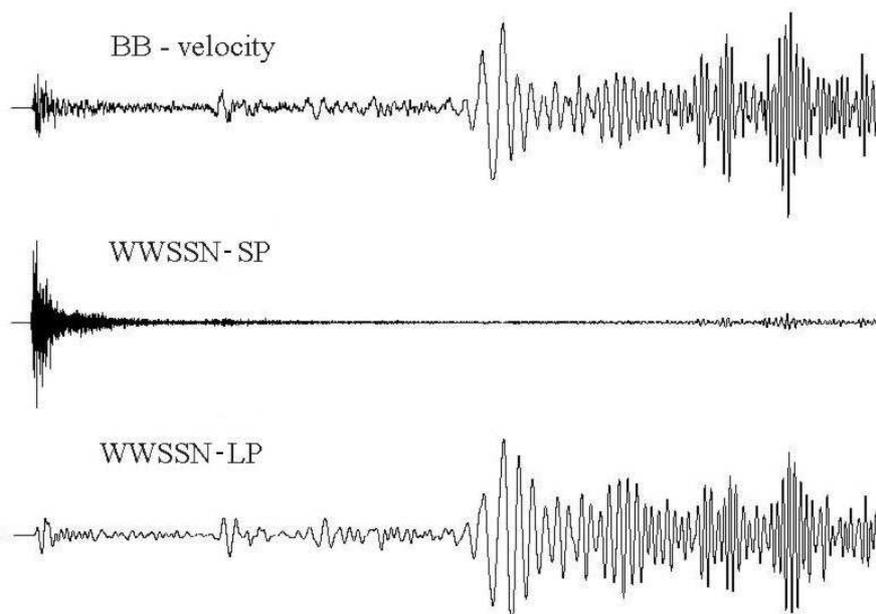
Fig. 11.29 BB-velocity seismogram (top) and simulated WWSSN-SP (middle) and WWSSN-LP seismograms (bottom). Note the strong dependence of waveforms and seismogram shape on the bandwidth of the simulated seismographs.

Both Fig.11.29 and 11.30 show clearly the strong influence of differences in bandwidth and center frequencies of the seismometer responses (compare with Fig. 11.27) on both the individual waveforms and the general shape of the seismogram. This is particularly obvious in the simulated teleseismic earthquake records. Fig. 11.30 shows the recordings of the teleseismic P-wave group of an earthquake in California on 16 Sept. 1999. Shown are the restitution of a BB-displacement seismogram derived from a BB-velocity seismogram and the simulations of WWSSN-SP and SRO-LP seismograms. In the BB-velocity seismogram one recognizes clearly the superposition of a low-frequency signal and a high-frequency wave group. The latter is clearly seen in the WWSSN-SP record but is completely absent in the SRO-LP simulation. From this comparison it is obvious that both the BB-velocity and the SP seismograms enhance short-period signal amplitudes. Therefore, only the former recordings are well suited for studying the fine structure of the Earth and determining the onset time and amplitude of short-period P waves. In contrast, BB-displacement seismograms and LP-filtered seismograms suppress the high-frequencies in the signals. Generally they are more suited to routine practice for surface-wave magnitude estimation and for the identification of most (but not all!) later phases (see Figs. 11.12, 11.13, 11.37, and Fig. 2.23).
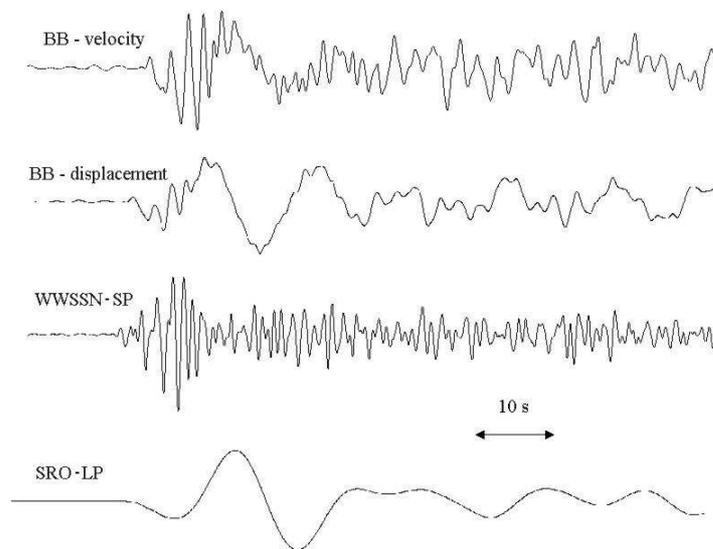
Fig. 11.30 From top to bottom: The original BB-velocity seismogram recorded at station GRFO; the BB-displacement record derived by restitution; the simulated WWSSN-SP; and the simulated SRO-LP seismograms of the P-wave group from an earthquake in California (16 Sept. 1999; D = 84.1°; Ms = 7.4).

Fig. 11.31 shows 10-days of a VBB record from an STS1 vertical-component seismograph (corner period T_c = 360s) at station MOX and simulated WWSSN-SP and SRO-LP seismograms for a short (40 min) time segment of this VBB record.
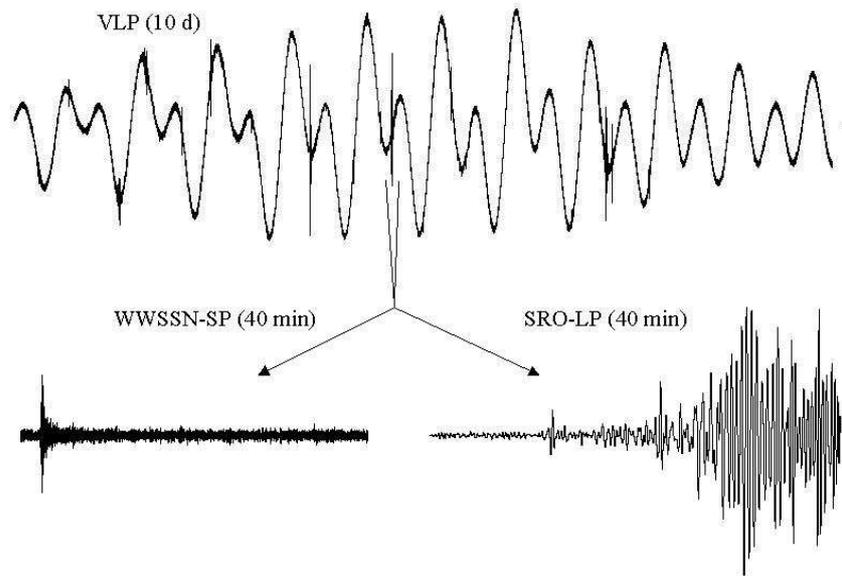
Fig. 11.31 STS1 (T_c = 360s) vertical-component seismogram with a length of 10 days (upper trace) as recorded at MOX station, Germany. In the seismogram we recognize Earth's tides and different earthquakes as spikes. For one of these earthquakes a WWSSN-SP and SRO-LP simulation filter was applied (lower traces). The length of the filtered records is 40 minutes.

Figs. 11.32a-d demonstrate, with examples from the GRSN and the GRF array in Germany, the restitution of ("true") displacement signals from BB-velocity records as well as the simulation of WWSSN-SP, Kirnos BB-displacement and SRO-LP records. All traces are time-shifted for the P-wave group and summed (they are aligned on trace 16). The summation trace forms a reference seismogram for the determination of signal form variations. Generally, this trace is used for the beam (see 11.3.5 below). The different records clearly demonstrate the frequency dependence of the spatial coherence of the signal. Whereas high-frequency signals are incoherent over the dimension of this regional network (aperture about 500 to 800 km) this is not so for the long-period records which are nearly identical at all recording sites.

The following features are shown in Figs. 11.32a-d:

a) Time shifted BB-displacement (traces 16-30) and BB-velocity seismograms (traces 1-15) with a duration of 145 s of the P-wave group from an earthquake in Peru on 23 June 2001 (Ms=8.1) as recorded at 15 stations of the GRSN. The BB-displacement seismogram suppresses the high-frequencies, which are clearly shown on the BB-velocity record.

b) WWSSN-SP simulations for the same stations as in Figure 11.32a. The high-frequency signals are enhanced but the shape and amplitudes of the waveforms are shown to vary considerably within the network, i.e., the coherence is low.

c) Kirnos SKD BB-displacement and d) SRO-LP simulations for the same stations as in Fig.11.32a. The high-frequency signals are masked. All traces show coherent waveforms.
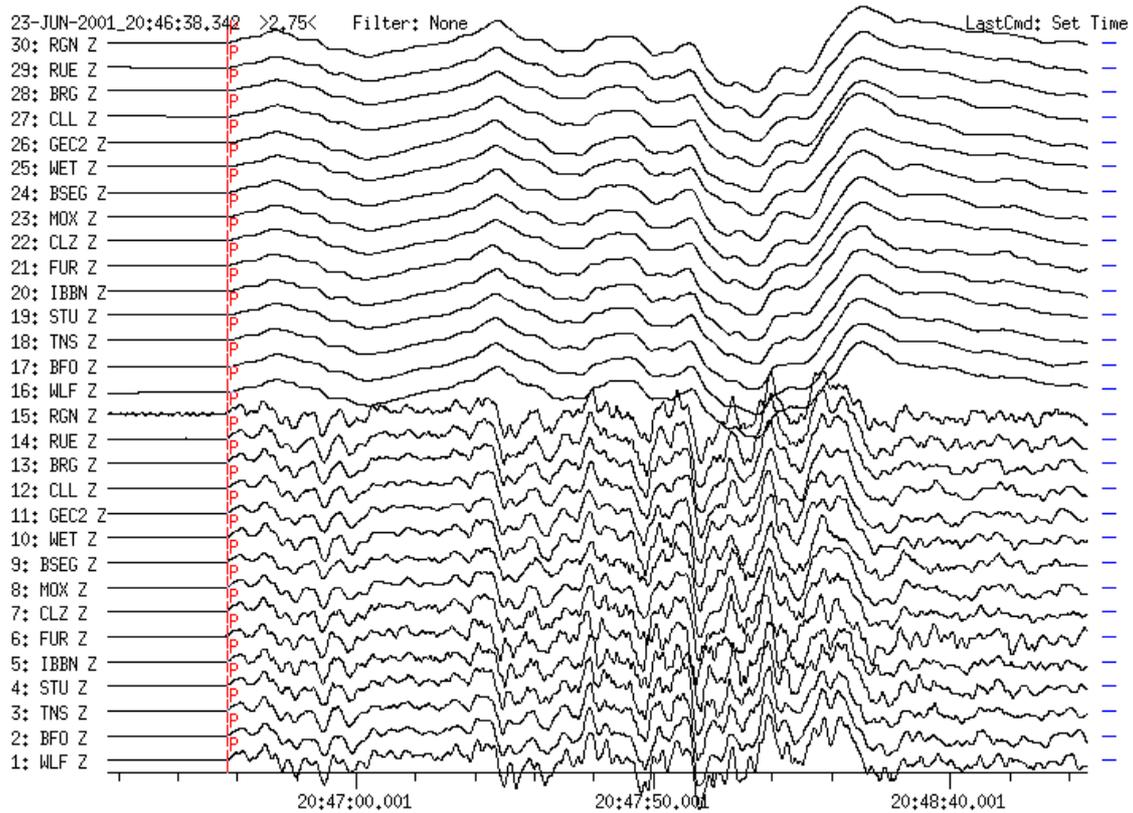
Fig. 11.32a (for explanation see text on page 48)
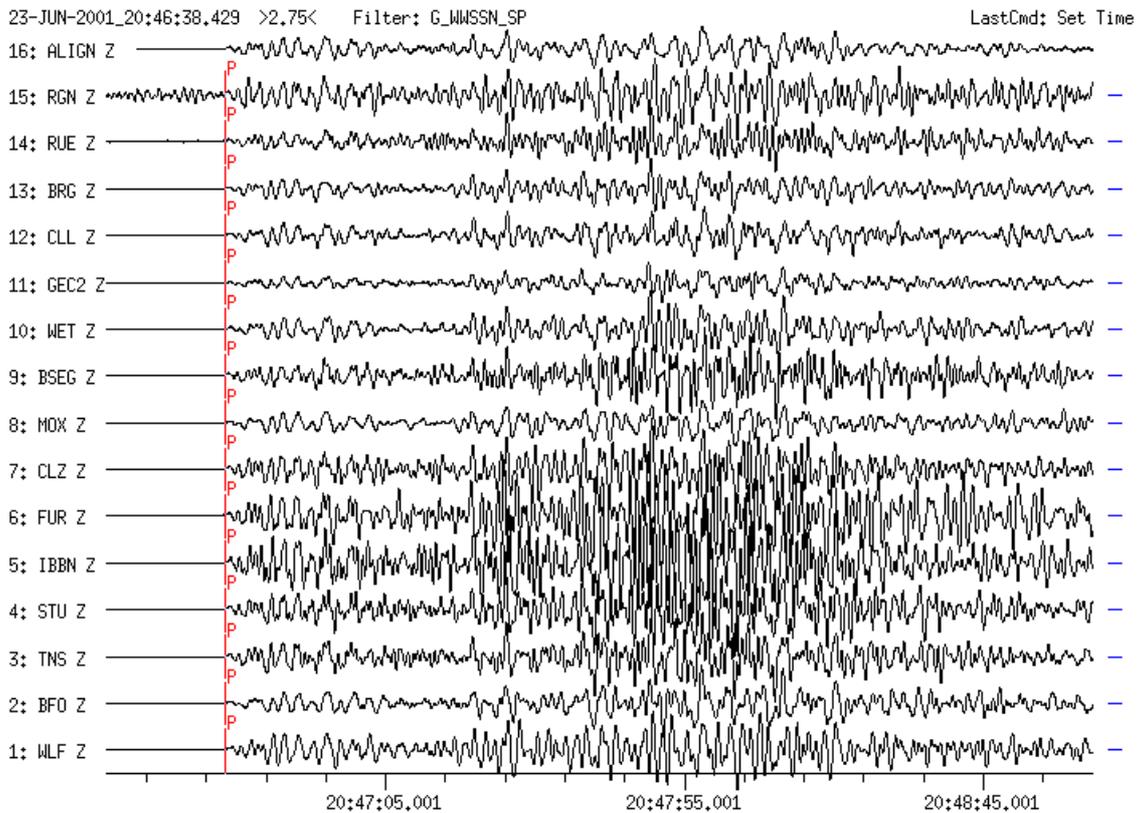
Fig. 11.32b As Fig. 11.32a however with short-period WWSSN-SP simulation.
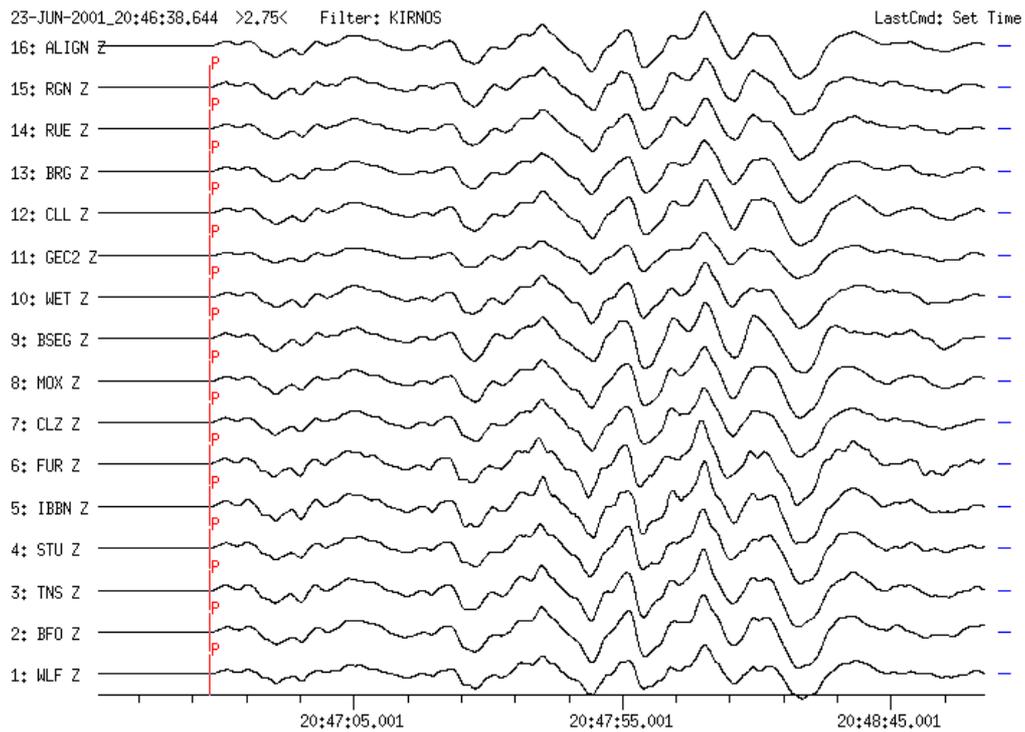
Fig 11.32c As Fig. 11.32a but for displacement-proportional Kirnos SKD simulation.
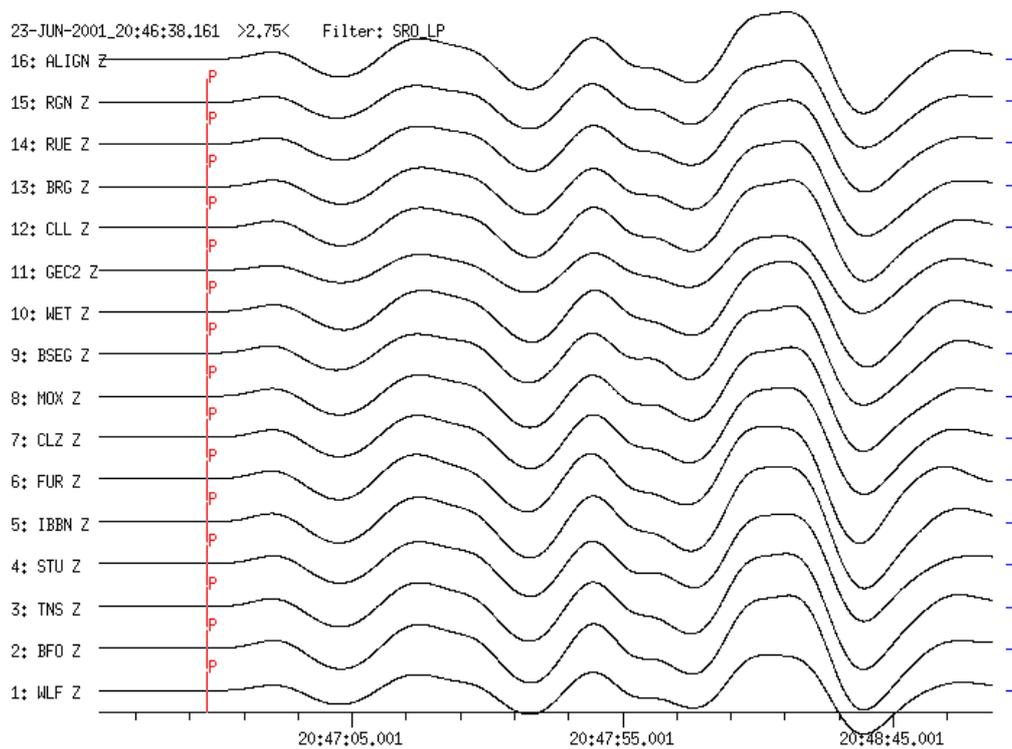
Fig. 11.32d As Fig. 11.32a but for long-period SRO-LP simulation.

Fig. 11.32a-d Restitution, simulation and coherency of seismograms demonstrated with records of the GRSN from an earthquake in Peru (23 June 2001, Ms = 8.1) in the epicentral distance range from 96° to 100°; for explanation see text).

11.3.3 Signal coherency at networks and arrays

Heterogeneous crustal structure and the array aperture limit the period band of spatially coherent signals. The larger the aperture of an array the more rapidly the signal coherence falls off with frequency. At short periods the array behaves like a network of single stations whereas at long periods the array behaves like a sensitive single station. For the GRF-array (aperture about 50 to 120 km) for instance, the signals are coherent for periods between about 1 and 50 s. For the GRSN the band of coherent signals is at longer periods than for the small aperture detection arrays like GERES in Germany or NORES in Norway (aperture 4 and 3 km, respectively) where signals are coherent at periods shorter than 1 s. In the coherency band itself, waveforms vary depending on their dominant frequency, apparent horizontal velocity and azimuth of approach. For instance, coherent waveforms are observed from the GRSN for BB-displacement records, Kirnos SKD simulation and all long-period simulated seismograms (see Figs. 11.32a-d) whereas for simulated WWSSN-SP seismograms the waveforms have low coherence or are incoherent.

Figs. 11.33a and b shows a comparison of the first 14 s of the P wave of the GRSN and the GRF-array. The coherence is clearly higher in the short-period range for the recordings at the smaller GRF-array than for the GRSN. The GRSN works as an array for periods longer than about 10 s but it is a network for shorter periods where the GRF-array works as an array down to periods of about 1 s. This discussion is valid for teleseismic signals only, where the epicentral distance is larger than the aperture of the station network or array.
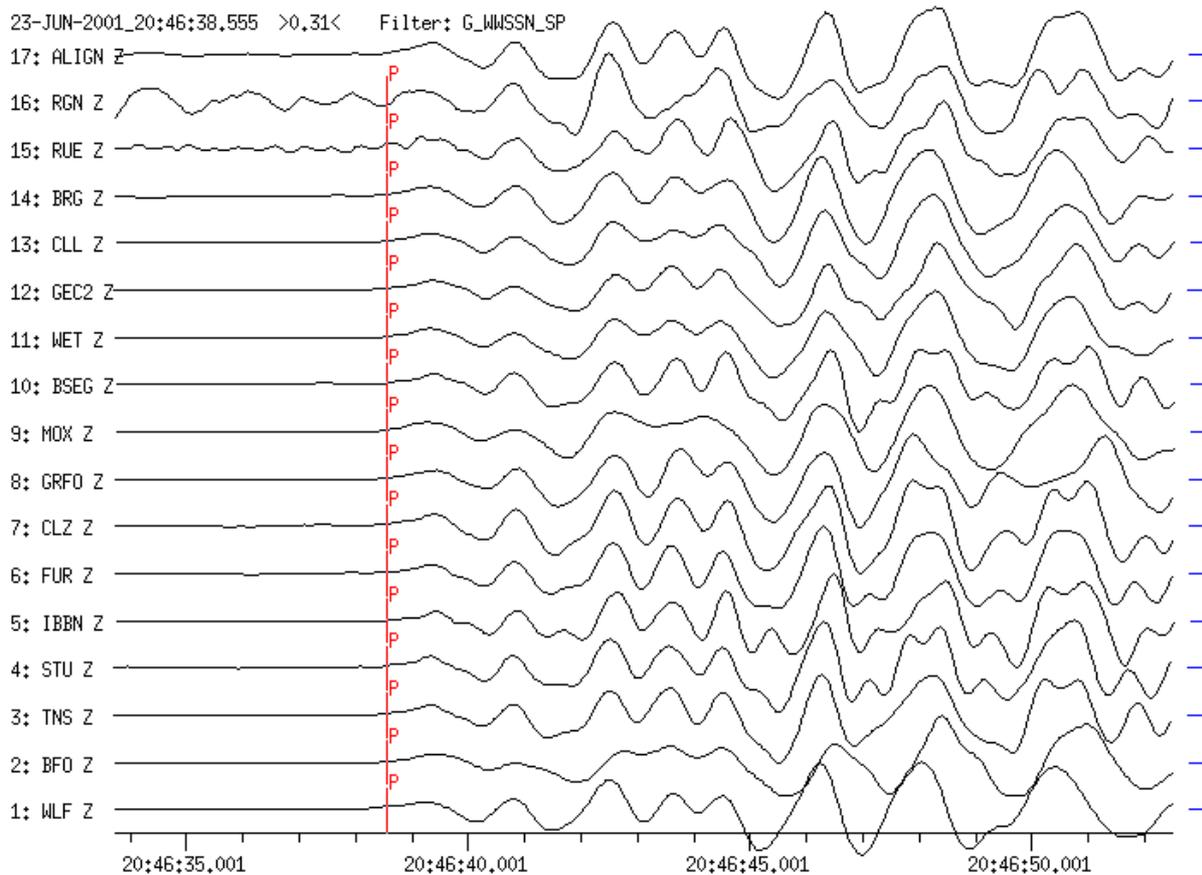
Fig. 11.33a (see figure caption below)
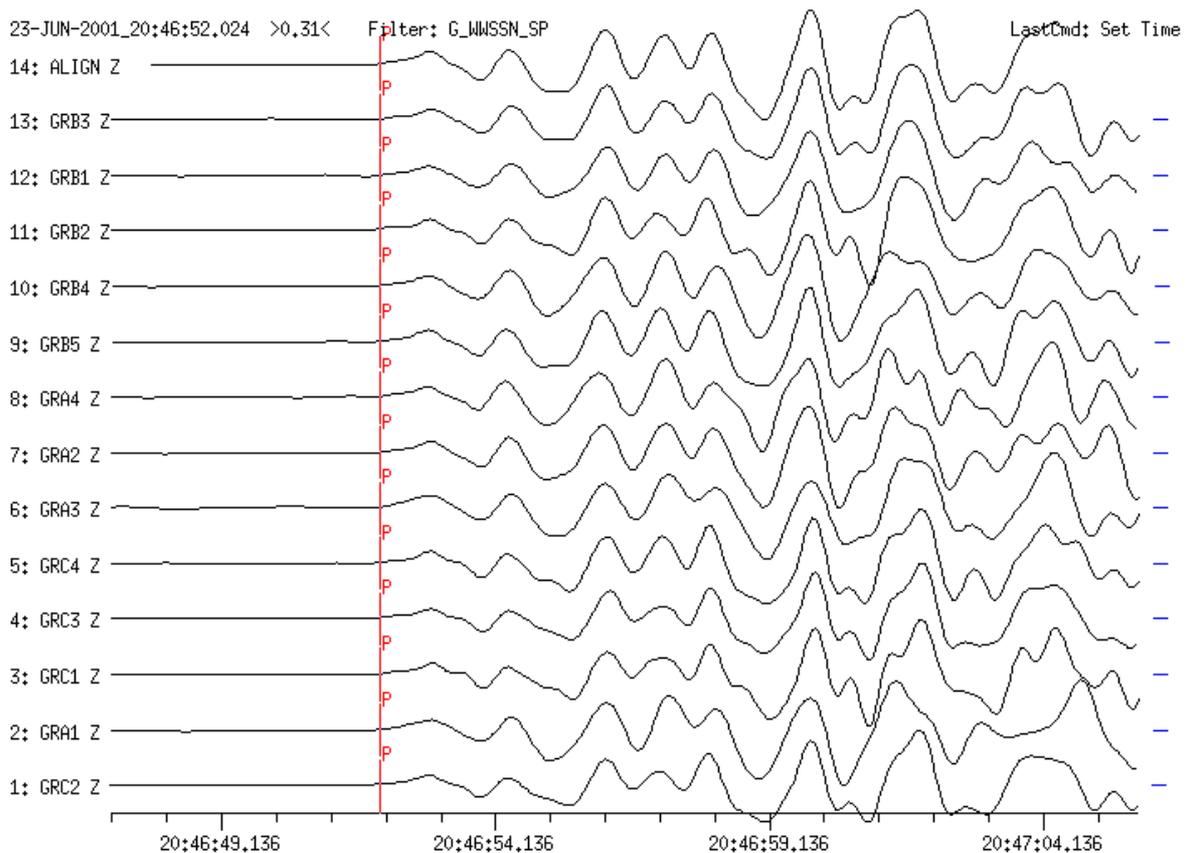
Fig. 11.33b (see figure caption below)

Fig. 11.33 WWSSN-SP simulations of the first 14 s after the P-wave onset from the same Peru earthquake as in Fig. 11.32. **a)** Recordings at the GRSN. **b)** Recordings at the GRF array. Note the lower coherence of the waveforms recorded at the stations of the regional network, which has an aperture much larger than the GRF-array (see Fig. 11.3a). The summation traces 17 and 14, respectively, are reference seismograms for the determination of signal waveform variations.

11.3.4 f-k and vespagram analysis

Array-techniques such as f-k and vespagram analysis should be applied only to records with coherent waveforms. Vespagram analysis or the velocity spectrum analysis is a method for separating signals propagating with different apparent horizontal velocities. The seismic energy reaching an array from a defined backazimuth with different slownesses is plotted along the time axis. This allows identification of later phases based on their specific slowness values. The best fitting slowness is that for which a considered phase has the largest amplitude in the vespagram. Fig. 11.34 shows the original records from the GRSN (top) and the related vespagram (bottom). More vespagrams are given in Figures 12e–g of DS 11.2.
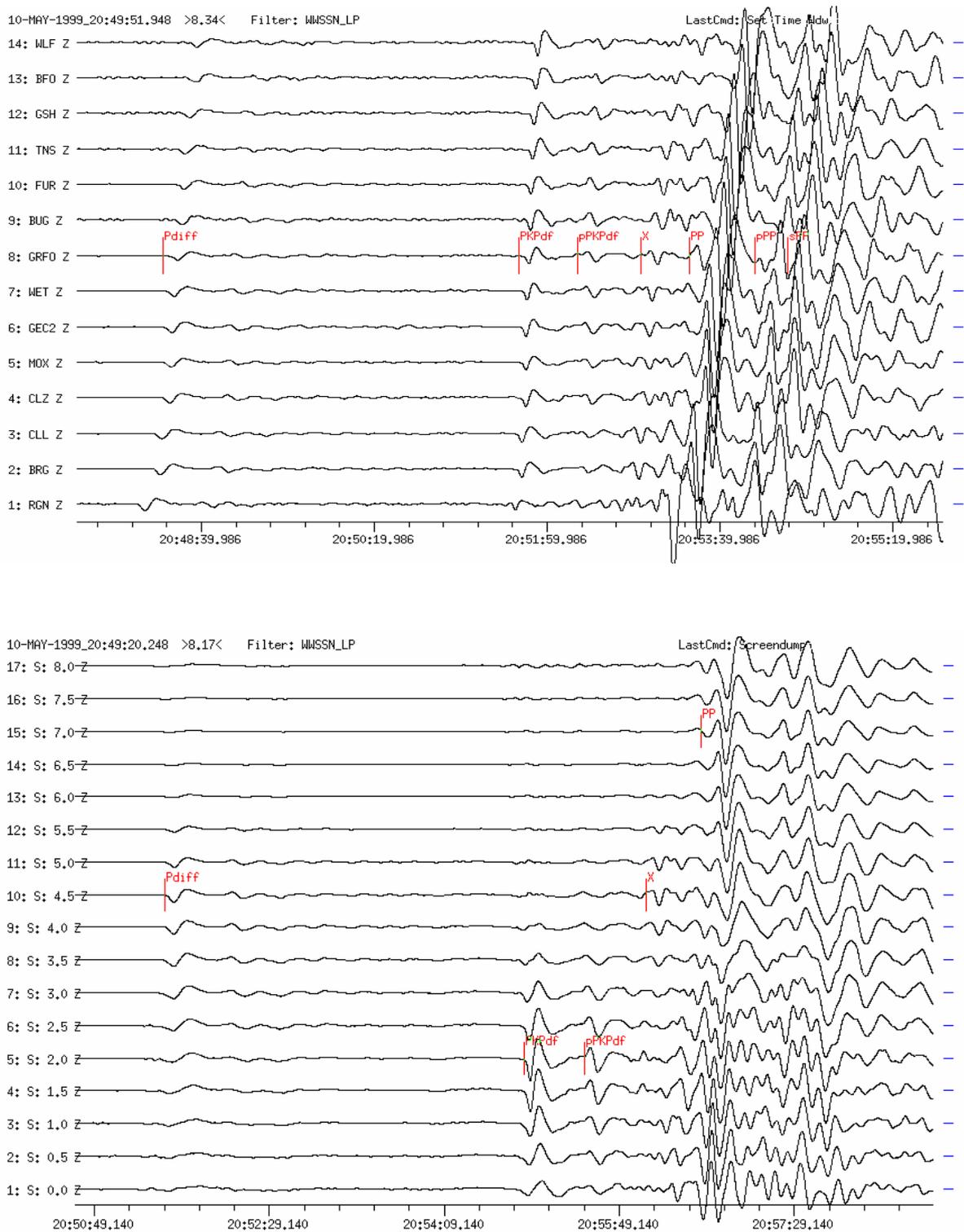
Fig. 11.34 **Top:** Simulated vertical-component WWSSN-LP seismograms from an earthquake in the region of Papua New Guinea. Source data NEIC-QED: 10 May 1999; depth 137 km; mb = 6.5; D = 124° to GRF, BAZ = 51°. The phases Pdif (old Pdiff), PKPdf, pPKPdf, PP, pPP, sPP and an unidentified phase X have been marked. **Bottom:** Vespagram of the upper record section. The analysis yields slowness values of 4.5s/° for Pdif, 2.0s/° for PKPdf and pPKPdf, 7.0s/° for PP, and a value that corresponds to the slowness for Pdif for the unknown phase X.

As an example an f-k analysis is shown in Fig. 11.35. The f-k analysis is used to determine slowness and backazimuth of coherent teleseismic wave groups recorded at an array. The epicentral distance must be much larger than the aperture of the recording array. The f-k analysis transforms the combined traces within a current time window (Fig. 11.35a and b) into the frequency-wavenumber domain. The result in the f-k domain is displayed in a separate window (Fig. 11.35c) with amplitudes (corresponding to wave energy) coded in color. A good result is achieved when there is a single, prominent color in the maximum (yellow in Fig. 11.35c). This maximum denotes slowness and backazimuth of the investigated phase and is helpful for source parameter determination and phase identification. The example was recorded at the GRF-array from an earthquake in Novaya Zemlya. Slowness and backazimuth values are 7.3 s/° and 11°, respectively. These values are used for producing the beam.
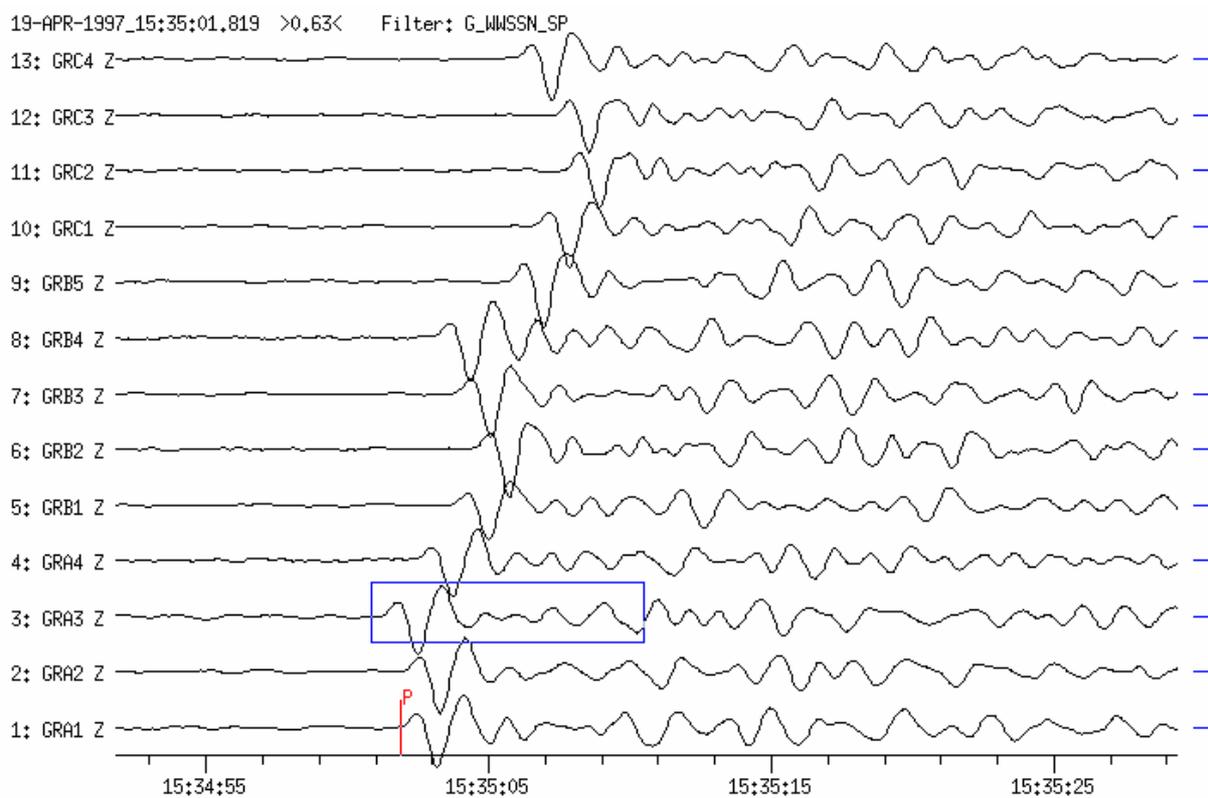
Fig. 11.35a

Figs. 11.35a-c Illustration of the procedure of frequency-wavenumber (f-k) analysis: a) coherent P-wave signals recorded at the GRF-array stations from an earthquake on 19 April 1997 (the box marks the time window selected for the f-k-analysis); b) the zoomed window used for the f-k-analysis; c) energy (coded in colors) in the frequency range 0.39-2.97 Hz as a function of wavenumber k. A good result is achieved because the single, prominent maximum (in yellow) shows the presence of a coherent signal. The estimated slowness and backazimuth values are 7.3 s/° and 11°, respectively.

19-APR-1997_15:35:01.862 >0.16<   Filter: G_WWSSN_SP   LastCmd: Set Time

13: GRC4 Z

12: GRC3 Z

11: GRC2 Z

10: GRC1 Z

9: GRB5 Z

8: GRB4 Z

7: GRB3 Z

6: GRB2 Z

5: GRB1 Z

4: GRA4 Z

3: GRA3 Z

2: GRA2 Z

1: GRA1 Z

P

15:35:01 15:35:02 15:35:03 15:35:04 15:35:05 15:35:06 15:35:07 15:35:08 15:35:09 15:35:10

Fig. 11.35b

19-APR-1997_15:35:01.100

width 9.50 sec

apparent veloc. :   0.14

slowness   :   7.39

azimuth   :   12.3

max. slow.   :   1.58,   7.22

slowness range :   15.00

frq. wdw.   :   0.39,   2.97

rel. power   :   0.85

abs. power   :   35.96

radial grid step 2

curr. slowness :   1.84, 6.88
vel, slo, az: 0.14   7.13   14.98
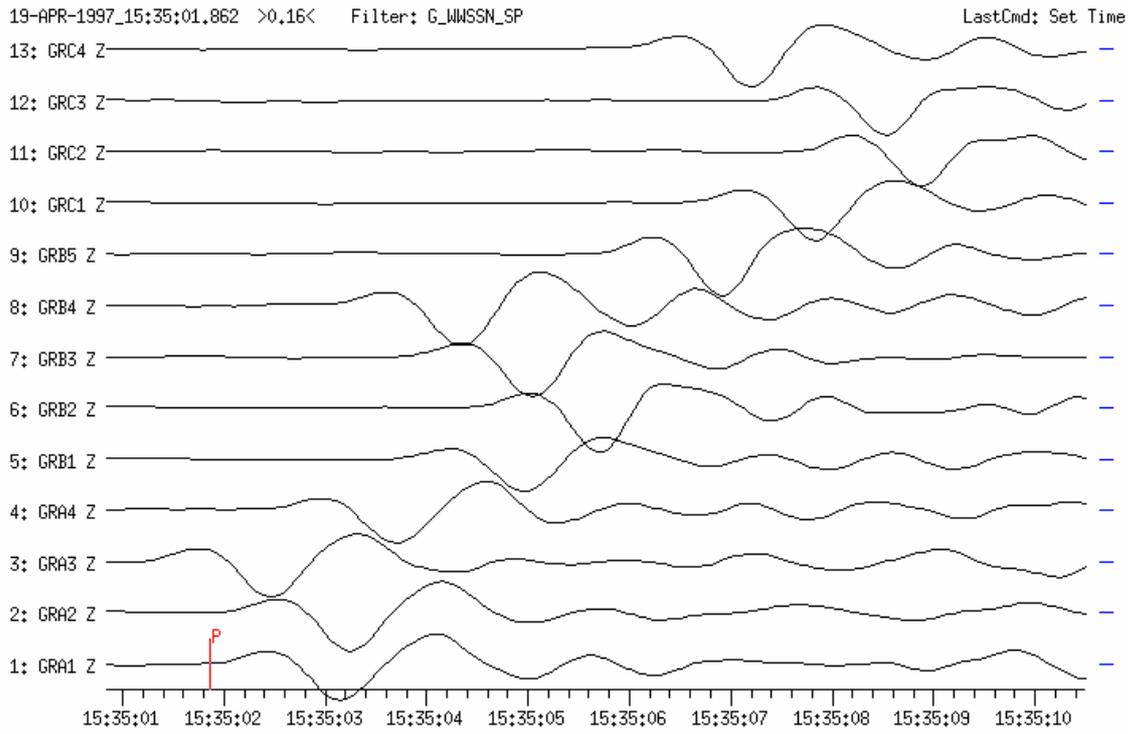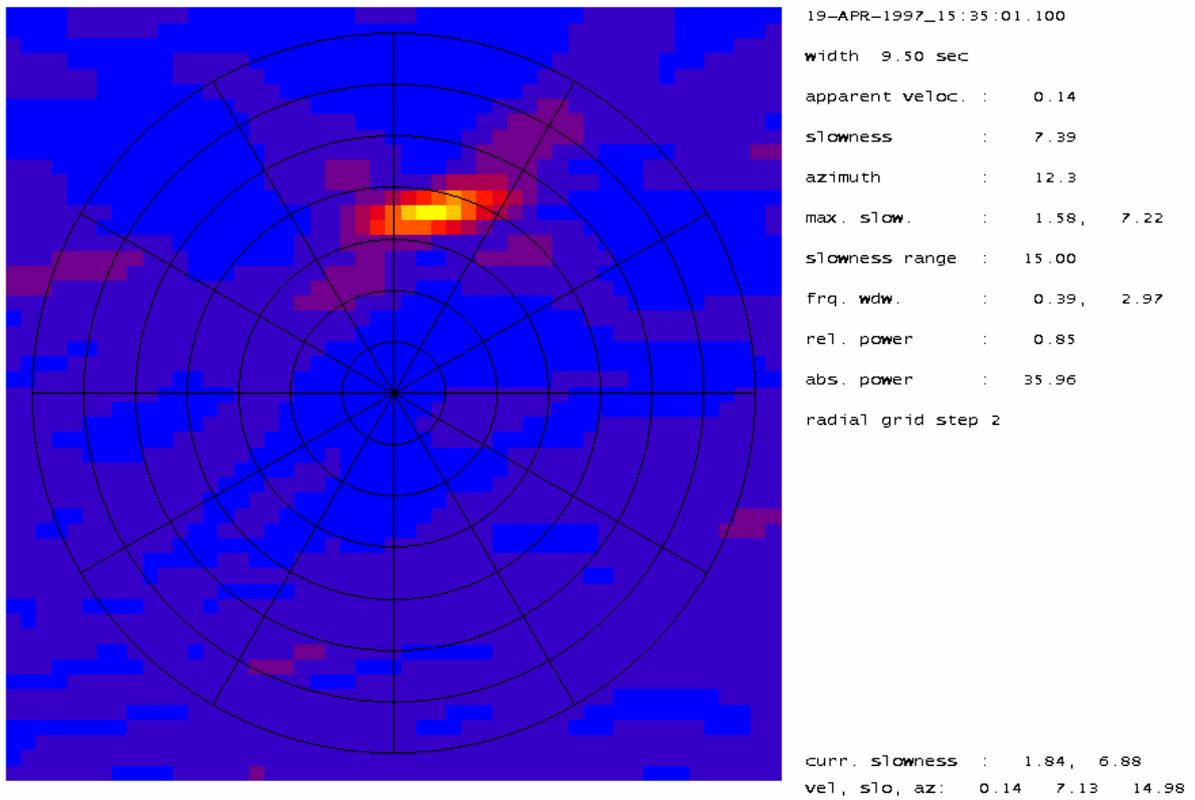
Fig. 11.35c

11.3.5 Beamforming

Beamforming improves the SNR of a seismic signal by summing the coherent signals from array stations (see 9.4.5). Signals at each station are time shifted by the delay time relative to some reference point or station. The delay time depends on ray slowness and azimuth and can be determined by trial and error or by f-k analysis. The delayed signals are summed "in phase" to produce the beam. Fig. 11.35d presents the array recordings of the signal shown in Figs. 11.35a-b time shifted, to correct for the time delay, and summed (trace 14; beam). In delay-and-sum beamforming with N stations the SNR improves by a factor $\sqrt{N}$ if the noise is uncorrelated between the seismometers. In the summation the increase in amplitude of the coherent signal is proportional to N. For incoherent waves (random seismic noise in particular), it is only proportional to $\sqrt{N}$. Thus, f-k analysis and beamforming are helpful for routine analysis if very weak signals have to be detected and analyzed.
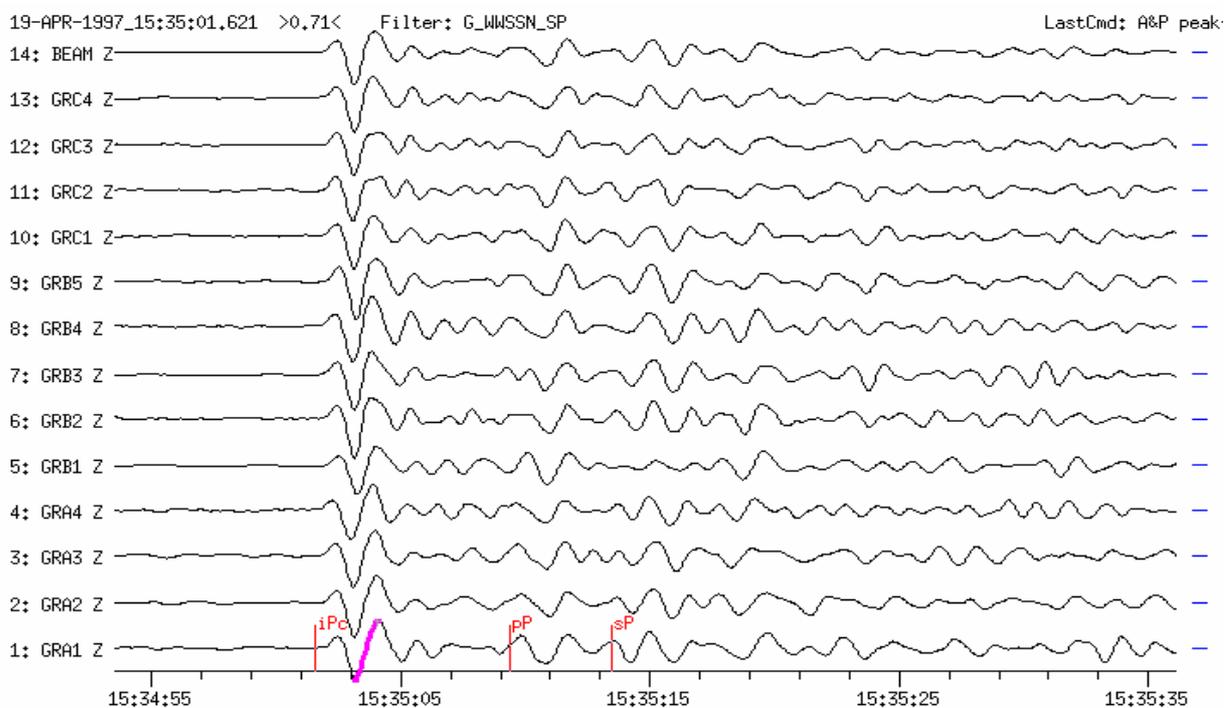
Fig. 11.35d The delay times for each of the array seismometers have been calculated from the slowness and azimuth of the signals shown in Figs. 11.35a-c. The time-shifted signals are summed "in phase" to produce the beam (top trace) which has the better signal-to-noise ratio than the recordings from the individual seismometers.

Fig. 11.36 shows another example of array processing with short-period filtered seismograms of the GRF array. The signal on the beam trace is the PKP wave of an underground nuclear explosion at Mururoa Atoll with an explosion yield equivalent of about 1 kt TNT. The onset time and signal amplitude of a weak seismic signal can only be read on the beam. The peak-to-peak amplitude is only about 2 nm with a period around 1 s.
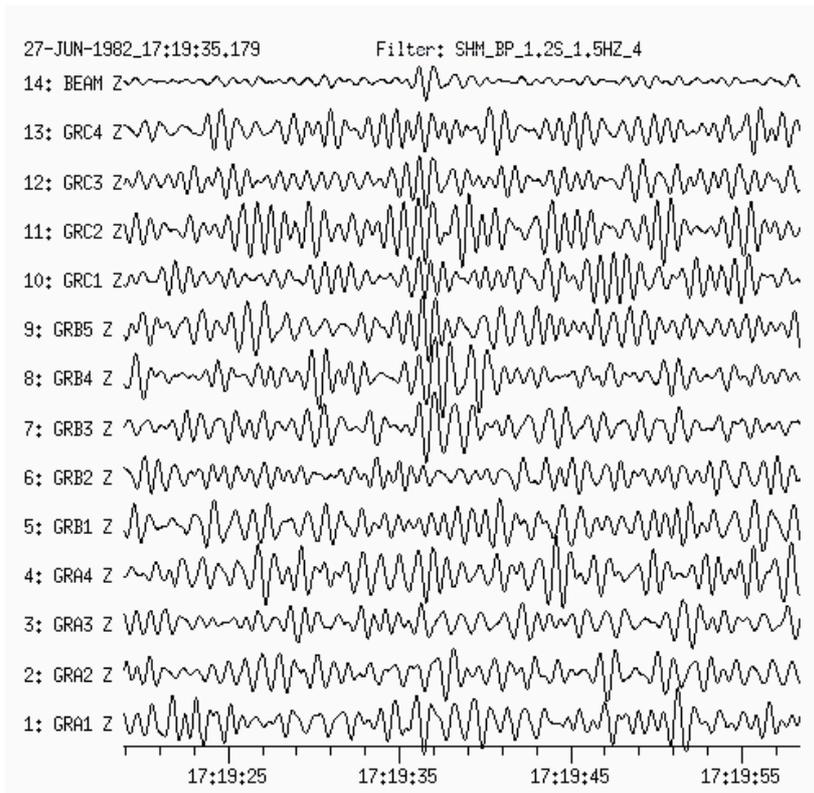
Fig. 11.36 Detection of the PKP wave of a nuclear explosion at Mururoa Atoll on 27 June 1982 at the Gräfenberg array using the delay-and-sum-method and a very narrowband Butterworth bandpass filter (BP) centered around 1 Hz. The event occurred at an epicentral distance of 146° and the explosion yield was approximately 1 kt TNT.

11.3.6 Polarization analysis

The task of polarization analysis is the transformation of recorded three component seismograms into the ray-oriented co-ordinate systems. For linearly polarized and single pulse P waves in a lateral homogeneous Earth, this task is simple, at least for signals with a high SNR; the direction of the polarization vector of the P wave clearly determines the orientation of the wave co-ordinate system. However, when propagating through heterogeneous and anisotropic media, the seismic waves have three-dimensional and frequency-dependent particle motions and the measured ray-directions scatter by ten degrees and more about the great circle path from the epicenter to the station (see Fig. 2.6).

Determination of particle motion is included in most of the analysis software. For identification of wave polarization and investigation of shear-wave splitting, the rotation of the traditional components N, E, and Z into either a ray–oriented co-ordinate systems or into the directions R (radial, i.e., towards the epicenter) and T (transverse, i.e., perpendicular to the epicenter direction) is particularly suitable for the identification of secondary later phases. An example for the comprehensive interpretation of such phases in a teleseismic record is given in Fig. 11.37.
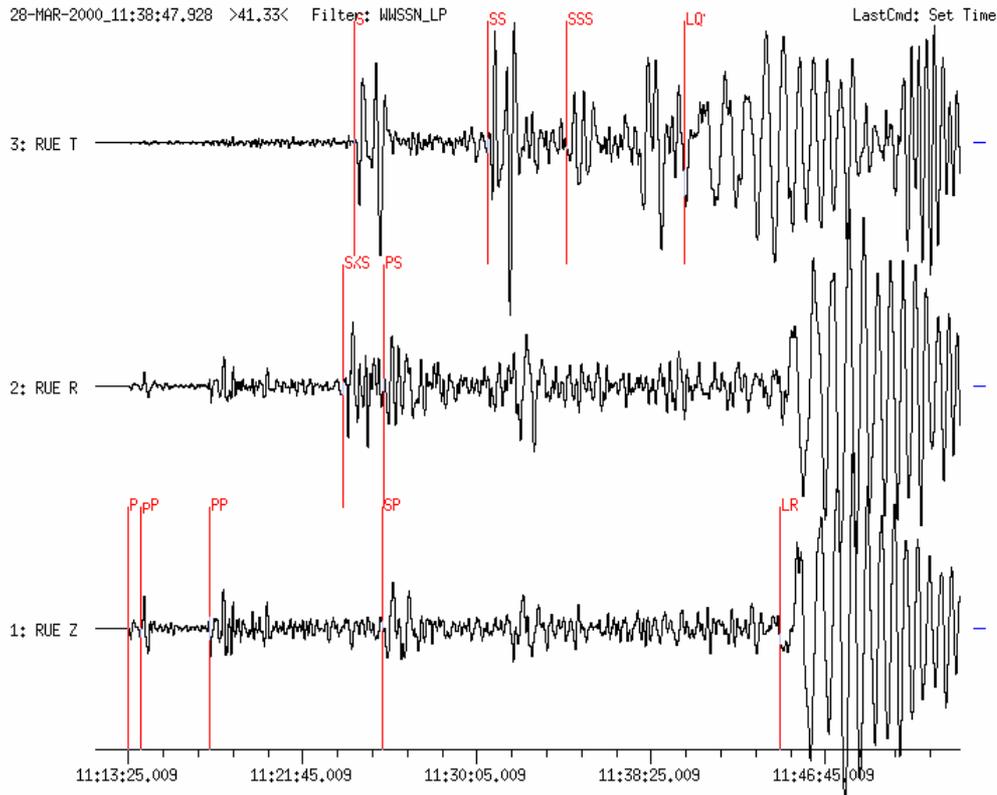
Fig. 11.37 Simulation of three-component WWSSN-LP seismograms of the Volcano Islands earthquake of 28 March 2000, recorded at station RUE in Germany (D = 94°, h = 119 km). The horizontal components N and E are rotated into R and T components. The phases P, pP, SP and the beginning of the dispersed surface Rayleigh wave train LR are marked on the vertical-component seismogram, SKS, PS on the radial component (R) and S, SS, SSS and the beginning of the Love waves LQ on the transverse component (T), respectively. Not marked (but clearly recognizable) are the depth phases sS behind S, sSS behind SS, and SSSS+sSSSS before LQ. The record length is 41 min.

11.4 Software for routine analysis

11.4.1 SHM

The Seismic Handler SHM is a powerful program for analyzing local, regional and teleseismic recordings. K. Stammler of the SZGRF in Erlangen has developed it for the analysis of data from the Graefenberg (GRF) array and the German Regional Seismic Network (GRSN). The program and descriptions are available via http://www.szgrf.bgr.de/sh-doc/index.html.

Main features of the program are:
- application of array procedures to a set of stations (slowness- and backazimuth determination by means of beamforming and f-k analysis);
- location algorithms (teleseismic locations using travel-time tables and empirical correction vectors, local and regional locations via external programs, e.g., LocSAT).

The basic program has some (more or less) standardized options, e.g.:
- manual and automatic phase picking (see Fig. 11.5);
- trace filtering with simulation and bandpass filters (see Figs. 11.28 and 11.29);
- determination of amplitudes, periods and magnitudes (see Fig. 11.4);
- display of theoretical travel times on the traces (see Fig. 11.37).

Furthermore, the following tasks are implemented:
- rotation of horizontal components (see Figs. 11.13 and 11.37);
- particle motion diagrams (see Fig. 2.6);
- trace amplitude spectrum (see Fig. 11.47);
- vespagram trace display (see Fig. 11.34);
- determination of signal/noise ratio (see Fig. 11.47); and
- trace editing functions.

Different data formats are supported on continuous data streams of single stations, networks and/or array stations. SHM is currently supported on UNIX and Linux. A screen display of SHM is shown in Fig. 11.38.
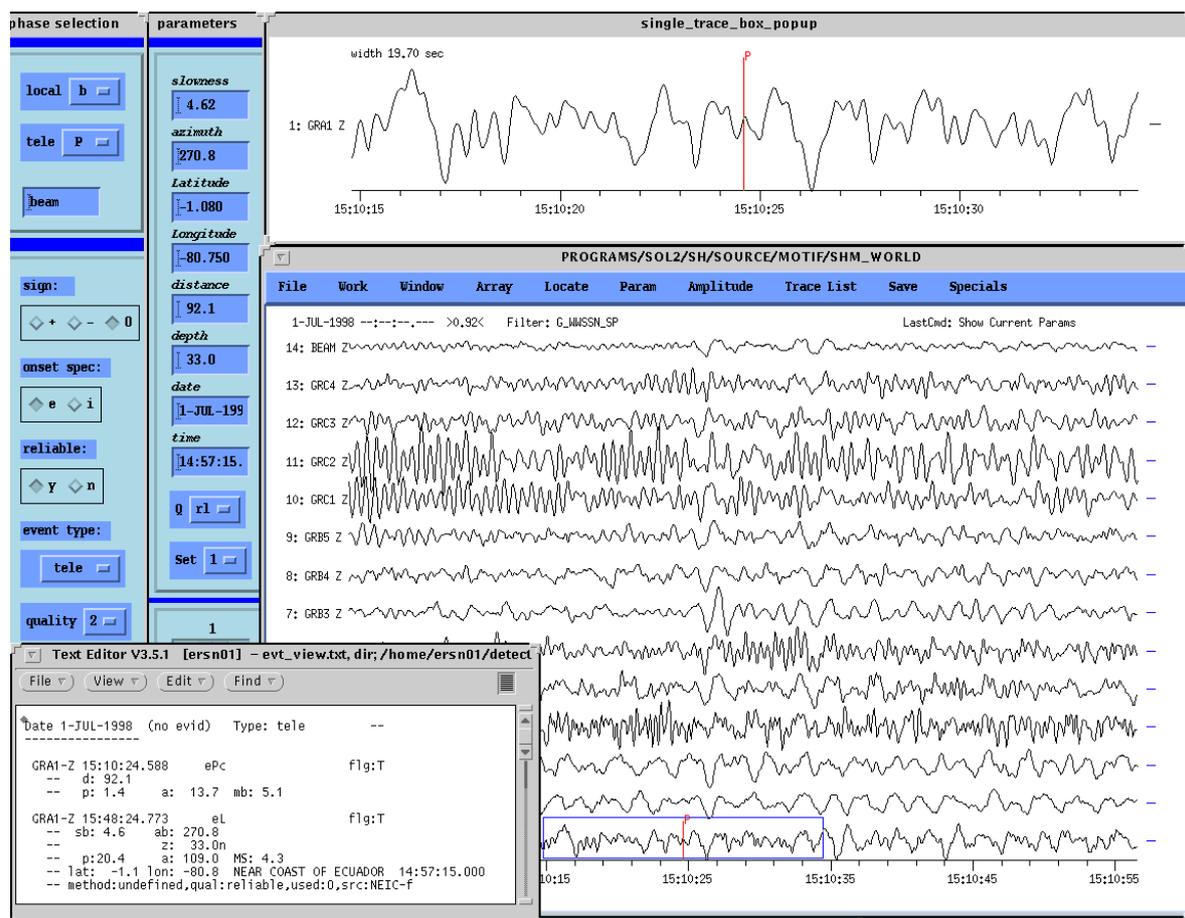
Fig. 11.38 Screen display of the seismic analysis program SHM. Different windows display a number of station recordings (large window), a zoomed single-station window, two seismogram and source parameter windows (left side) and an output window for the results of the seismogram analysis. Generally, the resulting parameters are stored in a database.

11.4.2 SEISAN

Another widely used seismic analysis system is SEISAN developed by J. Havskov and L. Ottemöller (1999). It contains a complete set of programs and a simple database for analyzing analog and digital recordings. SEISAN can be used, amongst other things, for phase picking, spectral analysis, azimuth determination, and plotting seismograms. SEISAN is supported by DOS, Windows95, SunOS, Solaris and Linux and contains conversion programs for the most common data formats. The program, together with a detailed Manual, is available via http://www.ifjf.uib.no/seismo/software/seisan/seisan.html.

11.4.3 PITSA

F. Scherbaum, J. Johnson and A. Rietbrock wrote the current version. It is a program for interactive analysis of seismological data and has numerous tools for digital signal processing and routine analysis. PITSA is currently supported on SunOS, Solaris and Linux and uses the X11 windowing system. It is available via http://lbutler.geo.uni-potsdam.de/service.htm.

11.4.4 GIANT

Andreas Rietbrock has written this program package. It is a system for consistent analysis of large, heterogeneous seismological data sets. It provides a graphical user interface (GUI) between a relational database and numerous analysis tools (such as HYPO71, FOCMEC, PREPROC, SIMUL, PITSA, etc.). The GIANT system is currently supported on SunOS, Solaris and Linux and uses the X11 windowing system and available via http://lbutler.geo.uni-potsdam.de/service.htm.

11.4.5 Other programs and ORFEUS software links

C. M. Valdés wrote the interactive analysis program PCEQ for IBM compatible PCs. It is widely used in conjunction with the location program HYPO71 for local events. The principal features are: picking P- and S-wave arrivals; filtering the seismogram for better P- and S-wave picks, and computing the spectra of selected seismogram sections. It is published in Volume 1 of the IASPEI Software Library (Lee, 1995).

Andrey Petrovich Akimov has written the program WSG (in English AWP: Automated workplace of seismologists), version 4.5 (in Russian). It works in an environment of Windows 95/98/NT and is used at single stations and seismic networks for estimating parameters from local, regional and teleseismic sources. The program converts different seismic data formats such as XDATA, PCC-1, CSS 2.8 and 3.0, DASS, CM6 GSE2 and can import via the TCP/IP protocol data from NRTS and LISS systems (miniSEED). The program and the program documentation in Russian is available via http://www2.gsras.ru/engl/mainms.htm.

ORFEUS (http://orfeus.knmi.nl/) presents a comprehensive list and links to available software in seismology. It concentrates on shareware. However, some relevant commercial sites are also included. Emphasis is laid on programs which run on UNIX/Linux platform.

11.5 Examples of seismogram analysis

The character of a seismogram depends on the source mechanism, the source depth, and whether the epicenter of the source is at local, regional or teleseismic distances. Seismograms of local earthquakes are characterized by short duration of the record from a few seconds to say one minute, higher frequencies, and a characteristic shape of the wave envelope, usually an exponential decay of amplitudes after the amplitude maximum, termed "coda" (see Figure 1b in DS 11.1 and Figure 2 in EX 11.1). In contrast, records at teleseismic distances show lower frequencies (because high-frequency energy has already been reduced by anelastic attenuation and scattering), and have a duration from say fifteen minutes to several hours (see Fig. 1.2). Regional events have intermediate features. The various wave groups, arriving at a station over different path, are called phases. They have to be identified and their parameters determined (onset time, amplitude, period, polarization, etc.). Phase symbols should be assigned according to the IASPEI recommended standard nomenclature of seismic phases. For phase names, their definition and ray paths see IS 2.1. Fig. 11.39 shows seismograms recorded at local, regional and teleseismic distances. They illustrate how the characteristics of seismic records vary with distance and depending on the source type. These characteristics will be discussed in more detail in the following sections.

There is no unique standard definition yet for the distance ranges termed "near" ("local" and "regional"), or "distant" ("teleseismic"; sometimes subdivided into "distant" and "very distant"). Regional variations of crustal and upper-mantle structure make it impossible to define a single distance at which propagation of local or regional phases stops and only teleseismic phases will be observed. In the following we consider a source as **local** if the direct crustal phases Pg and Sg arrive as first P- and S-wave onsets, respectively. In contrast, the phases Pn and Sn, which have their turning point in the uppermost mantle, are the first arriving P and S waves in the **regional** distance range. However, as discussed in 2.6.1 and shown in Fig. 2.40, the distance at which Pn takes over as first arrival depends on the crustal thickness, average wave speed and the dip of the crustal base. The "cross-over" distance x_{co} between Pn and Pg is - according to Eq. (6) in IS 11.1 for shallow (near surface) sources - roughly $x_{co} \approx 5 \times z_m$ where z_m is the Moho depth. Note, however, that as focal depth increases within the crust, x_{co} decreases, down to about $3 \times z_m$. Accordingly, the local distance range may vary from region to regions and range between about 100 km and 250 km. The CTBTO Technical Instructions (see IDC Documentation,1998) considers epicentral distances between 0° to 2°, where Pg appears as the primary phase, as local distance range.

The old Manual (Willmore, 1979) defines as near earthquakes those which are observed up to about 1000 km (or 10°) of the epicenter, and P and S phases observed beyond 10° as usually being **teleseismic** phases. However, regional phases such as Pn, Sn and Lg, will generally propagate further in stable continental regions than in tectonic or oceanic regions. According to the Earth model IASP91, Pn may be the first arrival up to 18°. The rules published in the IDC Documentation (1998) allow a transitional region between 17° and 20° in which phases may be identified as either regional or teleseismic, depending on the frequency content and other waveform characteristics. Accordingly, one might roughly define seismic sources as local, regional and teleseismic if their epicenters are less than 2°, between 2° and 20°, or more than 20° away from the station. Sometimes, the regional range is further subdivided into 2°-6°,where also the phase Rg may be well developed, and 6°-(17°)20° where only Sn and Lg are strong secondary phases. However, since we have not yet found good record examples with Pn beyond 15°, we will present and discuss our record examples for **near** (local and regional) and **teleseismic** sources in the ranges D ≤ 15° and D > 15°, respectively.
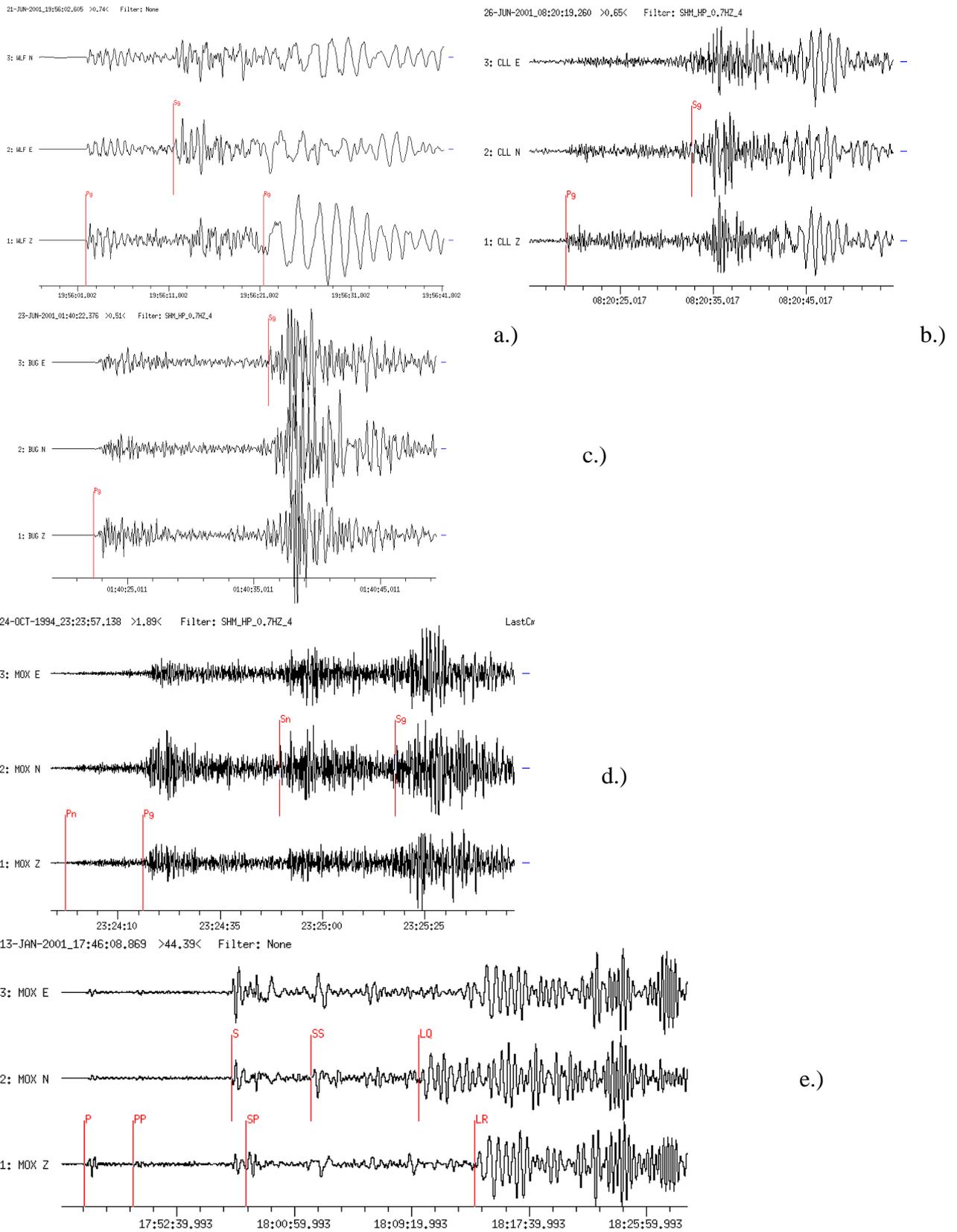
Fig. 11.39 Examples of 3-component seismograms recorded at a range of epicentral distances from one station: a) mining-induced earthquake (D = 80 km); b) quarry blast explosion (D = 104 km); c) local earthquake (D = 110 km); d) regional earthquake (D = 504 km); and e) teleseismic earthquake (D = 86.5°). Time scales are given below the records.

The methods used to analyze seismograms and to locate seismic sources depend on how close they are to the recording station. For near events different programs (ORFEUS software library; see 11.4.5) are used for source location. Differences in arrival times of phases and slowness and azimuth estimates from the plane-wave method or frequency-wavenumber (f-k) analysis can be used to locate distant sources with either array or network data. Time differences between phases often give reliable distance estimates and, together with azimuth determination from 3-component records, allow epicenters to be estimated from single station records (see EX 11.2). If depth phases are visible and can be identified, focal depth can be determined. Amplitude and period values of different phases are used for magnitude estimation. Both body waves and surface waves can be used to estimate magnitude.

11.5.1 Seismograms from near sources ($0° < D \leq 15°$)

Seismograms recorded at distances $D \leq 15°$ are dominated by P and S waves that have traveled along different paths through the crust and the uppermost mantle of the Earth. They are identified by special symbols for "crustal phases" (see IS 2.1). Pg and Sg, for example, travel directly from a source in the upper or middle crust to the station whereas the phases PmP and SmS have been reflected from, and the phases Pn and Sn critically refracted along (or beneath) the Moho discontinuity (see Fig. 11.40). Empirical travel-time curves are given in Exercise EX 11.1 (Figure 4) and a synthetic record section of these phases in Fig. 2.54. In some continental regions, phases are observed which have been critically refracted from a mid-crustal discontinuity or have their turning point in the lower crust. They are termed Pb (or P*) for P waves and Sb (or S*), for S waves, respectively. For shallow sources, crustal "channel-waves" Lg (for definition see IS 2.1) and surface waves Rg are observed after Sg-waves. Rg is a short-period Rayleigh wave ($T \approx 2$ s) which travels in the upper crust and is usually well developed in records of near-surface sources out to about 300 km and thus suitable for discriminating such events from local tectonic earthquakes (see Figs. 11.39a-c).
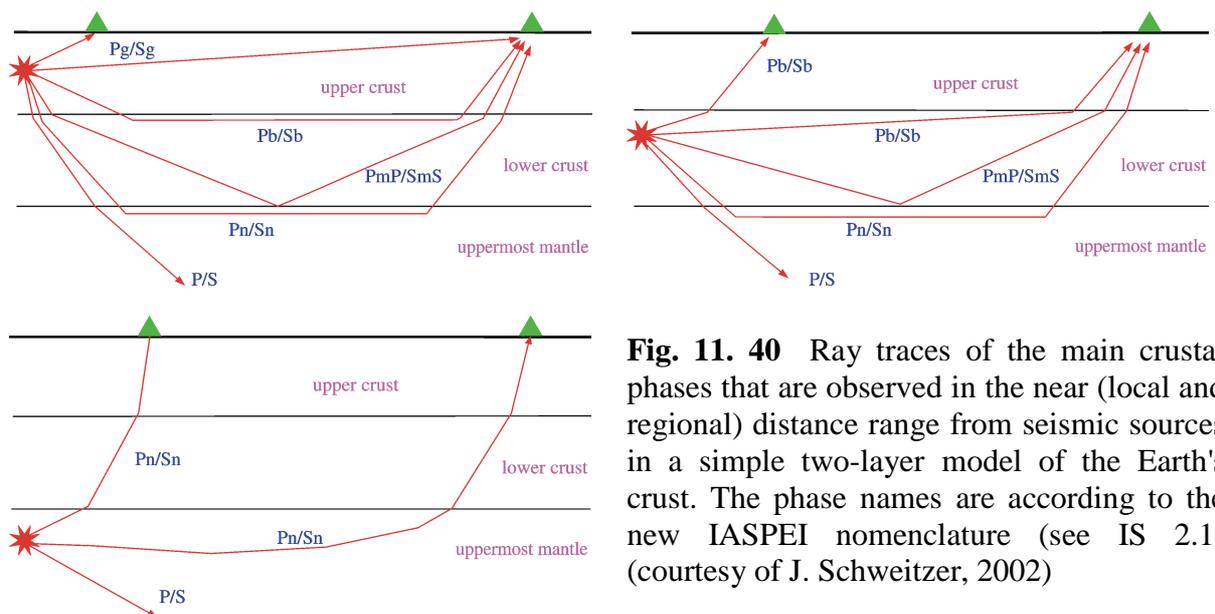
Fig. 11. 40 Ray traces of the main crustal phases that are observed in the near (local and regional) distance range from seismic sources in a simple two-layer model of the Earth's crust. The phase names are according to the new IASPEI nomenclature (see IS 2.1) (courtesy of J. Schweitzer, 2002)

Usually, Sg and SmS (the supercritical reflection, which often follows Sg closely at distances beyond the critical point; see Fig. 2.40) are the strongest body wave onsets in records of near seismic events whereas Pg and PmP (beyond the critical point) have the largest amplitudes in the early part of the seismograms, at least up to 200 – 400 km. Note that for sub-crustal earthquakes no reflected or critically refracted crustal phases exist. However, according to the new IASPEI nomenclature, P and S waves from sub-crustal earthquakes with rays traveling from there either directly or via a turning point in the uppermost mantle back to the surface are still termed Pn and Sn (see Fig. 11.40, lower left). At larger distances such rays arrive at the surface with apparent "sub-Moho" P and S velocities (see below).

Typical propagation velocities of Pg and Sg in continental areas are 5.5-6.2 km/s and 3.2-3.7 km/s, respectively. Note, that Pg and Sg are direct waves only to about 2° to 3°. At larger distances the Pg-wave group may be formed by superposition of multiple P-wave reverberations inside the whole crust (with an average group velocity around 5.8 km/s) and the Sg-wave group by superposition of S-wave reverberations and SV to P and/or P to SV conversions inside the whole crust. According to the new IASPEI phase nomenclature the definitions given for Lg waves and Sg at larger distances are identical, with the addition that the maximum energy of an Lg crustal "channel" wave travels with a group velocity around 3.5 km/s. In routine analysis, usually only the first onsets of these wave groups are picked without noting the change in character at larger distances. According to the Technical Instructions of the IDC Documentation (1998), stations of the CTBTO International Monitoring System (IMS) generally tend to name the strongest transverse arrival Lg and not Sg. A reliable discrimination is still a subject of research and not yet one of routine analysis and data reporting. Therefore, no simple and unique criteria for discrimination, which also depend on source type and propagation path, can be given here. They may be added to this Manual at a later time. Lg waves may travel in continental shield regions over large distances (see Fig. 2.15), even beyond 20° whereas Rg waves, which show clear dispersion and longer periods than Lg (see Fig. 2.16), are more strongly attenuated and generally not observed beyond 6°. The apparent velocities of Pn and Sn are controlled by the P- and S-wave velocities in the upper mantle immediately below the Moho and typically range between 7.5 - 8.3 km/s and 4.4 - 4.9 km/s, respectively.

Note: Seismograms from local and regional seismic sources are strongly influenced by the local crustal structure which differs from region to region and even between local stations. This may give rise to the appearance of other onsets (which may be strong) between the mentioned main crustal phases that can not be explained by a near-surface source in a single or two-layer crustal model. Some of these phases may relate to converted waves and/or depth phases such as sPmP (e.g., Bock et al., 1996). Also, at larger distances of up to about 30°, multiples such as PgPg, PbPb, PnPn, PmPPmP etc. and their related S waves may be well developed (see Fig. 11.19). However, usually these details can not be handled in routine data analysis and epicenter location and require specialized study. For routine purposes, as a first approximation, the IASP91 or AK135 global models (see DS 2.1) can be used for the analysis and location of near events based on the main crustal phases. However, one should be aware that crustal structure and velocities may differ significantly from region to region, and that the event location can be significantly improved when local travel-time curves or crustal models are available (see IS 11.1, Figures 11 and 12).

Fig. 11.41   shows seismograms of a shallow (h = 8 km) near earthquake from the Vogtland/NW Bohemia region in Central Europe, recorded at seven GRSN stations in the epicentral distance range 10 km (WERN) to 180 km (GEC2). Stations up to D = 110 km

(BRG) show only the direct crustal phases Pg, Sg, except GRFO, which in addition shows PmP. At GEC2 Pn arrives ahead of Pg with significantly smaller amplitude. The onset times of phases Pg, Sg and Pn were used to locate the epicenter of this event with a precision of about 2 km. If more stations close to the epicenter are included (e.g., Fig. 11.42; D = 6 – 30 km), the precision of the hypocenter location may be in the order of a few hundred meters.
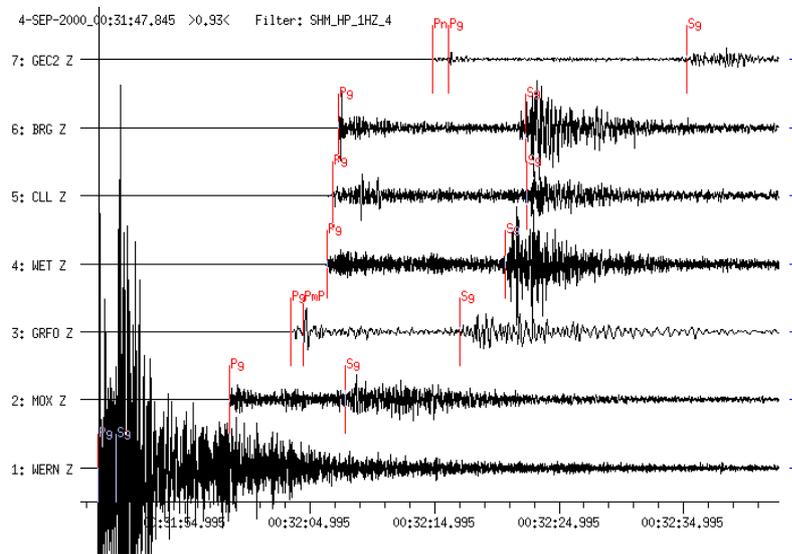

Fig. 11.41 Filtered short-period vertical component seismograms (4th order Butterworth high-pass filter, f = 1 Hz) from a local earthquake in the Vogtland region, 04 Sept. 2000 (50.27°N, 12.42°E; Ml = 3.3). Sampling rates at the stations differ: 80 Hz for MOX, WET, CLL, and BRG, 100 Hz for WERN and 20 Hz for GRFO and GEC2. Traces are sorted according to epicentral distance (from 10 to 180 km). The local phases have been marked (Pg and Sg at all stations, PmP at GRFO and Pn at the most distant station GEC2 (D = 180 km).
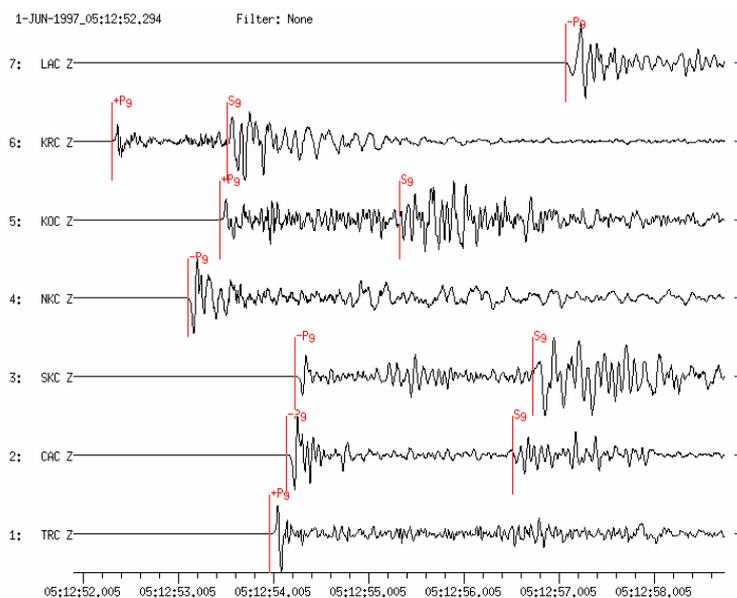
Fig. 11.42 Short-period recordings from stations of the local network of the Czech Academy in Prague from a small (Ml = 3.3) local earthquake in the German/Czech border region on June 1, 1997. The epicentral distance range is 6 km and 30 km. Such local networks allow hypocenters to be located to better than a few hundred meters.

Fig. 11.43 (left) shows for another Vogtland swarm earthquake, a record section with seismograms of 5 stations in the distance range 10 km to 130 km, together with the expected travel-time curves for Pg and Sg according to an average crustal model. Fig. 11.43 (right) shows some of the same seismograms on a map together with the station sites (triangles).
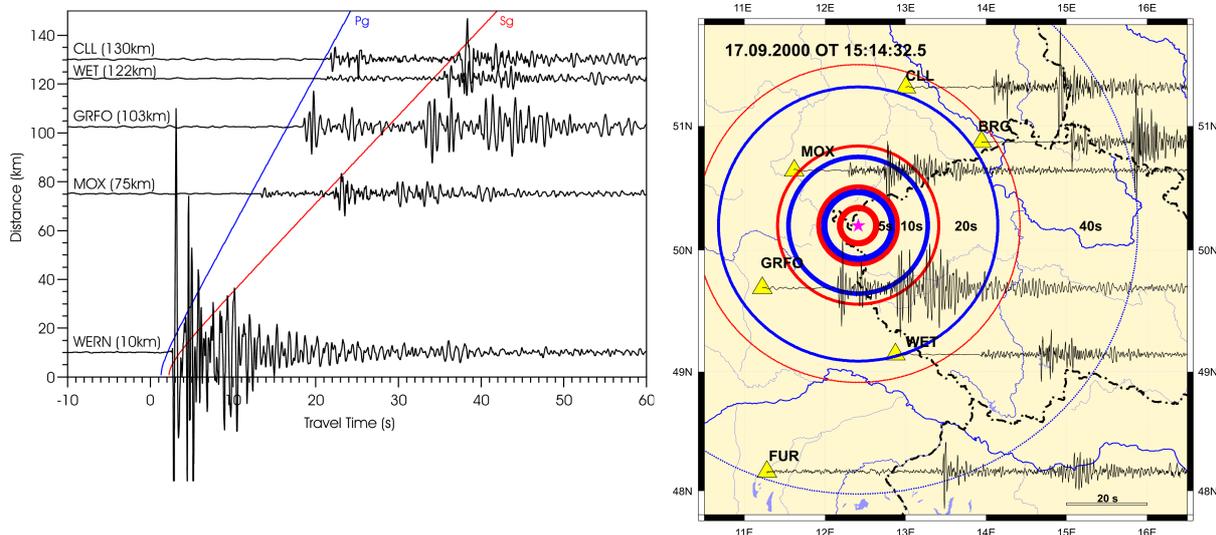
Fig. 11.43 Records of a Vogtland swarm earthquake (17 Sept. 2000; Ml = 3.1) at stations of a local network in Germany. Left: arranged by distance together with the expected travel times for Pg and Sg for an average crustal model; right: on a map view with station positions. The circles indicate the position of the wavefronts of Pg (blue) and Sg (red) after 5, 10, 20 and 40 s, respectively (see also file 1 in IS 11.3 and related animation on CD-ROM).

From these two figures the following conclusions can be drawn:

- at some stations the arrival times are in good agreement with the times predicted from an average crustal model, at other stations they are not, which implies crustal structure varies laterally; and
- the amplitude ratio Pg/Sg varies strongly with the azimuth because of the different radiation patterns for P and S waves. This variation can be used to derive the fault-plane solution of the earthquake (see Figs. 3.25 and 3.26 and section 3.4.4).

Other examples of local seismograms are shown in Figs. 11.44 and 11.45. Fig. 11.44 shows recordings from an earthquake in the Netherlands (Ml = 4.0) in the distance range 112 km to 600 km, and Fig. 11.45 those from a mining-induced earthquake in France (Ml = 3.7) in the range 80 km to 500 km. These records again show obvious variation in the relative amplitudes of Pn, Pg and Sg. The relative amplitudes depend on the distance and azimuth of the station relative to the radiation pattern of the source, and particularly with respect to the differences in take-off angles of the rays for the direct and the critically refracted waves (see Fig. 11.40). The source depth with respect to the major crustal discontinuities may also influence the relative amplitude ratio between these various phases.

Generally, for near-surface sources and distances smaller than about 400 km, Pn is much smaller than Pg (see also Figures 3a and 3c in Datasheet 11.1). For larger distances however, the relative amplitudes of Pn and Sn may grow so that these phases dominate the P and S

arrivals (see Fig. 2.15 and the uppermost traces in Figs. 11.44 and 11.45). This is not only because of the stronger attenuation of the direct waves that travel mostly through the uppermost heterogeneous crust but also because P and S near the critical angle of refraction at the Moho form so-called "diving" phases which are not refracted into the Moho but rather travel within the uppermost mantle with sub-Moho velocity. The recognition of these crustal body waves and the precision of onset-time picking can be significantly improved by stretching the time scale in digital records (compare Figures 3a and 3c in DS 11.1).

The great variability in the appearance of waveforms and relative amplitudes in near-earthquake recordings is also illustrated by Fig. 11.46. Even seismic records at the same station from two different sources at nearly the same distance and with similar azimuth may look very different. This may be because the waves from the two earthquakes travel along slightly different paths through the highly heterogeneous Alpine mountain range. However, the fault-plane orientation and related energy radiation with respect to the different take-off angles of Pn and Pg, may also have been different for these two earthquakes.
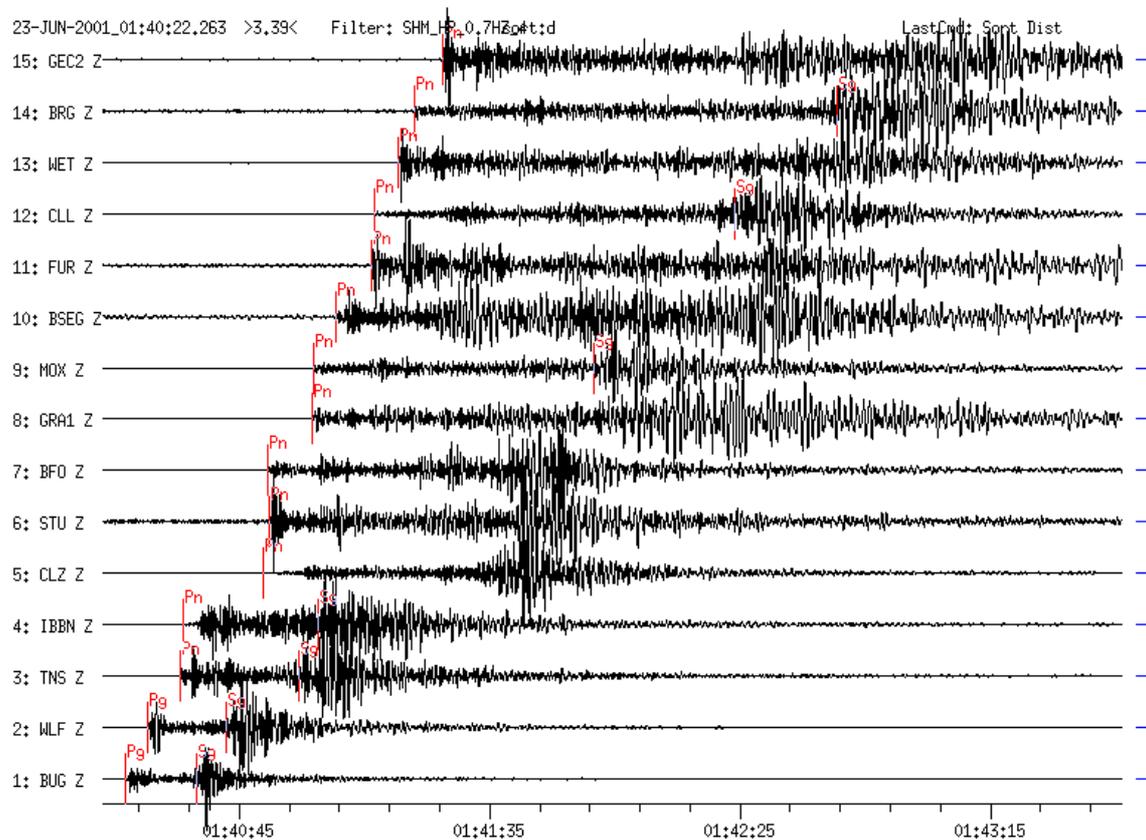
Fig. 11.44 Vertical-component short-period filtered broadband seismograms (4th order Butterworth high-pass filter, f = 0.7 Hz; normalized amplitudes) from a local earthquake at Kerkrade, Netherlands, recorded at 15 GRSN, GRF, GERES and GEOFON stations. Ml = 4.0; epicentral distances between 112 km (BUG) and 600 km (GEC2). Note the variability of waveforms and relative phase amplitudes of local/regional earthquakes in network recordings in different azimuths and epicentral distances. The suitability of filters for determination of local phase onsets has to be tested. Local magnitudes determined from a Wood-Anderson simulation.
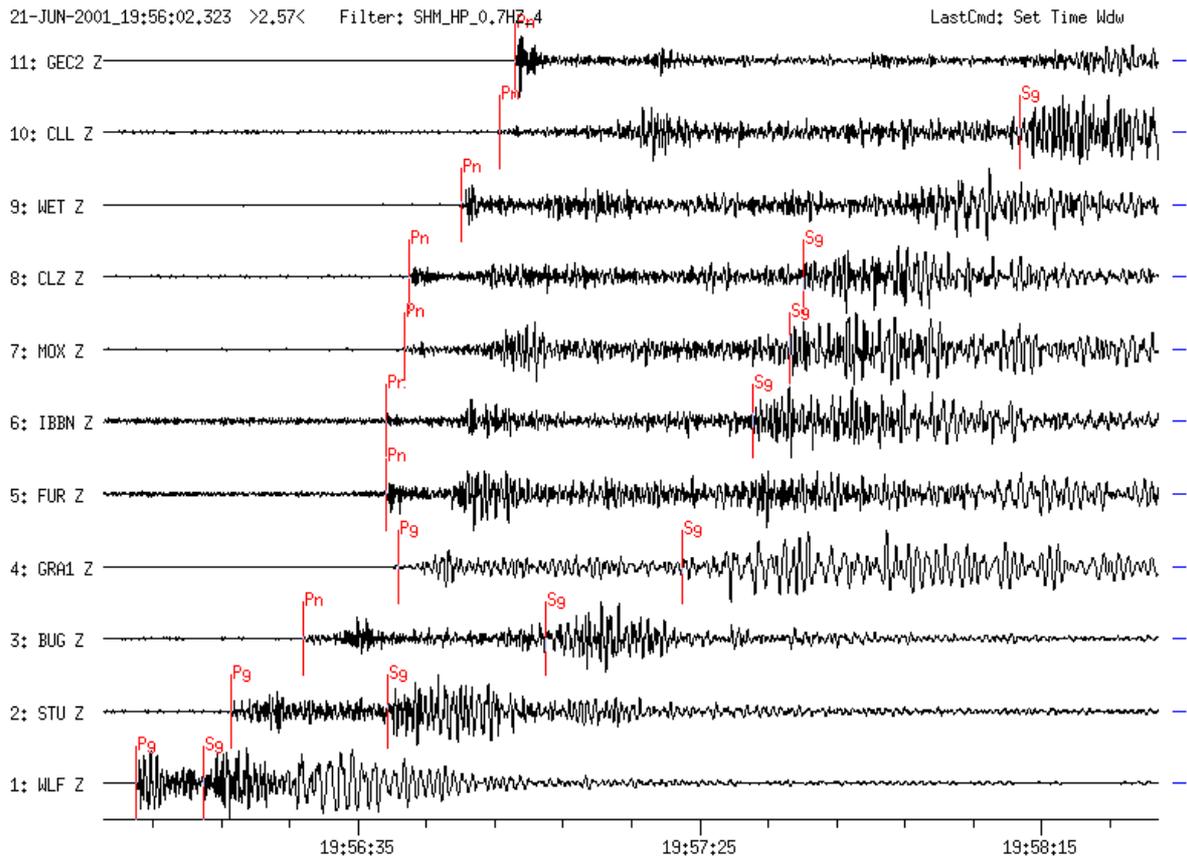
Fig. 11.45 Vertical-component short-period filtered BB seismograms (4th order Butterworth high-pass filter, f = 0.7 Hz, normalized amplitudes) from a local mining-induced earthquake at the French-German border recorded at 11 GRSN, GERES and GEOFON stations (Ml = 3.7; epicentral distances between 80 km (WLF) and 501 km (GEC2).

Note that in Figs. 11.39a and b and Fig. 11.45 (e.g., station WLF), the longer period Rg waves, following Sg, are particularly well developed in records of near-surface quarry blasts or shallow mining-induced earthquakes but not in the natural earthquake records (as in Fig. 11.43).

As mentioned above, at distances beyond about 600 to 800 km, Pn and Sn become the dominating body-wave onsets that for shallow sources are followed by well-developed surface-wave trains. Figure 6a in DS 11.1 shows a typical 3-component BB-velocity record of such an earthquake in Italy made at station GRA1 in Germany (D = 10.3°). Figure 6c shows the respective BB recordings of the same shock at 10 stations of the GRSN (D = 8°- 12°). Pg and Sg are no longer recognizable. In fact, Pn and Sn at these regional distances are no longer pure head waves from the Moho discontinuity but rather so-called diving phases of P and S which have penetrated into the uppermost mantle but travel also with the sub-Moho velocity of Pn of about 8 km/s. These diving phases may be of longer periods than Pn at shorter distances. One should also be aware that local and regional earthquakes do not only appear in short-period recordings. Strong near events with magnitudes above 4 usually generate also strong long-period waves (see Figs. 11.8 and 11.10).
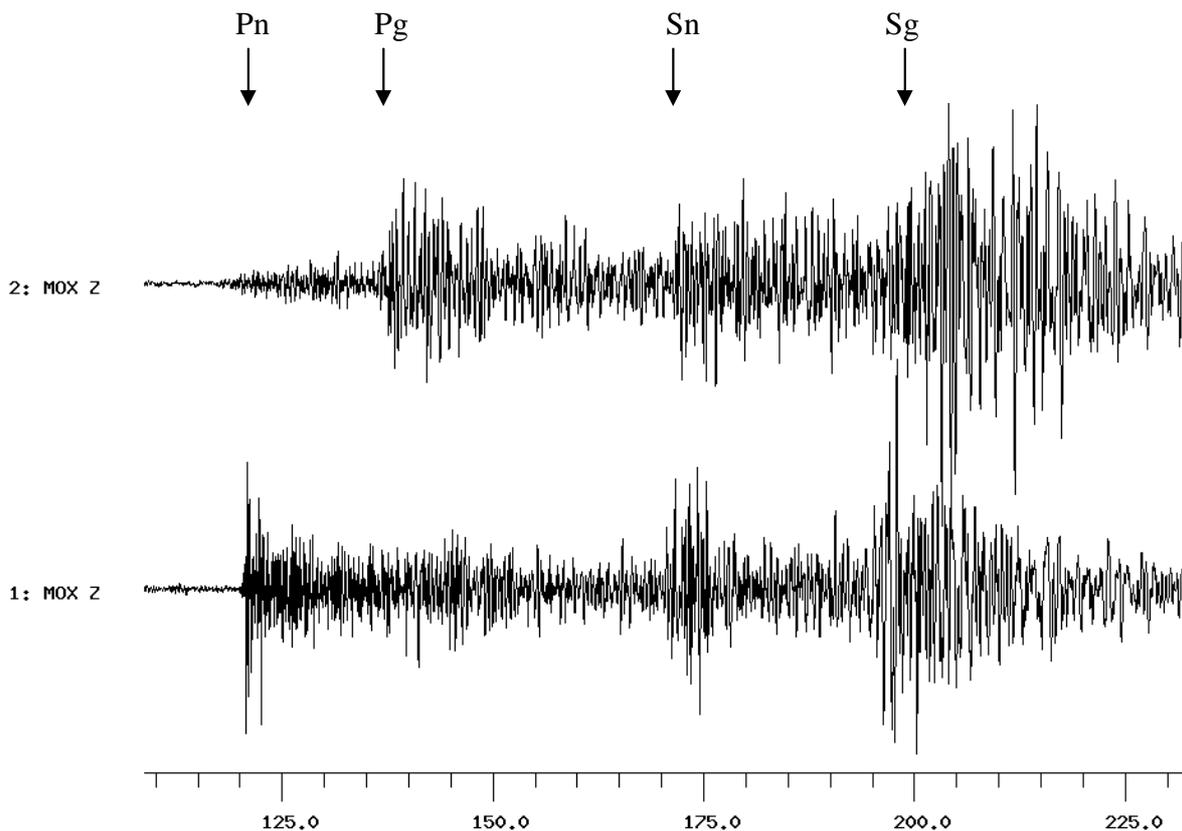
Fig. 11.46 Comparison of Z-component short-period filtered records at station MOX, Germany, of two earthquakes in Northern Italy (trace 1: 28 May 1998; trace 2: 24 Oct. 1994) at about the same epicentral distance (D = 505 km and 506 km, respectively) and with only slightly different backazimuth (BAZ = 171° and 189°, respectively). Note the very different relative amplitudes between Pn and Pg, due to either crustal heterogeneities along the ray paths or differences in rupture orientation with respect to the different take-off angles of Pn and Pg rays.

In general, regional stations and local networks complement each other in the analysis of smaller sources at local distances. Additionally, source processes and source parameters can be estimated using local station data. For this purpose, first motion polarities (compression c or +, dilatation d or -) for phases Pg, Pn, Sg and amplitude ratios (P/SV) should be measured for fault plane solution and moment tensor inversion (see 3.4 and 3.5). In regions with a poor station coverage, the mean precision of location may be several kilometers and source depths may then only be determined with teleseismic depth phases by way of waveform modeling (see 2.8).

An important aspect to consider in digital recordings and data analysis of local and regional seismograms is the sampling rate. Sampling with more than 80 s.p.s. is generally suitable for near seismic events. With lower sampling rate ssome of the most essential information about the seismic source process such as the corner frequency of the spectrum and its high-frequency decay, may be lost. Fig. 11.47 gives an example.
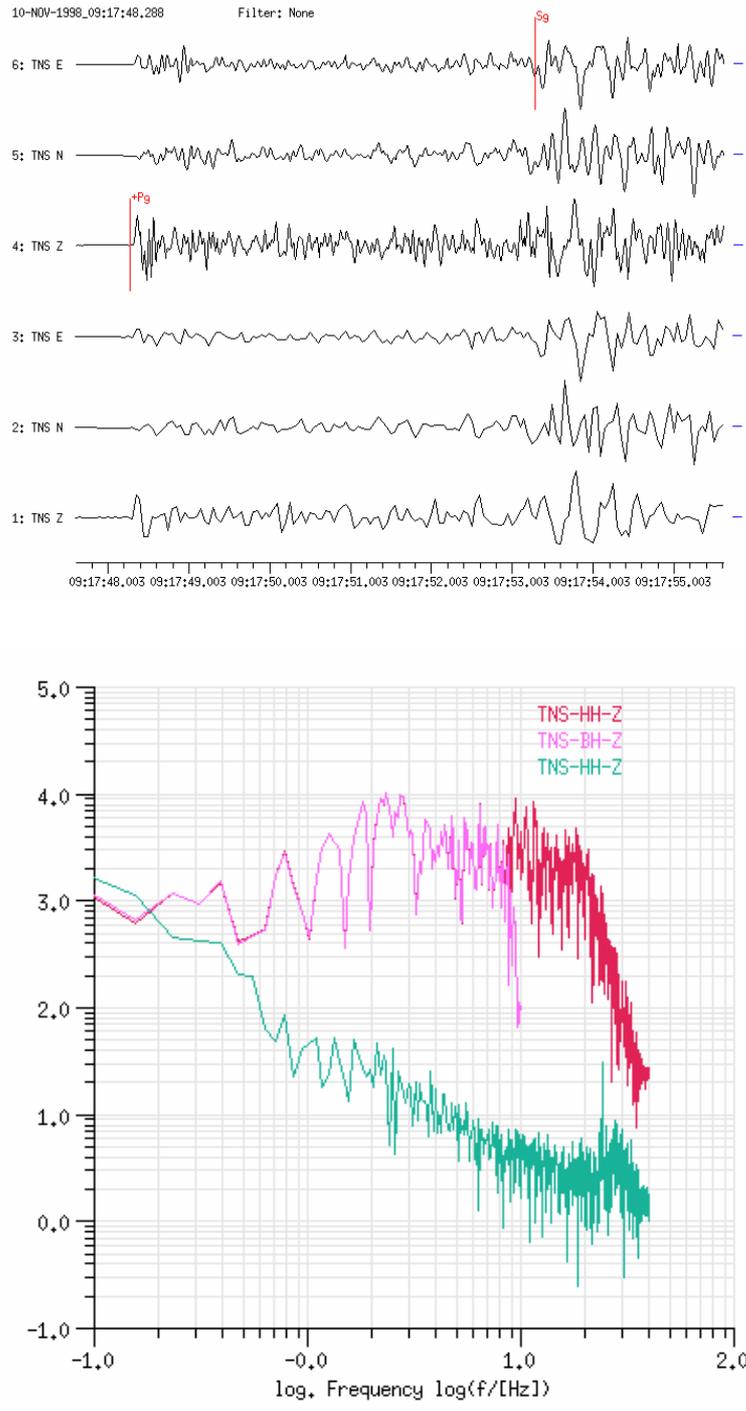
Fig. 11.47 Top: BB-velocity seismogram from a local earthquake near Bad Ems (11 Oct. 1998; Ml = 3.2) recorded at the GRSN station TNS (D = 40 km). Different sampling rates were used for data acquisition. Traces 1 – 3 were sampled at 20 Hz and traces 4 – 6 at 80 Hz. In the records with the higher sampling rate, the waveforms are much more complex and contain higher frequencies. The high frequency content is suppressed with the lower sampling rate. **Bottom:** Fourier spectrum of traces 1 (sampling rate 20 Hz – pink) and 4 (sampling rate 80 Hz – red). The lower sampling rate cuts off the high-frequency components of the seismic signal. Thus the corner frequency of the signal at about 20Hz and the high-frequency decay could not be determined from the pink spectrum. The green spectrum represents the seismic noise.

In the example considered in Fig. 11.47 only the 80 Hz data stream with a Nyquist frequency of 40 Hz allows the corner frequency near 20 Hz to be determined. However, in some regions, or when studying very small local earthquakes, still higher frequencies have to be analyzed. This may require sampling rates between 100 and 250 Hz.

Note, that besides the regional phases Sn and Lg the teleseismic phase PcP also may be observed in the far regional distance range (6°-20°) in short-period seismograms of strong events (Ml > 4). PcP, which gives a good control of source depth, can be identified in array recordings because of its very small slowness.

In Box 1 below a summary is given of essential features that can be observed in records of local and regional seismograms. For more records in this distance range see DS 11.1.

BOX 1: General rules for local and regional events

- The frequency content of local events (D < 2°) is usually high (f ≈ 0.2 - 100 Hz). Therefore they are best recorded on SP or SP-filtered BB instruments with sampling rates f ≥ 80 Hz. The overall duration of short-period local and regional (D < 20°) seismograms ranges between a few seconds and to several minutes.
- Strong local/regional sources radiate long-period energy too and are well recorded by BB and LP seismographs. In the far regional range the record duration may exceed half an hour (see Fig. 1.2).
- Important seismic phases in seismograms of local sources are Pg, Sg, Lg and Rg and in seismograms of regional sources additionally Pn and Sn, which arrive beyond 1.3°-2° as the first P- and S-wave onsets. The P waves are usually best recorded on vertical and the S waves on horizontal components.
- Note that Pg is not generally seen in records from sources in the oceanic crust. Also, deep (sub-crustal) earthquakes lack local and regional crustal phases.
- For rough estimates of the epicentral distance D [km] of local sources, multiply the time difference Sg-Pg [s] by 8, and in the case of regional sources the time difference Sn-Pn [s] by 10. For more accurate estimates of D use local and regional travel-time curves or tables or calculations based on more appropriate local/regional crustal models.
- The largest amplitudes in records of local and regional events are usually the crustal channel waves Lg (sometimes even beyond 15°), and for near-surface sources the short-period fundamental Rayleigh mode Rg. For near-surface explosions or mining-induced earthquakes, Rg, with longer periods than Sg, may dominate the record, however usually not beyond 4°.
  - For routine analysis the following station/network readings should be made: (1) the onset time and polarity of observed first motion phases; (2) onset times of secondary local and regional phases; (3) local magnitude based either on maximum amplitude or duration. If local/regional calibration functions, properly scaled to the original magnitude definition by Richter (1935), are not available it is recommended to use the original Richter equation and calibration function, together with local station corrections.

11.5.2 Teleseismic earthquakes (15° < D < 180°)

11.5.2.1 Distance range 15° < D ≤ 28°

At distances beyond 15°, sometimes referred to as "far-regional", Pn and Sn amplitudes become too small (except in some shield regions) and the first arrival phase has a travel path through deeper parts of the upper mantle. The common nomenclature for these waves with longer periods than Pn and Sn is P and S, respectively. For the next 12°, the records look rather simple in one respect, namely, that only three major wave groups are recognizable (P, S, and surface waves, see Fig. 11.48).
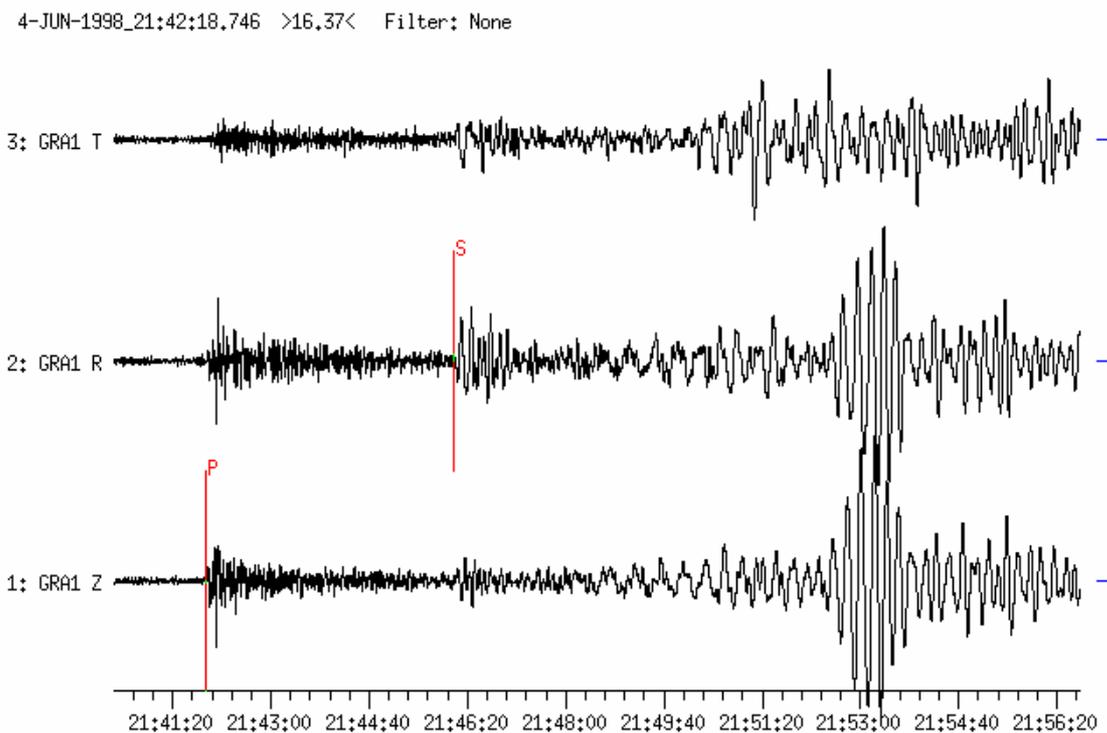
Fig. 11.48 Three-component broadband seismograms from an earthquake in Iceland on 04 June 1998, recorded at GRF-array station GRA1 (D = 22.5°). P, S and surface waves are recognizable. Horizontal traces have been rotated (R = Radial, T = Transverse) with R showing into the source direction. The overall duration of the record is about 15 min.

The body-wave groups themselves, however, are rather complicated because of the refraction and reflection of P and S at the pronounced velocity increase at the bottom of the upper mantle (410 km discontinuity) and at the bottom of the transition zone to the lower mantle (660 km discontinuity). These strong increases/gradients in wave velocity give rise to the development of two triplications of the P-wave travel-time curve with prograde and retrograde branches which in some distance ranges follow closely each other (see Fig. 2.29), thus forming a sequence of successive P- (and S-) wave onsets (see Fig. 11.49). The largest amplitudes occur in the range of the left-side cusp of the 660 km discontinuity triplication (P660P) between about 18° and 20° (also termed "20°-discontinuity") but with weaker P-wave first arrivals some 5 to 10 s earlier. Accordingly, small differences in epicentral distance

can lead to large differences in the appearance of the body-wave groups in seismic records (see Fig. 11.49). Generally, P waves are rather complex and wave onsets emergent. Surface waves of shallow earthquakes, however, are strong, clearly separated from S waves and very useful for surface wave magnitude (Ms) estimation.

Fig. 11.49 shows BB-velocity seismograms from an earthquake in Turkey recorded at stations of the GRSN in the distance range between about 14.5° and 19.5°. Note the increase of the P-wave amplitudes with distance when approaching "20°-discontinuity".
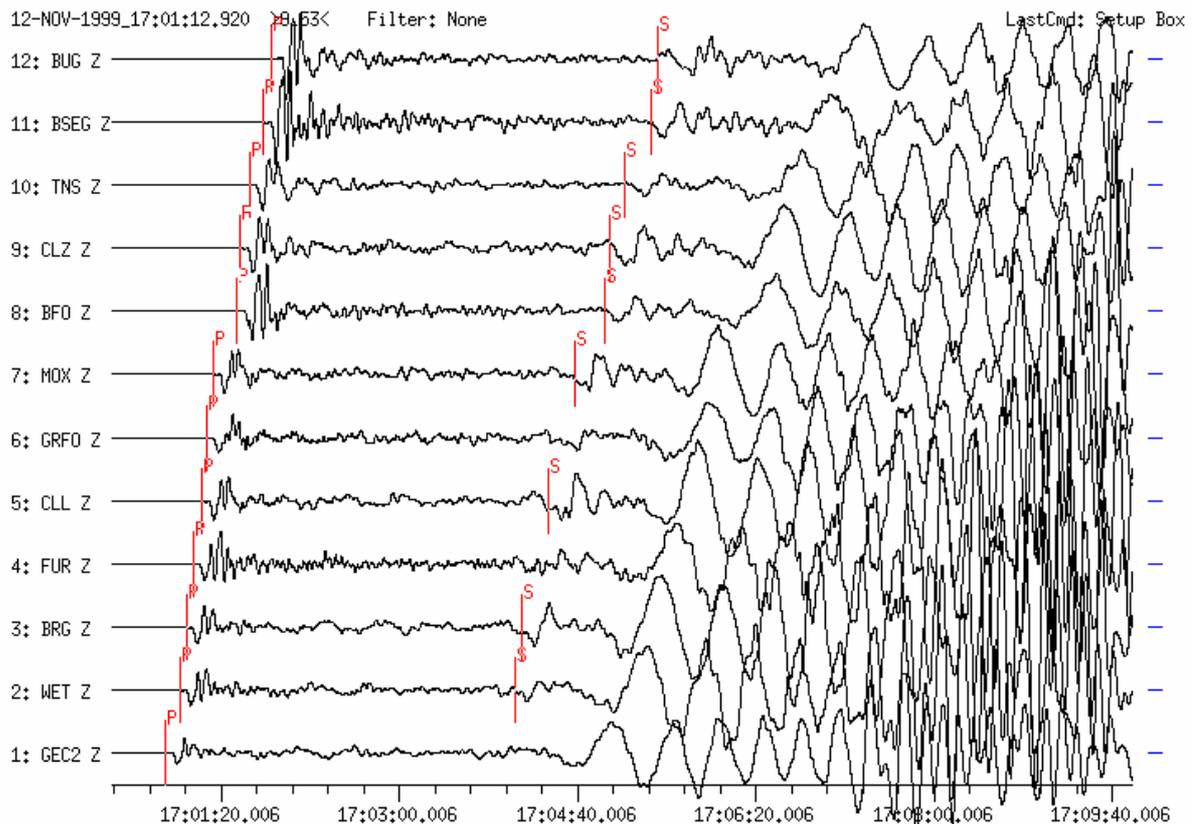
Fig. 11.49 Vertical-component BB-velocity seismograms from the damaging earthquake in Düzce, NW-Turkey, recorded at 12 GRSN-stations in the distance range 14.5° to 19.5°. (Source data from NEIC-QED: 12 Nov. 1999, OT 16:57:20; 40.79°N, 31.11°E; h = 10 km; Mw = 7.1; D = 16.5° and BAZ = 115° from GRFO). Traces are sorted according to distance. Incoherent and complex P waves are followed by weak S waves and distinct and clearly dispersed surface waves, which have longer periods than the S waves. The body waves P and S are affected by upper mantle discontinuities. Note the increase in P-wave amplitudes with distance due to the cusp of P660P around 18° to 19° (see Fig. 2.29).

Fig. 11.50 shows 3-component records (Z, R, T) demonstrating the presence of the 20° discontinuity in another part of the world. The seismograms are from an earthquake that occurred in the southern part of the New Hebrides at 35 km depth, recorded between 16.9° and 23.6° by a regional network of portable broadband instruments deployed in Queensland, Australia (seismometers CMG3ESP; unfiltered velocity response). The complex P wavelets

appear in Z and R only. In their later parts they may contain PnPn arrivals. Similarly complex S-wave groups appear in R and T, and may include SnSn.
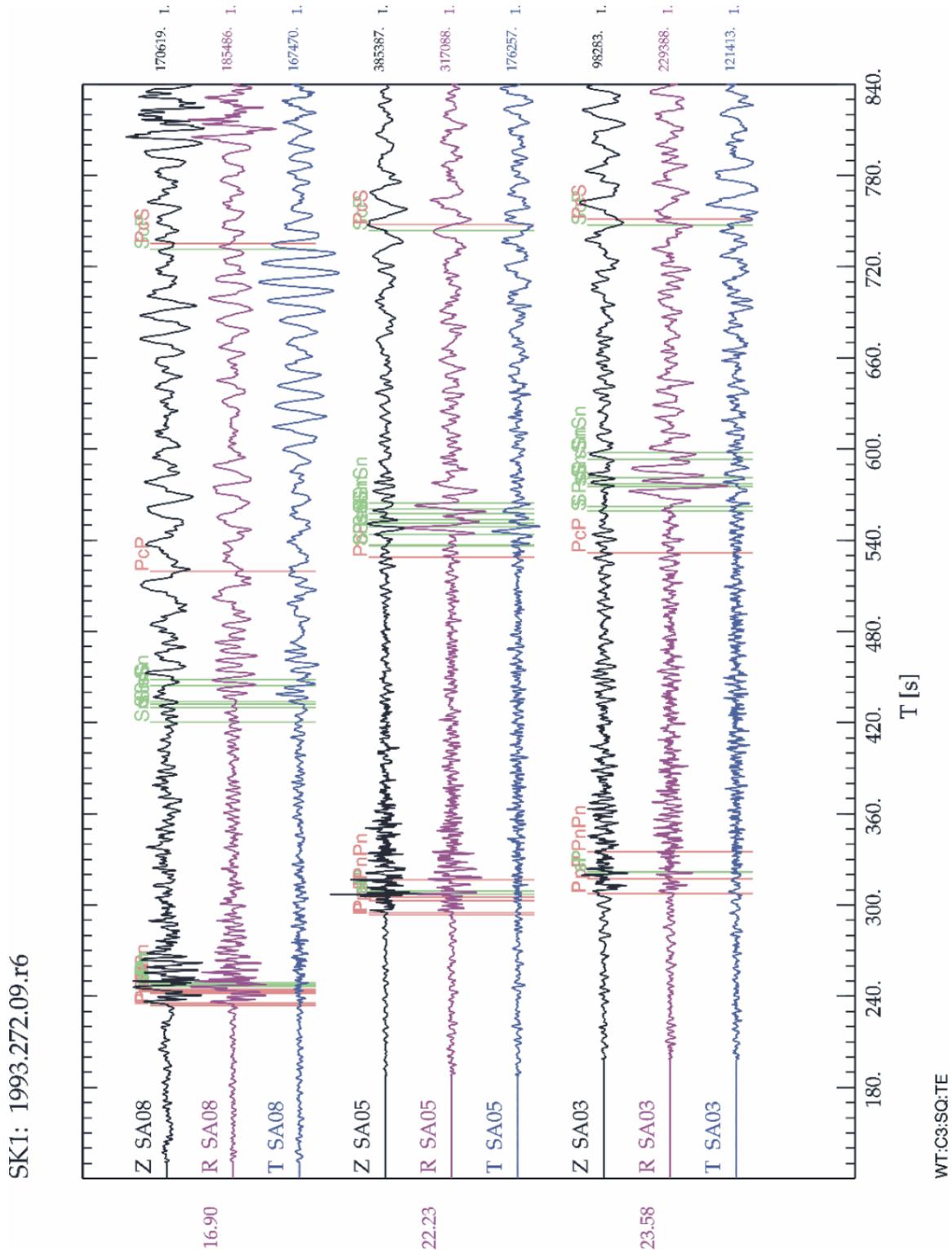
Fig. 11.50 Three-component BB records made in Queensland, Australia, from an earthquake in the New Hebrides between D = 16.9° and 23.6°. Note the complexity of P- and S-wave arrivals around the 20° discontinuity. On each set of records the predicted phase arrival times for the AK135 model (see Fig. 2.53) are shown as faint lines. However, there might be no

clear onset visible at these times above the noise or signal-coda level of previous phases. Never use such theoretical onset marks for picking onset times! (Courtesy of B.L.N. Kennett).

11.5.2.2 Distance range 28° < D ≤ 100°

The main arrivals at this distance range up to about 80°, have traveled through the lower mantle and may include reflections from the core-mantle boundary (CMB) (Fig. 11.53). The lower mantle is more homogeneous than the upper mantle (see Fig. 2.53). Accordingly, P and S waves and their multiples form rather simple long-period seismograms (Figs. 11.9 and 11.52; see also files 4 and 5 in IS 11.3 and animation on CD-ROM). Between 30° and 55°, the waves reflected from the core (e.g., PcP, ScP etc.) are also often recorded as sharp pulses on short-period records, particularly on records of deep earthquakes where depth phases appear well after the core reflections (see Fig. 11.16). At around 40°, the travel-time curve of PcP intersects those of PP and PPP (see Fig. 11.53) and in horizontal components PcS intersects S, and ScS intersects SS and SSS. This complicates proper phase separation, at least for the later phases on long-period records, where SS and SSS may be strong. ScP, however, may also be rather strong on short-period vertical components (see Fig. 11.53). Note that PP, PS, SP and SS are Hilbert-transformed (see 2.5.4.3). Their onset and amplitude picks can be improved by inverse Hilbert transformation, which is part of modern analysis software such as Seismic Handler (SH and SHM). The amplitudes of the core reflections decrease for larger distances but they may be observed up to epicentral distance of about 80° (ScP and ScS) or 90° (PcP), respectively, beyond which ScS merges with the travel-time curves of SKS and S and PcP with that of P (compare travel-time curves in Figure 4 of EX 11.2 with Figs. 11.16 and 11.55).
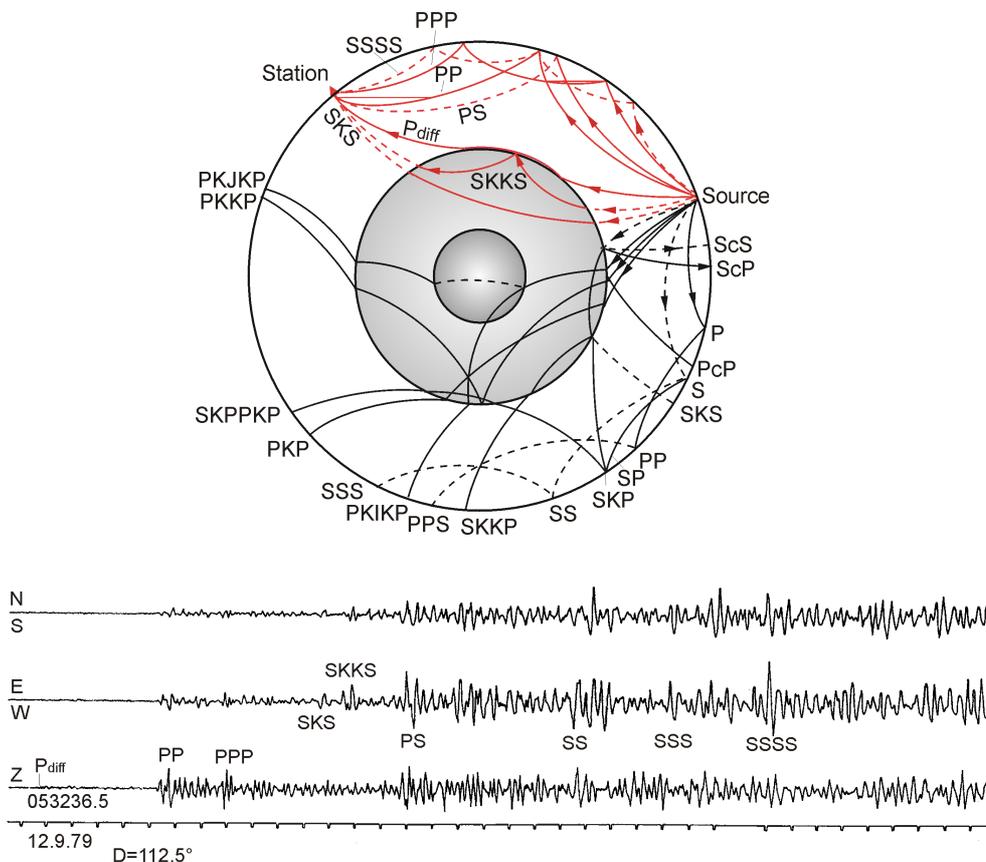
Fig. 11.51 Seismic ray paths through the mantle and core of the Earth with the respective phase names according to the international nomenclature (see Fig. 2.48 and overlay for related

travel-time curves, and IS 2.1 for phase names and their definition). The red rays relate to the 3-component analog Kirnos SKD BB-displacement record of body waves from an earthquake at D = 112.5° at station MOX, Germany.
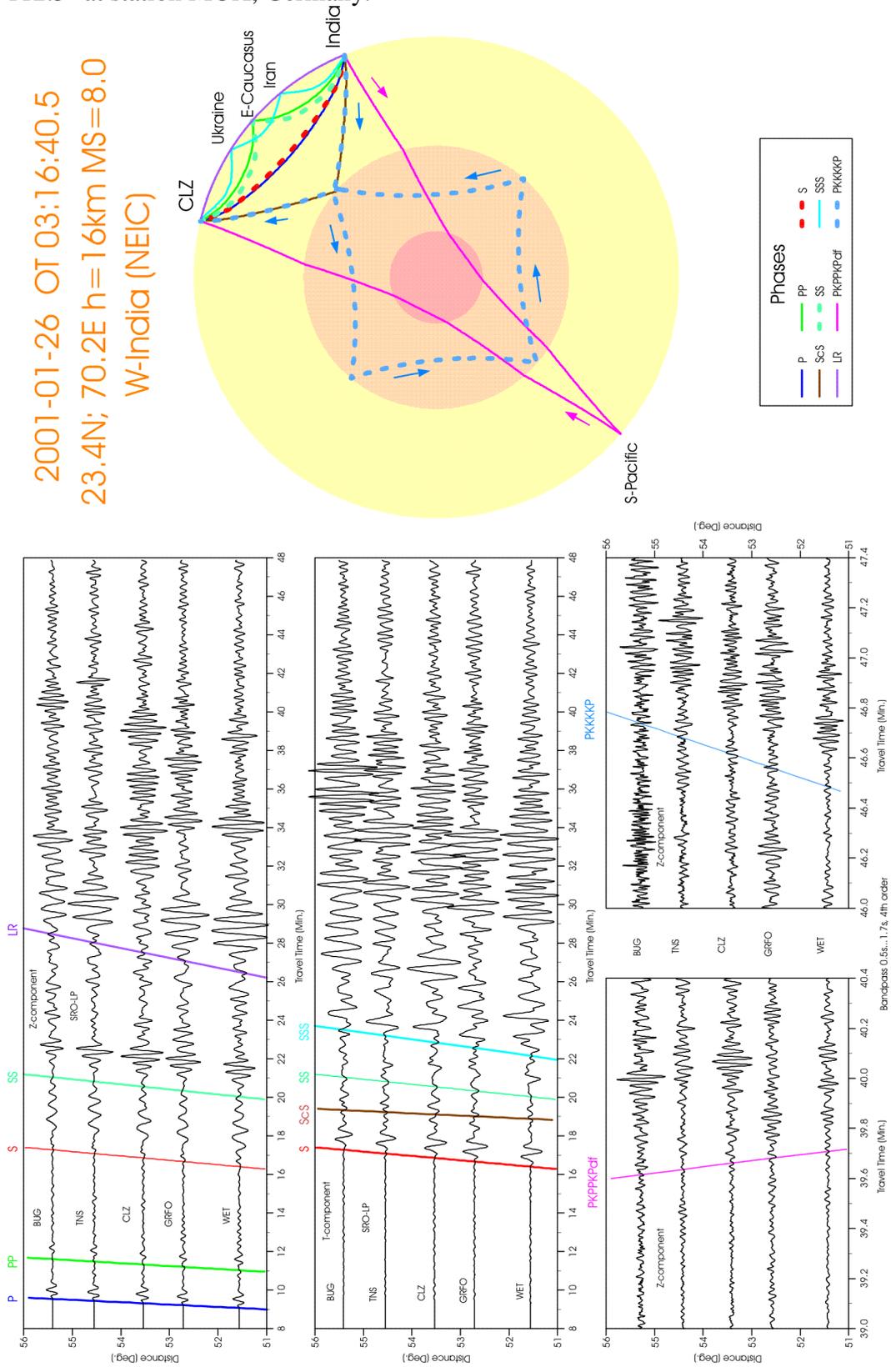

Fig. 11.52 Long-period Z- (left) and T-component seismograms (middle) of a shallow earthquake in western India recorded in the distance range 51° to 56° at stations of the GRSN.

Two cutout sections from short-period Z-component records of multiple core phases are shown on the right and the related ray paths at the top (for animation see file 4 in IS 11.3).
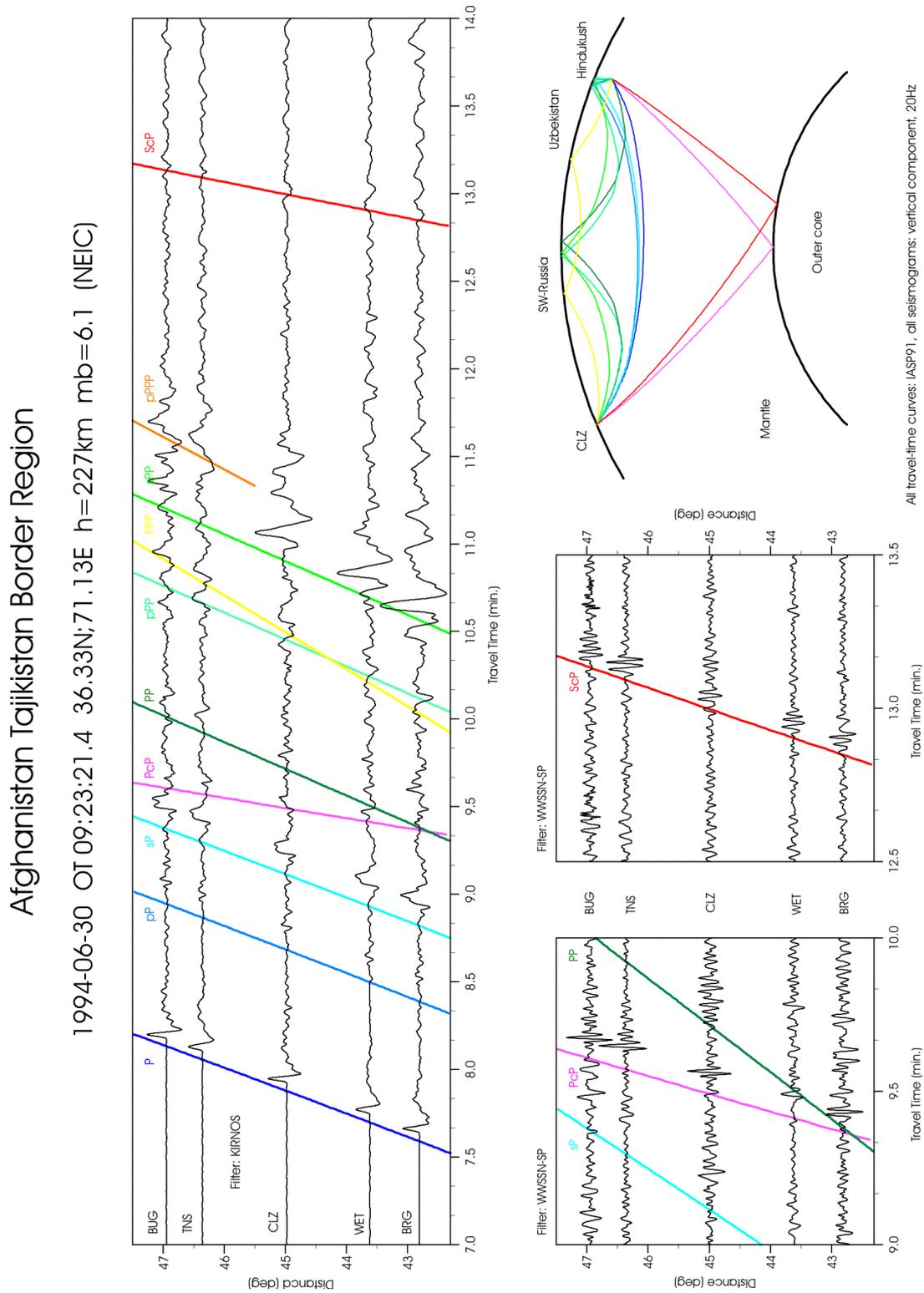
Fig. 11.53 Vertical-component Kirnos SKD BB-displacement (left) and WWSSN-SP seismograms (right) from an intermediate depth (h = 227 km) earthquake in the Afghanistan-Tajikistan border region recorded at stations of the GRSN. Besides P the depth phases pP, sP, pPP, sPP and pPPP and the core reflections PcP and ScP are clearly visible, particularly on

the short-period records. The ray traces of these phases are shown in the upper right corner (see also file 3 in IS 11.3 and related animation on CD-ROM).

Fig. 11.54 shows the ray paths for S, ScS and SKS and their related travel-time curves according to the IASP91 model for the whole distance range from 60° to 180° and Fig. 11.55 both short- and long-period records for these waves between 50° and 80°.

S/Sdif, ScS, SKSac/SKSdf
Raypaths and traveltime-curves (IASP91, h=0km)
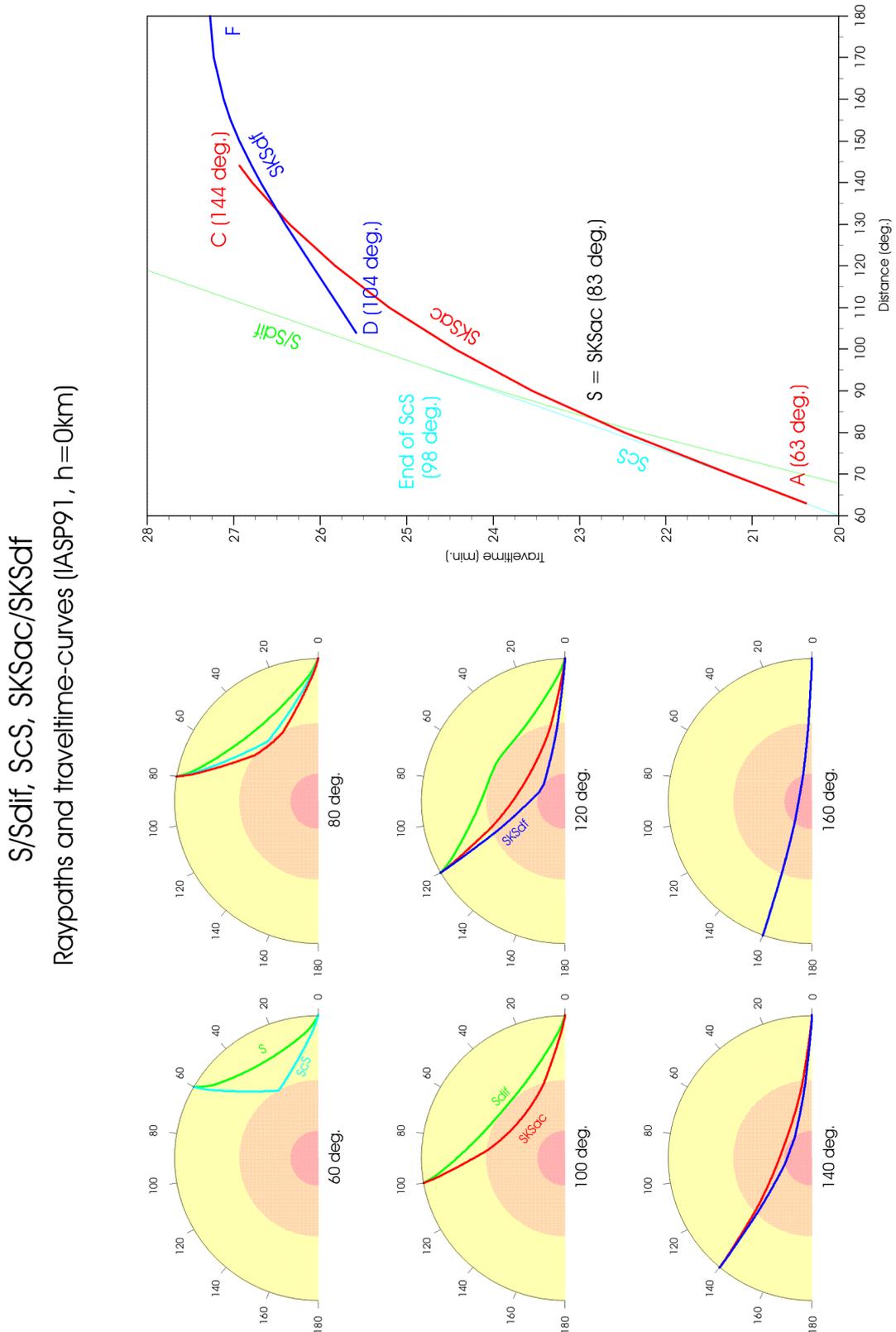
Fig. 11.54 Ray paths for S, ScS and SKS and their related travel-time curves according to the IASP91 model for the whole distance range from 60° to 180°.
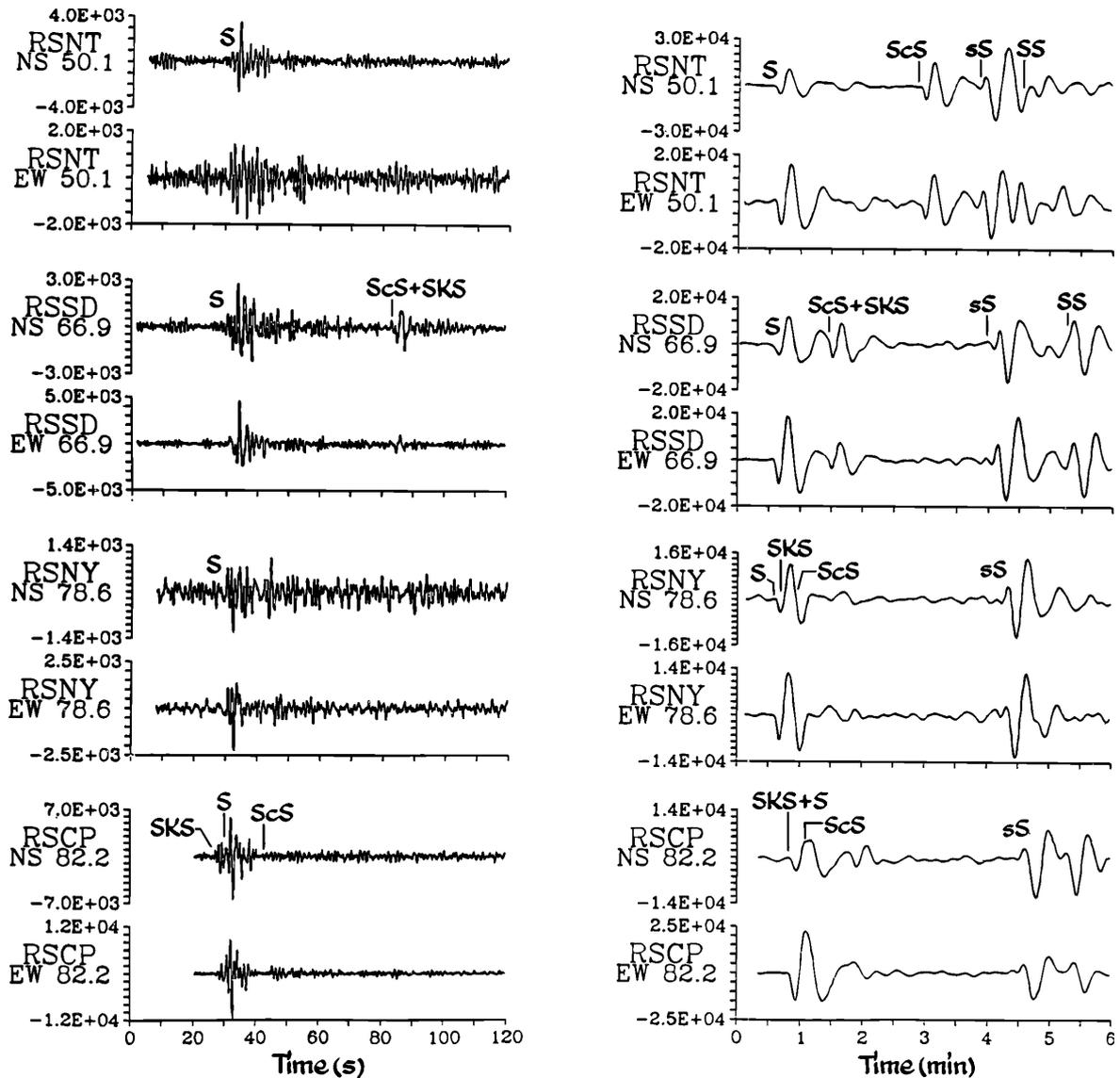
Fig. 11.55 SP (left) and LP (right) horizontal-component seismograms from a deep-focus earthquake in the Sea of Okhotsk (20 April 1984, mb = 5.9, h = 588 km) recorded by stations in the distance range 50.1° to 82.2°. Note the different amplitude scaling. Accordingly, the amplitudes of various transverse phases are 2 to 10 times larger in long-period records when compared with short-period records. Four distinct phases are identified: S, ScS, sS and SS. SKS, which emerges at distances larger than 60° however, overlaps with ScS between about 65° and 75°. S, ScS and SKS start to coalesce as distance increases toward 82°. Beyond this distance SKS arrives before S, SKKS and ScS (reprinted from Anatomy of Seismograms, Kulhánek, Plate 40, p.137-138; © 1990; with permission from Elsevier Science).

Arrays and network records, which also allow f-k and vespagram analysis are very useful for identifying the core reflections PcP, ScP and ScS because their slownesses differ significantly from those of P, S and their multiple reflections (see Fig. 11.52 as well as Figures 6a and b

and 7b in DS 11.2). Surface reflections PP, PPP, SS and SSS are well developed in this distance range in long-period filtered records and converted waves PS/SP at distances above 40°. Sometimes the surface reflections are the strongest body-wave onsets at large distances (see Figures 10c and 11b in DS 11.2). Their identification can be made easier when network records are available so vespagram analysis can be used (e.g., Figure 11c in DS 11.2). In short-period filtered network records it is sometimes also possible to correlate well in this distance range multiple reflected core phases such as PKPPKP or P'P', SKPPKP and even SKPPKPPKP (see Fig. 1.4).

Beyond 83° SKS moves ahead of S and its amplitude relative to S increases with distance. Network and array analysis yields different slowness values for S and SKS because of their diverging travel-time curves (see Fig. 11.54). This helps to identify these phases correctly. Note that the differential travel time SKS-P increases only slowly with distance (see Figure 4 in EX 11.2). Misinterpretation of SKS as S may therefore result in an underestimation of D by up to 20°! Since SKS is polarized in the vertical plane it can be observed and separated well from S in radial and vertical components of rotated seismograms (see Figures 10c, 13e, 14e, and 15b in DS 11.2). The same applies for PcS and ScP, which are also polarized in the vertical plane in the direction of wave propagation.

In the distance range between about 30° and 105° multiple reflected core phases P'N or between about 10° < D° < 130° the phases PNKP, with N-1 reflections either at the free surface (P'N) or from the inner side of the core-mantle boundary (PNKP) may appear in short-period records some 13 min to 80 min after P. An example for PKPPKP (P'P') and PKKKKP (P4KP) is given in Fig. 11.52. These phases are particularly strong near caustics, e.g., P'P' (see Fig. 11.69) and P'P'P' (P'3) near 70° and PKKP near 100° (see Fig. 11.71) but they are not necessarily observable at all theoretically allowed distances. Figures 9 and 10 in EX 11.3, however, document the rather wide distance range of real observations of these phases at station CLL (for P'P' between 40° and 105° and for PKKP between 80° and 126°). Note the different, sometimes negative slowness of these phases. More record examples, together with the ray paths of these waves, are presented in a special section on late core phases (11.5.3). For differential travel-time curves PKKP-P and PKPPKP-P see Figures 9 and 10 in EX 11.3. Also PKiKP, a weak core phase reflected from the surface of the inner core (ICB), may be found in short-period array recordings throughout the whole distance range, about 4.5 to 12 min after P. Its slowness is less than 2s/°. Beyond 95°, P waves show regionally variable, fluctuating amplitudes. Their short-period amplitudes decay rapidly (see Fig. 3.13) because of the influence of the core (core-shadow) while long-period P waves may be diffracted around the curved core-mantle boundary (Pdif, see Figs. 11.59 and 11.63 as well as Figures 1, 2, 4b and 6c and b in DS 11.3).

In any event, comprehensive seismogram analysis should be carried out for strong earthquakes which produce many secondary phases. Unknown phase arrivals should also be reported for further investigations into the structure of the Earth. When reporting both identified and unknown phases to international data centers the IASPEI-proposed international nomenclature should strictly be observed (see IS 2.1).

11.5.2.3 Distance range 100°< D ≤ 144°

Within this distance range, the ray paths of the P waves pass through the core of the Earth. Due to the large reduction of the P-wave velocity at the core-mantle boundary (CMB) from

about 13.7 km/s to 8.0 km/s (see Fig. 2.53) seismic rays are strongly refracted into the core (i.e., towards the normal at this discontinuity). This causes the formation of a "core shadow". This "shadow zone" commences at an epicentral distance around 100°. The shadow edge is quite sharp for short-period P waves but diffuse for long-period P and S waves that are diffracted around the curved CMB (compare Figures 6b and c as well as 7a and b in DS 11.3).
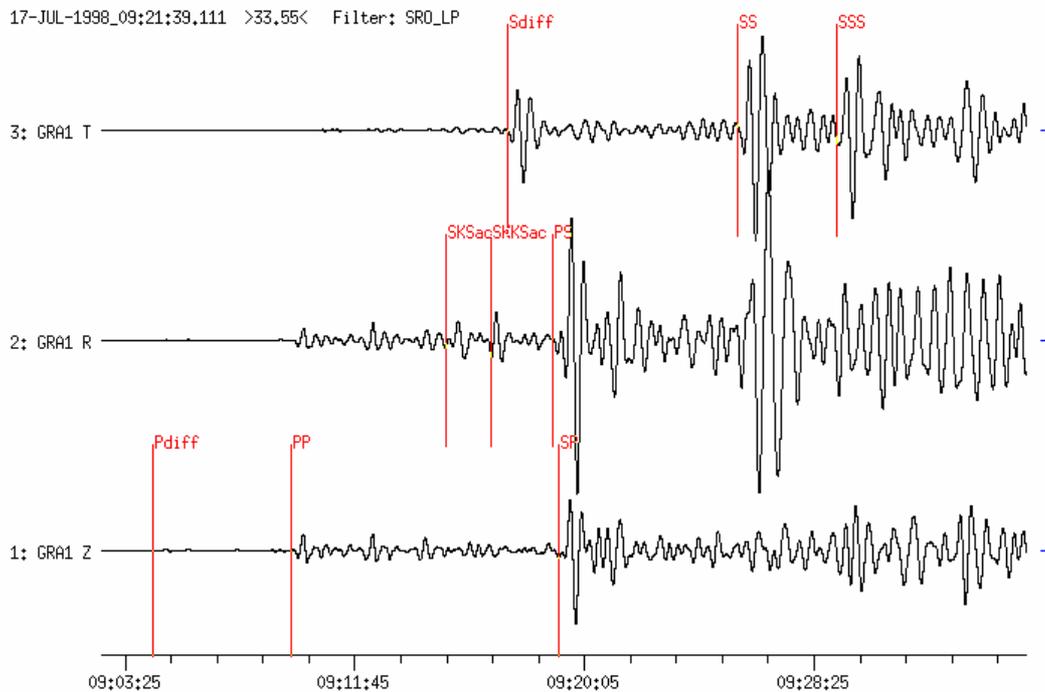
For strong earthquakes Pdif and Sdif may be observed out to distances of about 150° (see Figs. 11.56, 11.59 and 11.63).

Fig. 11.56 SRO-LP filtered 3-component seismograms at station GRA1, Germany, in D = 117.5° from an earthquake in Papua New Guinea (17 July 1998, Ms = 7.0). The N and E components have been rotated into the R and T directions. Phases Pdif, PP, PPP (not marked) and a strong SP are visible on the vertical component, whereas the phases SKS, SKKS and PS, which are polarized in the vertical propagation plane, are strong on the radial (R) component (as are PP and PPP). Sdif, SS and SSS are strong on the transverse (T) component. Note that Pdiff and Sdiff are still acceptable alternative phase names for Pdif and Sdif.

Fig. 11.57 shows rotated (R-T) horizontal component SRO-LP recordings at GRSN stations from two intermediate deep events in the Chile-Bolivia border region and in the Mariana Islands, respectively. The related ray paths are depicted in the upper part. The records cover the transition from the P-wave range into the P-wave core shadow. Magnified cut-outs, also of the related Z-component records, are presented for both earthquakes in Figures 1 and 2 of DS 11.3. They show more clearly the first arriving longitudinal waves and their depth phases. The following conclusions can be drawn from a comparison of these figures:

- Pdif arrives about 4 minutes (at larger distance up to 6 min; see Fig. 11.63) earlier than the stronger PP;
- The largest phases (see also Fig. 11.60) are usually PP, PPP, PS, SP, Sdif, SKS, SKKS, SS and SSS;

- SKS is the first arriving shear wave, followed by SKKS, SP or PS (and the related depth phases), all on the R component;
- S/Sdiff and SS may be strong(est) in T or R, or even in both components, depending on the SV/SH ratio of shear-wave energy radiated by the source.
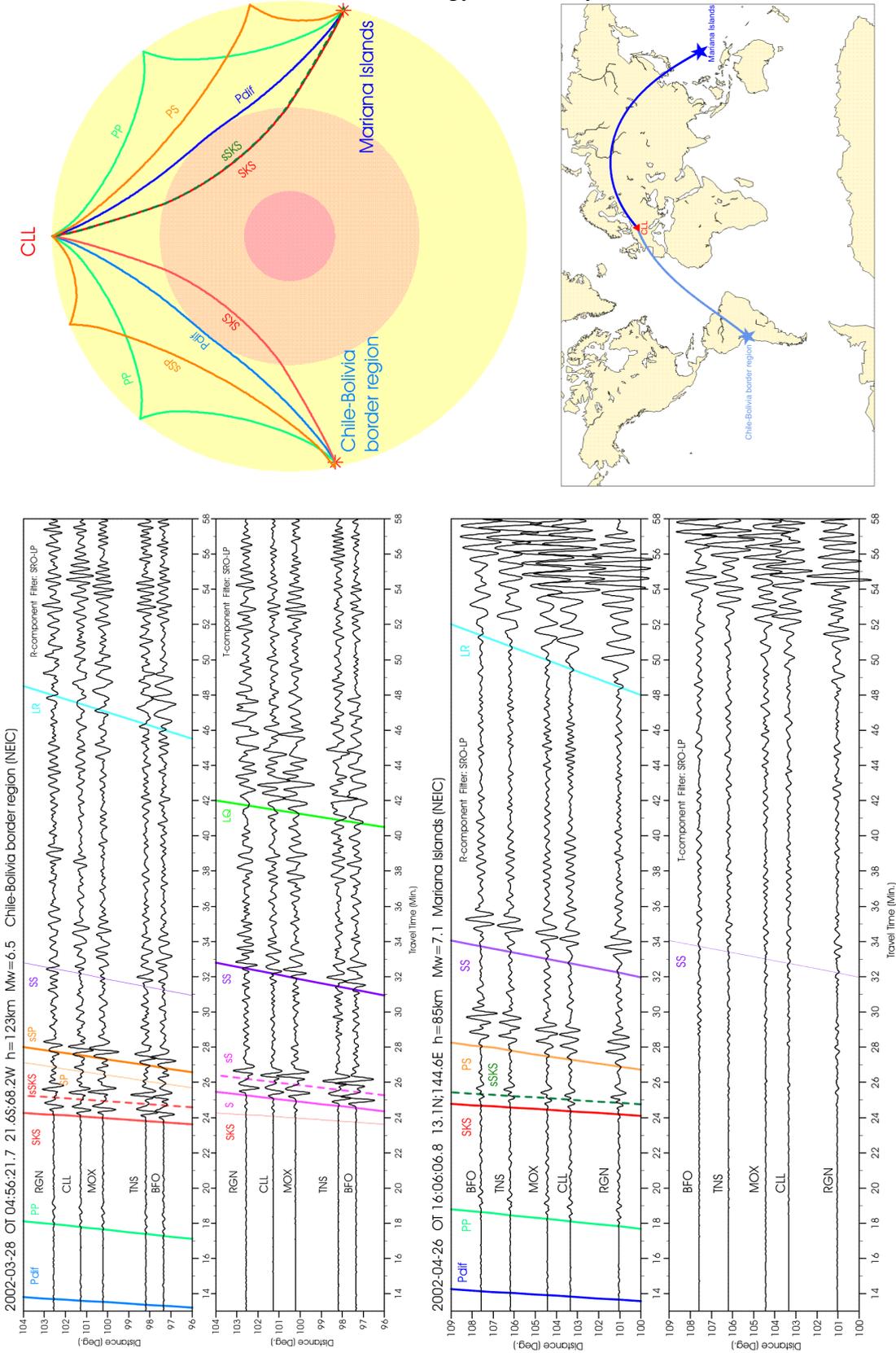
Fig. 11.57 SRO-LP filtered records of GRSN stations on R and T components in the distance range between 96° and 109° from two earthquakes on opposite backazimuth. Left: Chile-Bolivia Border region; right: Mariana Islands (source data according to the NEIC).

If no Pdif is observed, PKiKP is the first arrival in short-period records up to 113° (see Figure 3b in DS 11.3). For distances beyond 114° PKiKP follows closely after PKPdf (alternatively termed PKIKP). The latter has traveled through the outer and inner core and arrives as first onset for D ≥ 114°. PKPdf is well recorded in short-period seismograms but usually with emergent onsets and, up to about 135° distance, still with weaker amplitudes than PKiKP. Fig. 11.58 shows the amplitude-distance relationship between PKiKP, PKPdf and the other direct core phases PKPab and PKPbc, which appear with largest amplitudes beyond 143°. Fig. 11.59 depicts the ray paths and travel-time curves of Pdif, PKiKP, PKPdf, PKPab and PKPbc (for more complete ray paths see IS 2.1). Also PKKP (with its branches ab and bc) is often clearly recorded between 110° and 125° (see Figures 3c and d in DS11.3).
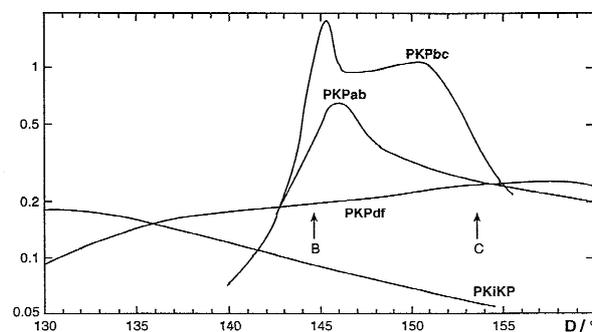
Fig. 11.58 Smoothed amplitude-distance relationships for the core phases PKiKP, PKPdf, PKPab and PKPbc as calculated for the model 1066B in the distance range 130° to 160° (modified from Houard et al., Amplitudes of core waves near the PKP caustic,…Bull. Seism. Soc. Am., Vol. 83, No. 6, Fig. 4, p. 1840, © 1993; with permission of Seismological Society of America).

Fig. 11.60 presents records of GRSN stations in the distance range 121° to 127° from an earthquake of intermediate depth (h = 138 km) in the region of New Britain (see file 7 in IS 11.3 and animation CD). They show the PKPdf arrivals about 3.5 min after Pdif together with the dominant phases in this range, namely PP, PPP, PS, PPS and the Rayleigh-wave arrival LR in the Z component and the SS, SSS and the Love-wave arrival LQ in the T component. Also shown, together with the ray paths, is the core phase P4KPbc, which has been reflected 3 times at the surface of the Earth, and which is recognizable only on the short-period filtered vertical component. Between about 128° and 144° some incoherent waves, probably scattered energy from "bumps" at the CMB, may arrive as weak forerunners up to a few seconds before PKPdf. They are termed PKPpre (old PKhKP). PKPdf is followed by clear PP, after about 2 to 3 minutes, with SKP or PKS arriving about another minute later (see Fig. 11.61).

SKP/PKS have their caustics at about 132° and thus, near that distance, usually have rather large amplitudes in the early part of short-period seismograms (see Fig. 11.61). For medium-sized earthquakes these phases may even be the first ones to be recognized in the record and be mistaken for PKP. Note that for near-surface events SKP and PKS have the same travel time, but with the former having relatively larger amplitudes in the Z component whereas PKS is larger in the R component. For earthquakes at depth, PKS and SKP separate with the latter arriving earlier the deeper the source (Fig. 11.61). Beyond 135° there are usually no clear phases between SKP and SS. Misinterpretation (when Pdif is weak or missing) of PP

and SKS or PS waves as P and S may in this distance range result in strong underestimation of D (up to 70°). This can be avoided by looking for multiple S arrivals (SS, SSS) and for surface waves which follow more than 40 min later (see Table 5 in DS 3.1). For more records see DS 11.3, examples 1 to 7.

Pdif and PKiKP/PKPdf/PKPbc/PKPab
Raypaths and travel-time curves (IASP91)
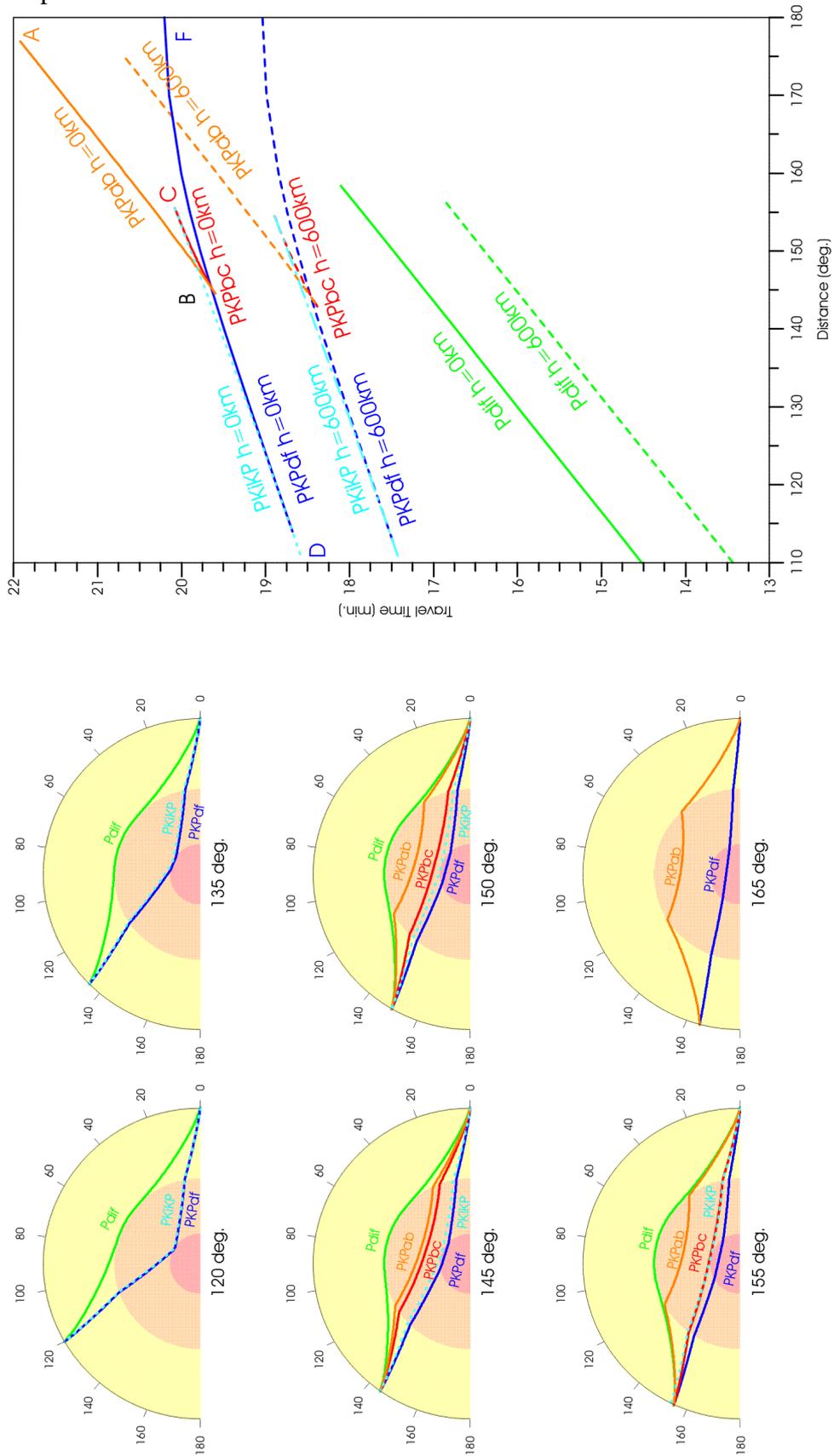
Fig. 11.59 Ray paths of Pdif, PKPdf, PKPab and PKPbc and their travel-time curves for surface focus and deep focus (h = 600 km) events.
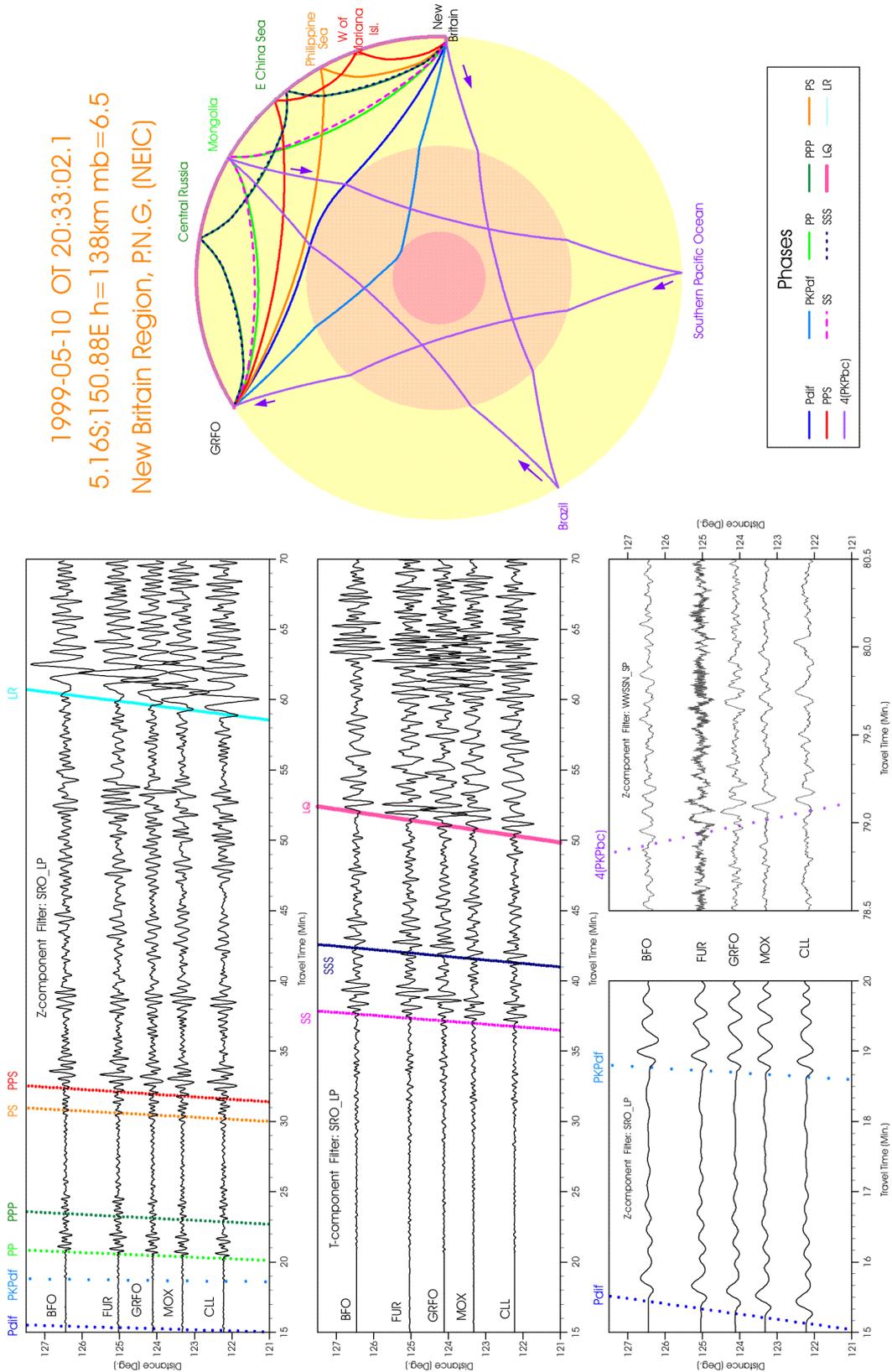
Fig. 11.60 Main seismic phases in the distance range 121° to 127° on records made at GRSN stations. Left and middle: SRO-LP filtered Z and T component, respectively. Right: SRO-LP and WWSSN-SP components. Top right: Ray traces of phases shown (see also file 7 in IS 11.3 and animation on CD-ROM).
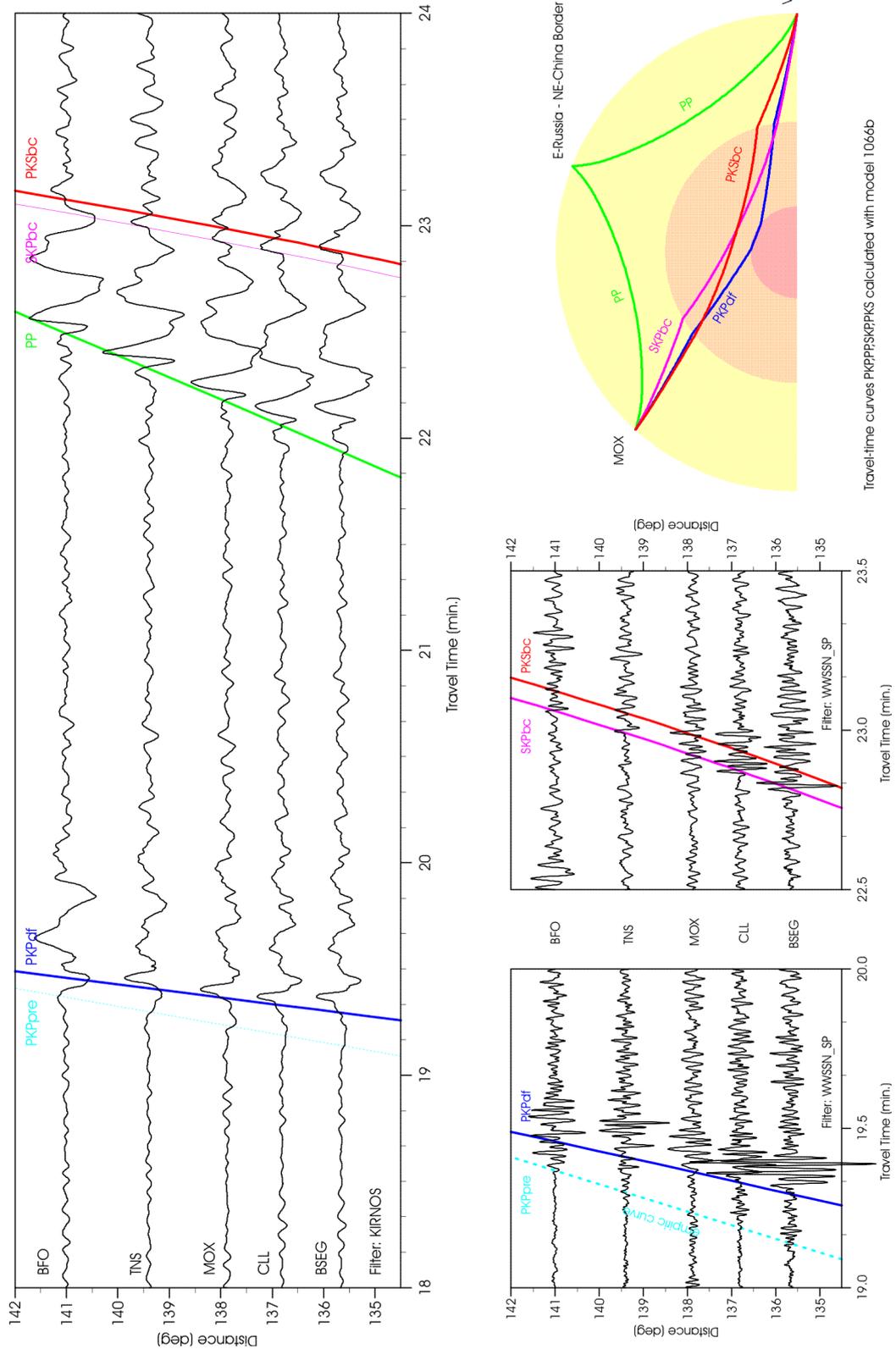
Fig. 11.61 Vertical-component seismograms at GRSN stations recorded in the distance range 135° to 141°. Left: Kirnos SKD BB-displacement; right: WWSSN-SP; top: ray paths of the phases PKPdf , PP and SKP/PKS bc. Note the precursor PKPpre.

11.5.2.4 Core distance range beyond 144°

Between 130° and 143° the first onsets of longitudinal core phases are relatively weak and complex in short-period records, but their amplitudes increase strongly towards the caustic around 144°. At this epicentral distance three PKP waves, which have traveled along different ray paths through the outer and inner core, namely PKPdf, PKPbc (old PKP1) and PKPab (old PKP2) arrive at the same time (see Fig. 11.59) so their energies superimpose to give a strong arrival with amplitudes comparable to those of direct P waves at epicentral distances around 40° (compare with Fig. 3.13). Beyond the caustic the travel-time curves of these three PKP waves split into the branches AB (or ab), BC (or bc) and DF (or df) (see Fig. 11.59). Accordingly, the various arrivals can be identified uniquely by attaching to the PKP symbol for a direct longitudinal core phase the respective branch symbol (see Figs. 11.59 and 11.62). Note that the PKPbc branch shown in Figs. 11.59 between the point B and C is ray-theoretically not defined beyond 155°. However, in real seismograms one often observes weak onsets between PKPdf and PKPab up to about 160° or even slightly beyond in the continuation of the PKPbc travel-time curve. This phase is a PKP wave diffracted around the inner core boundary (ICB) and named PKPdif (see Fig. 11.62 and 11.63).
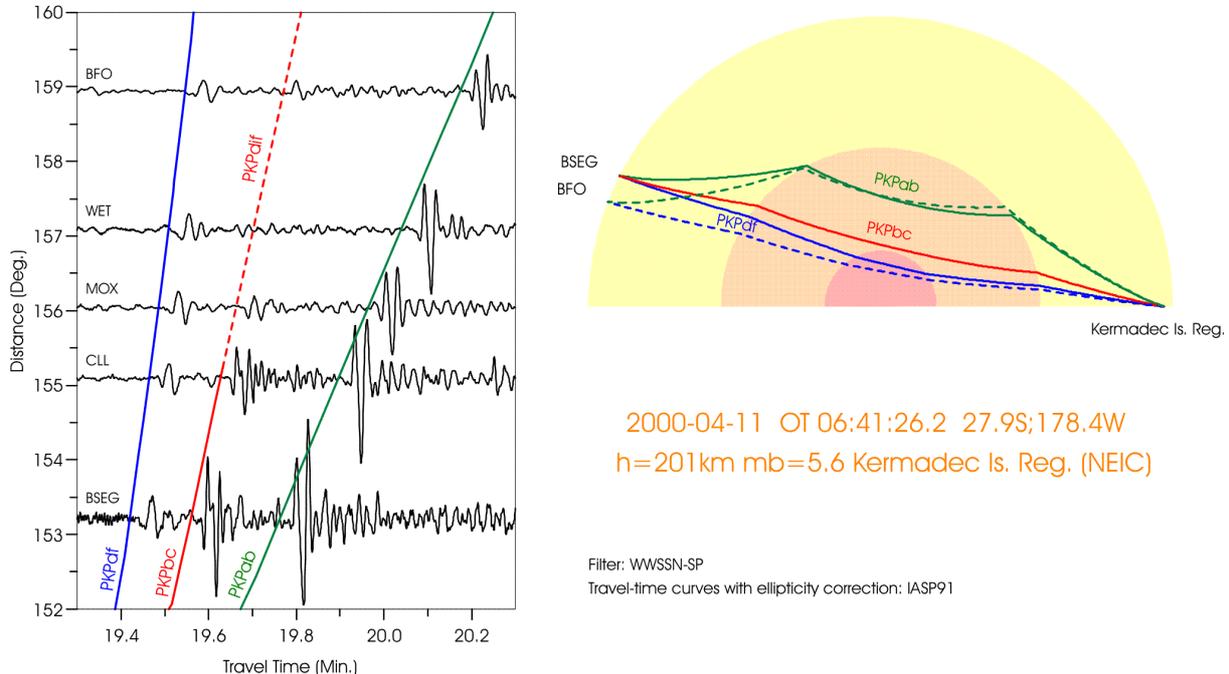

Fig. 11.62 Left: Records of the direct core phases PKPdf, PKPbc and PKPab as well as of the diffracted phase PKPdif from a Kermadec Island earthquake at stations of the GRSN in the distance range between 153° and 159°; **right:** ray paths through the Earth.

The relative amplitudes between the three direct longitudinal core phases change with distance. In SP records these three phases are well separated beyond 146°, and PKPbc is the dominant one up to about 153° though the separation between these three phases is not clear within this range in LP records (Fig. 11.63 upper part and Figures 9a-c in DS 11.3).
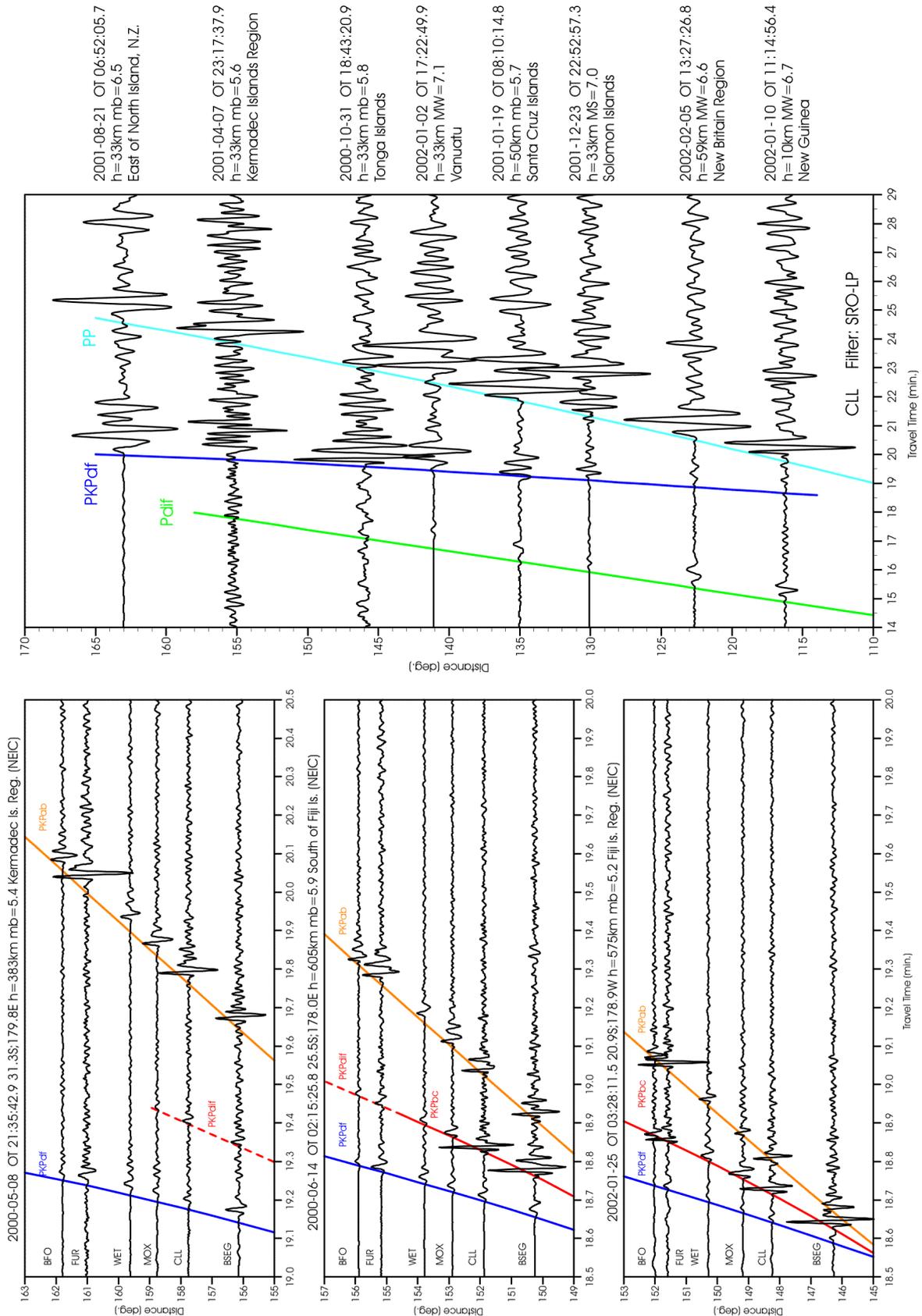
Fig. 11.63 Short-period (bottom) and long-period (SRO-LP) filtered broadband records of GRSN stations of PKP phases in the distance range 116° to 163°. In the LP records additionally the onsets of Pdif and PP have been correlated with their travel-time curves.

On short-period records the phases PKPdf, PKPbc and PKPab are easy to identify on the basis of their typical amplitude and travel-time pattern. D can be determined with a precision better than 1.5° by using differential travel-time curves for the different PKP branches (see EX 11.3). On records of weaker sources, PKPbc is often the first visible onset because the PKPdf, which precedes the PKPbc, is then too weak to be observed above noise. On long-period records superposed different onsets may be recognizable only at distances larger than 153°. Then PKPab begins to dominate the PKP-wave group on short-period records (compare Figs. 11.63). Towards the antipode, however, PKPdf (PKIKP) becomes dominating again whereas PKPab disappears beyond 176°.

On LP and BB records the dominant phases on vertical and radial components are PKP, PP, PPP and PPS while on the transverse component SS and SSS are dominant. For deep sources, their depth phases sSS and sSSS may be strongest (see Fig. 11.64). Besides PP, which has traveled along the minor arc (epicentral distance D) the phase PP2, which has taken the longer arc to the station (360° - D), may be observable, as well as phases such as PcPPKP and others (see Fig. 11.65 as well as file 9 in IS 11.3 and related animation on CD-ROM). SKKS, SKKKS, SKSP etc. may still be well developed on radial component records (see also Figs. 2.48 and 2.49 with the related travel-time curve overlay). The whole length of BB or LP seismograms in this distance range between the first onsets and the surface wave maximum is more than an hour (see Tab. 5 in DS 3.1).

11.5.3 Late and very late core phases

For large magnitude sources, reflected core phases may be observed in addition to the direct ones, sometimes with up to 4 (or even more) repeated reflections. These phases may be observed at practically all teleseismic distances with delays behind the first arriving P or PKP onsets ranging from about 10 minutes up to about 80 minutes, depending on the number of multiple reflections. These phases are clearly discernible only in high-magnifying SP (or appropriately filtered BB) records. Most frequently observable are the single surface reflection P'P' (also termed PKPPKP), and the single reflection from the inner side of the core-mantle boundary, PKKP. As for the direct core phases, these multiple reflections develop different travel-time branches according to their different penetration depth into the outer core (see also figures in IS 2.1). Figs. 11.66 and 11.67 show the ray paths for P'P' and PKKP waves, respectively, together with their related IASP91 travel-time curves (Kennett and Engdahl, 1991) for sources at depth h = 0 km and h = 600 km. Where there is more than one reflection the respective phases are often written P'N or PNKP, respectively, with the number of reflections being N-1. Ray paths and short-period record examples for P'N with N = 2 to 4 are shown in Figs. 11. 68 to 11.70 and for PNKP with N = 2 to 5 in Figs. 11.70 and 71. Fig. 11.64 shows a P5KP (PKKKKKP), which has been four times reflected from the inner side of the CMB. It is observed nearly 37 min after PKP. The phase P7KP has been found in a record at Jamestown, USA, of an underground nuclear explosion on Novaya Zemly in 1970.

All these figures show that these late arrivals may still have a significant SNR. Since they appear very late and thus isolated in short-period records, station operators may wrongly interpret them

as being P or PKP first arrivals from independent events. This may give rise to wrong phase associations and event locations, which, particularly in a region of low seismicity, may give a seriously distorted picture of its seismicity. This was demonstrated by Ambraseys and Adams (1986) for West Africa.
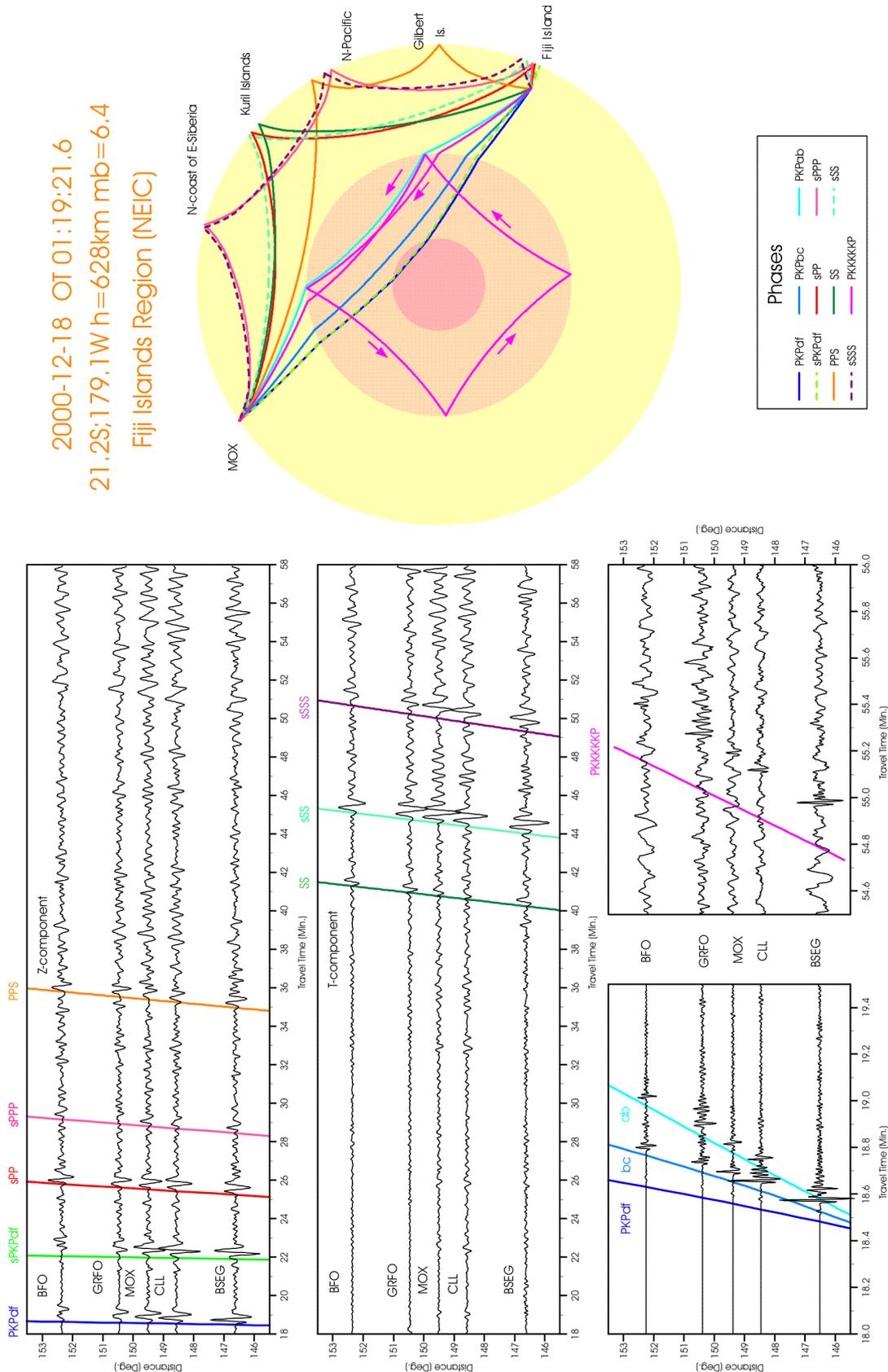
Fig. 11.64 Records of GRSN stations of a deep earthquake in the Fiji Island region. Top: ray paths and source data; bottom: records on the Z component (LP left and SP right) and T component (middle) (see also file 8 in IS 11.3 and related animation on CD-ROM).
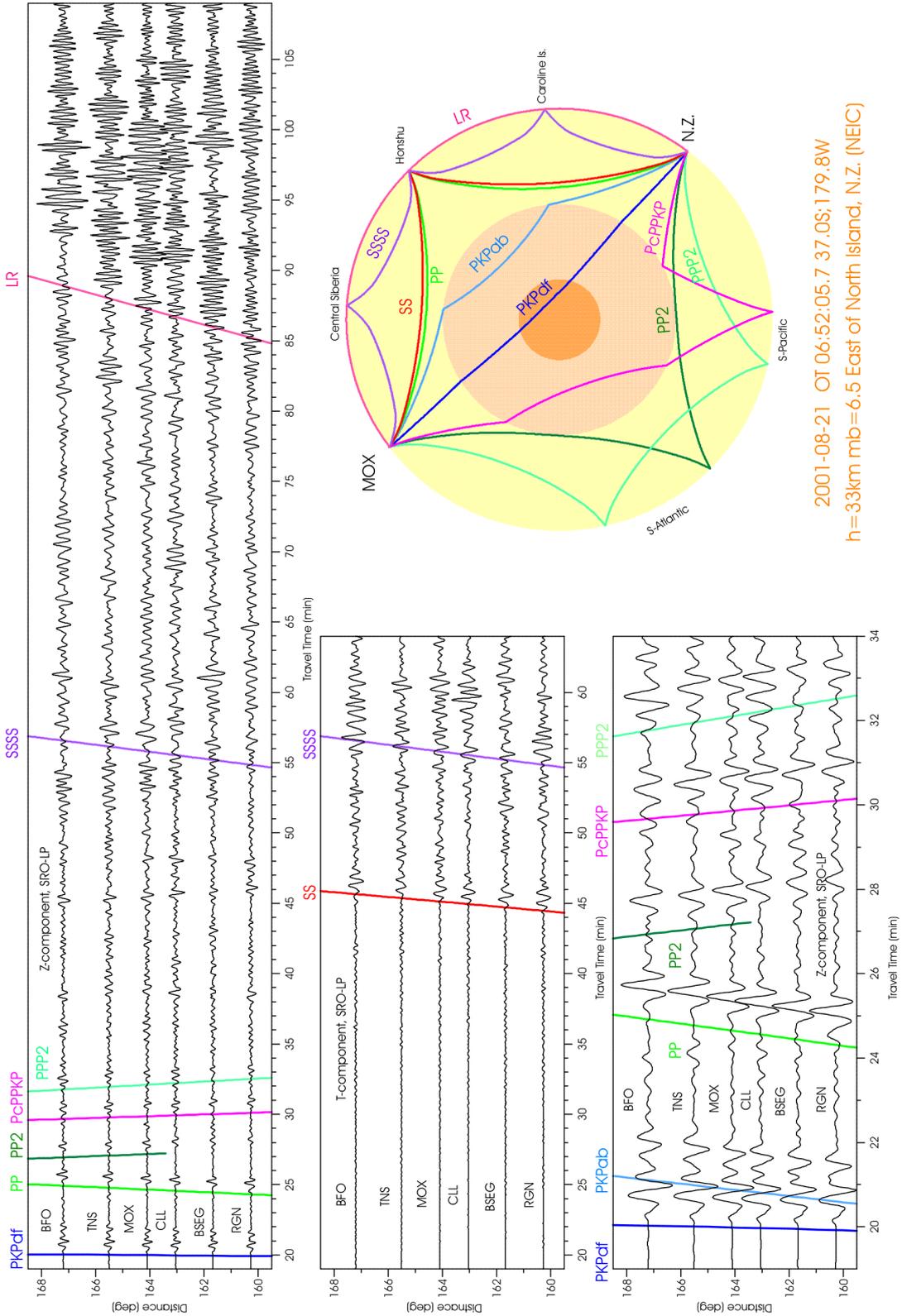
Fig. 11.65 Records of GRSN stations of a shallow (crustal) earthquake east of the North Island of New Zealand. Upper right: ray paths, source data and wavefronts of PP and PP2 arriving in Germany; bottom: records on long-period components (Z left and right; T middle). An animation has been produced that shows the ray propagation and seismogram formation for this earthquake (see file 9 in IS 11.3 and related CD-ROM).

P and P'P'df/P'P'bc/P'P'ab

Raypaths and travel-time curves (IASP91)
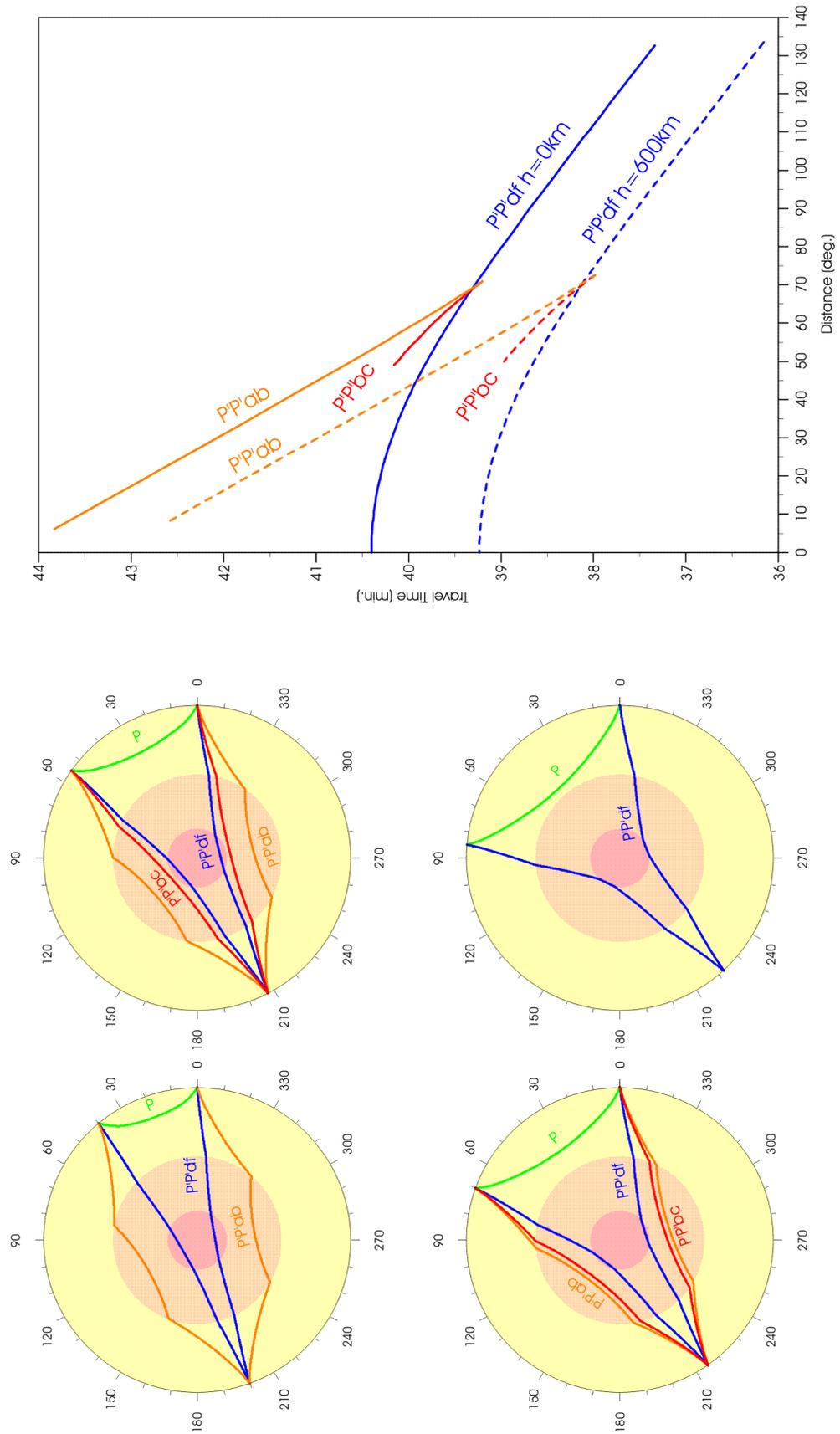
Fig. 11.66 Ray paths and travel-time curves for P'P' according to the Earth model IASP91 (Kennett and Engdahl, 1991).

PKKPdf, PKKPbc, PKKPab: Raypaths and travel-time curves
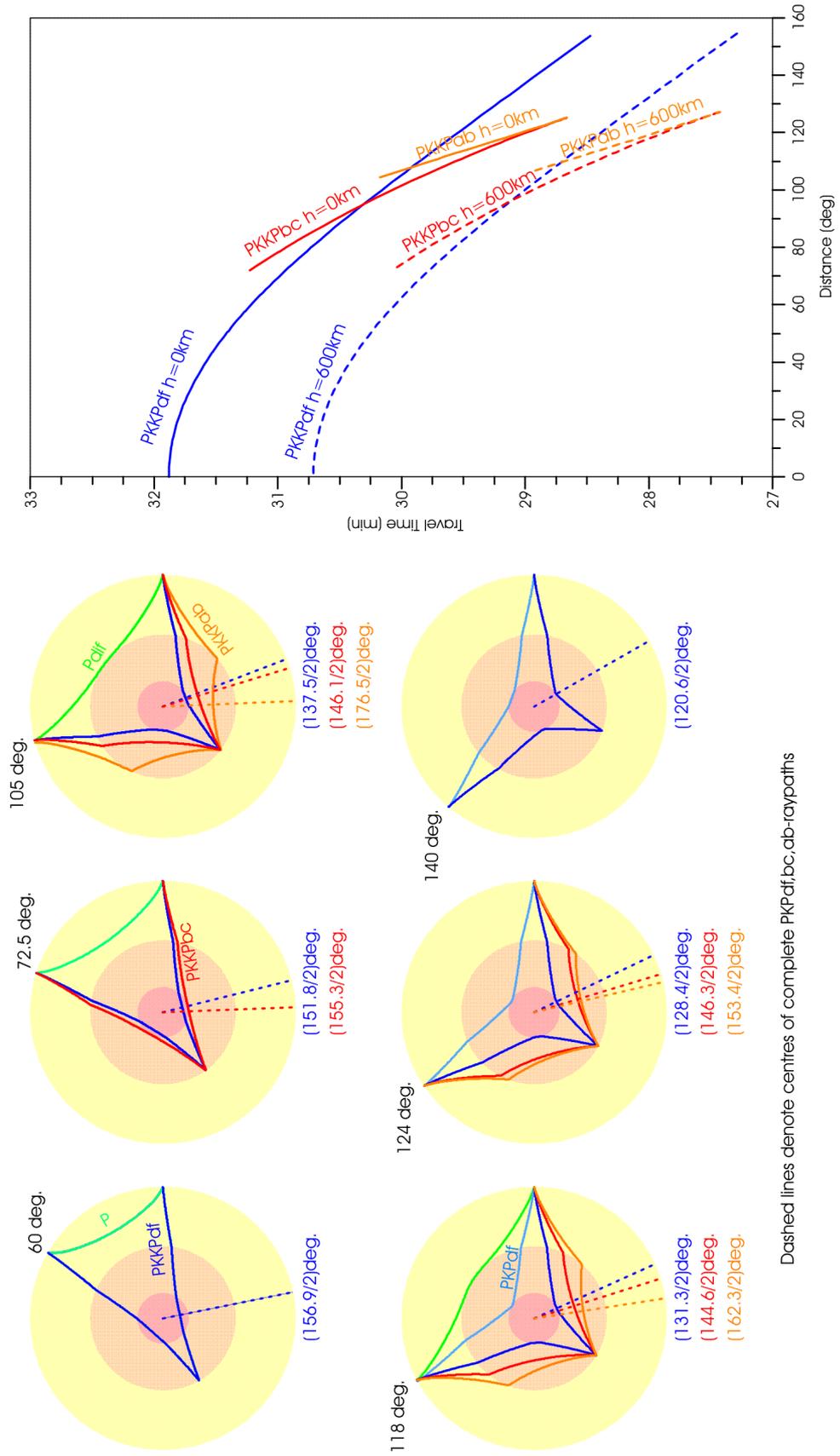

Fig. 11.67 Ray path and travel-time curves for PKKP according to the Earth model IASP91 for epicentral distances of the source between 60° and 140°.
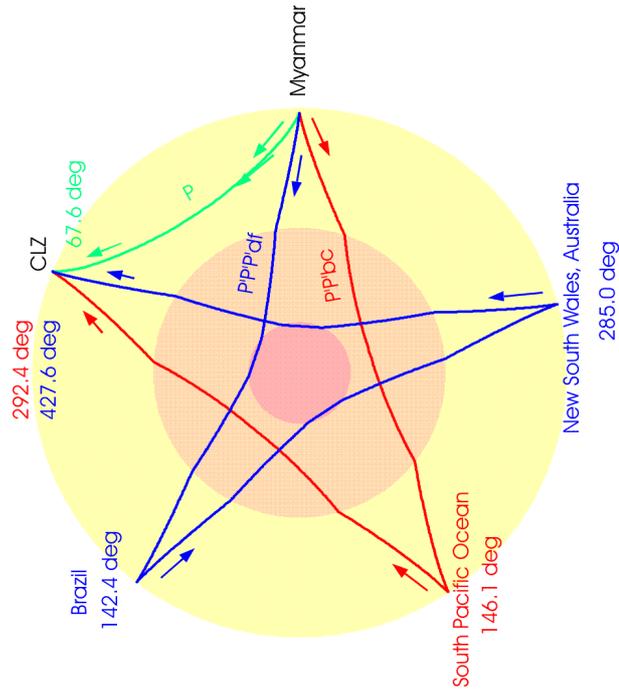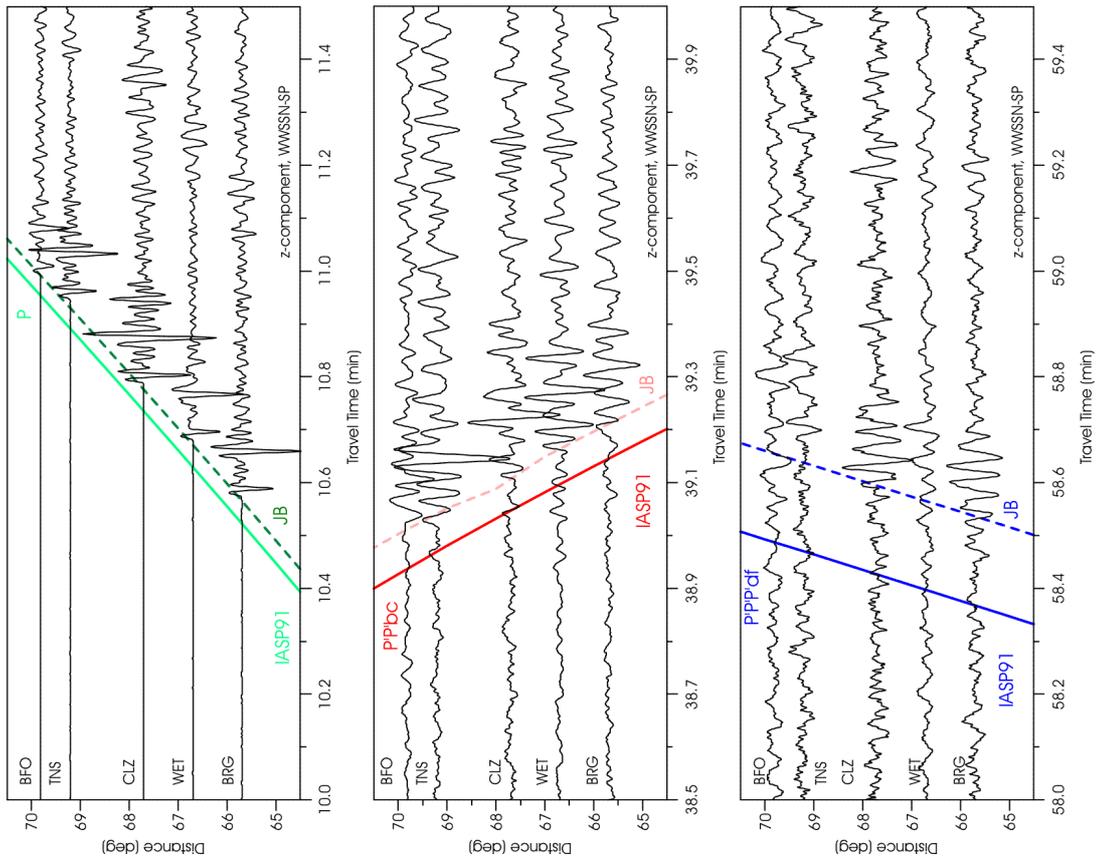
Fig. 11.68 Ray path (top) and short-period Z-component records at stations of the GRSN (bottom) of P, P'P' and P'3 together with their theoretically expected arrival times according to the IASP91 and JB tables. Earthquake in Myanmar; distance range 65° < D < 70°.
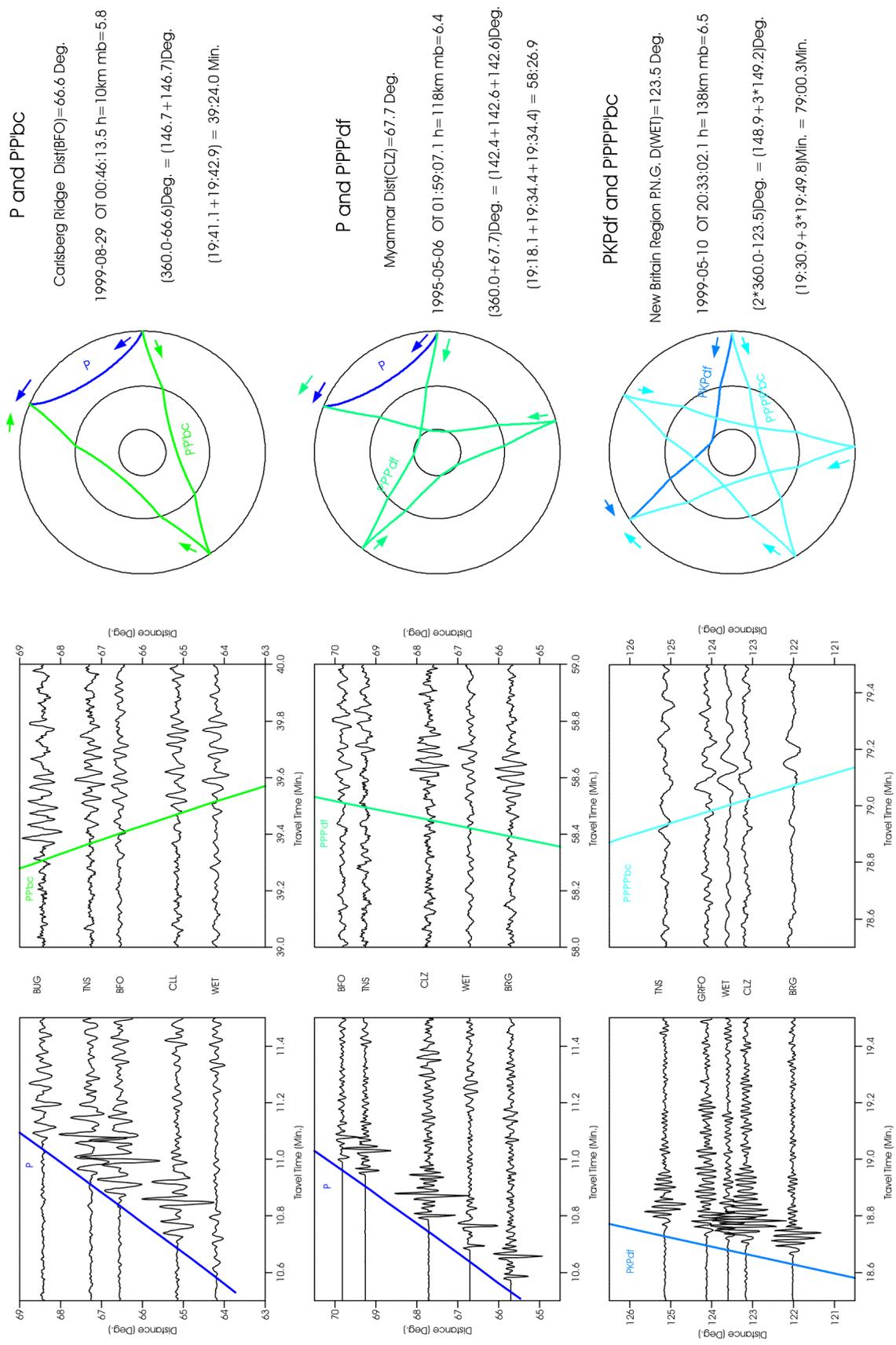
Fig. 11.69 Short-period record segments showing P and PKPdf (bottom) together with P'2, P'3 and P' 4 (middle) at GRSN stations. Top: Related ray paths and source data. Note the negative slowness for P'2 and P'4. The theoretical travel-time curves relate to IASP91. Record length is one minute.
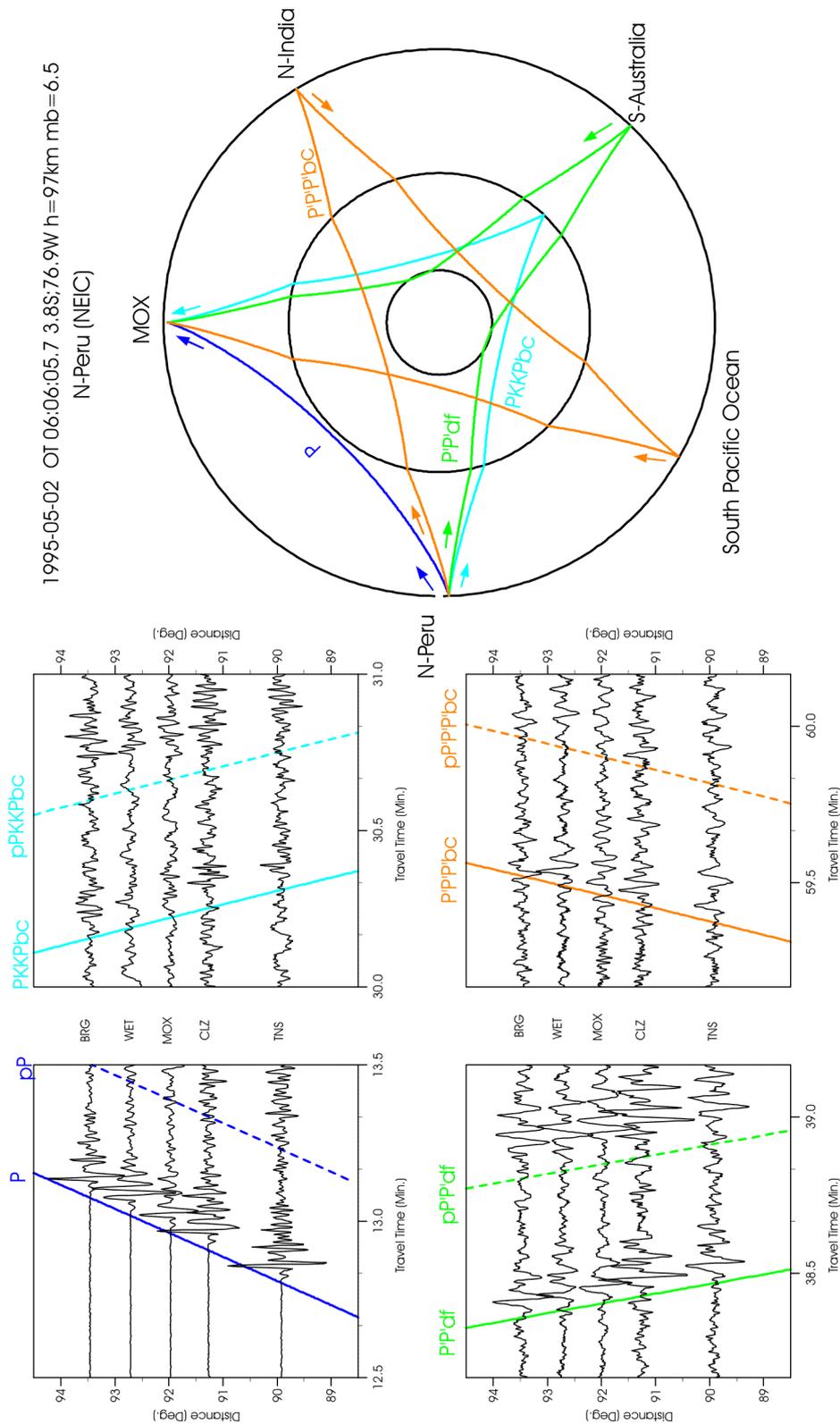
Fig. 11.70 Late and very late multiple core phases PKKP, P'2 and P'3, respectively, together with their depth phases in short-period filtered record segments of GRSN stations from an earthquake in Northern Peru at an epicentral distance around 92°. For an animation of ray propagation and seismogram formation from this source see file 6 in IS 11.3 and related CD.

PKKP, P3KP, and P5KP

Pdif and PKPbc

Santiago del Estero Prov., Arg. Dist(GRFO)=101.6Deg.
2000-04-23 OT 09:27:22.8 h=604km Mw=6.9 (NEIC)

first half of PKPbc (15.9+112.7)Deg.
is a part of PKPbc (145.9Deg and h=604km)

second half of PKPbc (112.7+17.3)Deg.
is a part of PKPbc (147.3Deg. and h=0km)

P and PKKKP

Crete Dist(MOX0=14.4Deg.

1995-06-15 OT 00:15:48.7 h=14km mb=6.1 (NEIC)

The 3 sections of PKKKP (22.1+100.5)Deg., 100.5Deg.,
and (100.5+22.1)Deg. are parts of 3 PKP (144.6Deg.)

PKPdf and PKKKKKP

Fiji Islands Region Dist(MOX)=145.9Deg.

1998-03-29 OT 19:48:16.2 h=537km mb=6.5 (NEIC)
P5KP contains 5 equal inner sections of 90.4Deg.

Travel time and ray path in general calculated with IASP91

Fig. 11.71 Short-period record segments of P and PKPdf (bottom) together with those of PKKP, P3KP and P5KP (middle) at GRSN stations. Top: Related ray paths and source data. Note the negative slowness for PKKP and P3KP. The theoretical travel-time curves relate to IASP91. Record length is one minute.

In Figs. 11.62 to 11.71 the theoretical travel-time curves for core phases have been shown. For consistency, they are based on the travel-time model IASP91 (Kennett and Engdahl, 1991), as in all earlier record sections shown for the teleseismic distance range. An exception is Fig. 11.68, which shows additionally the theoretical travel-time curve for the JB model (Jeffreys and Bullen , 1940). One recognizes, that the model IASP91 yields onset times for core phases that tend to be earlier than the real onsets in the seismograms. This applies to both direct and multiple reflected core phases. The agreement between real and theoretical onsets of core phases is better when using the JB model. The JB model is still regularly used for the location of teleseismic sources at the international data centers in Boulder (NEIC), Thatcham (ISC) and Moscow whereas the IDC of the CTBTO uses IASP91. The more recent model AK135 (Kennett et al., 1995) is more appropriate than IASP91 for core phases. No recommendations have been made yet by IASPEI for using a best fitting global 1-D Earth model as standard at all international data centers. However, the NEIC is currently rewriting its processing software so that it will allow to use different Earth models, and AK135 will probably be its "default" model.

Note that the difference between the azimuth of the P wave and that of P'P' and PKKP, respectively, is 180° (see Figs. 11.66 and 11.67)**.** The related angular difference of the surface projections of their ray paths is 360°–D where D is the epicentral distance. Accordingly, the slowness of P'P' as well as of any even number P'N is negative, i.e. their travel time decreases with D. This also applies to PKKP and P3KP, as can be seen from Fig. 11.71. The surface projection of the travel paths of P'3 is 360° + D and that of P'4 is 2 × 360°–D. PKPPKP is well observed between about 40° < D ≤ 105°. In this range it follows the onset of P by 33 to 24 min (see Figure 10 in EX 11.3 with observed data). The existence of P'N is not limited to PKPbc. Fig. 11.68 shows an example of P'3df, recorded at a distance of about 67°. P'4 is sometimes observed in the distance range 112° to 136°. An example is given in Fig. 11.69.

Similar ray paths can be constructed for PNKP, the phase with (N-1) reflections from the inner side of the core-mantle boundary (see Fig. 11.71). Figure 9 in EX 11.3 gives the differential travel-time curves for PKKP to the first arrivals P or PKP, respectively, in the distance range between 80° and 130° together with the observed data. In this range PKKP arrives 13 to 19 min behind P or 9.5 to 12 min behind PKPdf. Higher multiple reflections from the inner side of the CMB such as P3KP, P4KP and P5KP are observed, if at all, at 37 ± 1 min after the first arriving wave. The latter is true for P3KP following P at around 10°, for P4KP following P between 45° < D < 75° and for P5KP following the onset of PKPdf between about 130° < D < 150° (called "37- min" rule- of- thumb).

A particular advantage of these multiple reflected core phases is the small depth dependence of their travel-time differences to P and PKP, respectively. Consequently, their identification allows very good distance estimates to be made from single station records even when the source depth is not known. Because of the inverse differential travel-time curves of PKPPKP and PKKP with respect to P and PKP their identification can be facilitated by comparing the onset times at neighboring stations (e.g., Fig. 11.70). The polarization of both the first arrival and the possible PKKP or PKPPKP onset, determined from 3-component records, can also aid identification because their azimuths should be opposite to that of P or PKIKP, respectively. Sometimes, also converted core reflections such as SKPPKP or SKKP can be observed in short-period recordings. However, direct or reflected core phases, which have traveled along both ray segments through the mantle as S waves (such as SKS, SKKS, etc.) are mostly observed in broadband or long-period records.

11.5.4   Final remarks on the recording and analysis of teleseismic events

Box 2 below, summarizes the key criteria that should be taken into account when recording and analyzing seismograms from sources at teleseismic distances (see also 11.2.6.1).

Box 2: General rules for recording and analyzing teleseismic events

- The overall duration of teleseismic records at epicentral distances larger than 15^o(or 20°) ranges from tens of minutes to several hours. It increases both with epicenal distance and the magnitude of the source.
- High frequencies, of S waves in particular, are attenuated with distance so recordings at long range are generally of lower ($f \approx 0.01$ - 1 Hz) frequency than local or regional recordings.
- Usually only longitudinal waves, both direct or multiple reflected P and PKP phases, which are much less attenuated than S waves, are well recorded by short-period, narrow-band seismographs (or their simulated equivalents) with high magnification of frequencies around 1 Hz. However, S waves from deep earthquakes may sometimes be found also in SP teleseismic records.
- Because of the specific polarization properties of teleseismic body and surface waves, polarization analysis is an important tool for identifying the different types of wave arrivals.
- According to the above, teleseismic events are best recorded by high-resolution 3-component broadband seismographs with large dynamic range and with sampling rates $f = 20$ Hz.
- The main types of seismic phases from teleseismic sources are (depending on distance range) the longitudinal waves P, Pdif, PKP, PcP, ScP, PP, and PPP and the shear waves S, Sdif, SKS, ScS, PS, SS, and SSS. The longitudinal waves are best recorded on vertical and radial components whereas the shear waves appear best on transverse and/or radial components.
- Multiple reflected core phases such as P'N and PNKP, which appear on SP records as isolated wavelets, well separated from P or PKP, may easily be misinterpreted as P or PKP arrivals from independent seismic sources if no slowness data from arrays or networks are available. Their proper identification and careful analysis helps to avoid wrong source association, improves epicenter location and provides useful data for the investigation of the deeper interior of the Earth.
- Several body wave phases such as PP, PS, SP, SS, PKPab and its depth phases, SKKSac, SKKSdf, PKPPKPab, SKSSKSab undergo phase shifts and wavelet distortions at internal caustics (see 2.5.4.3). This reduces the accuracy of their time and amplitude picks and their suitability for improving source location by waveform matching with undistorted phases. Therefore it is recommended that seismological observatories correct these phase shifts prior to parameter readings by applying the inverse Hilbert-transformation, which is available in modern software for seismogram analysis.
- Surface waves of shallow events have by far the largest amplitudes while surface wave amplitudes from deep earthquakes and large (nuclear) explosions are small at teleseismic distances.
- At seismic stations or network centers the following parameter readings should be obligatory during routine analysis: onset time and, if possible,

polarity of the first arriving phase; maximum P amplitude A [nm] and period T [s]; onset time of secondary phases; and for shallow sources additionally the maximum surface-wave amplitude A [μm] and period T [s].

- P-wave amplitudes for the determination of the short-period body-wave magnitude mb have to be measured on standard short-period (WWSSN-SP simulated) records in the period-range 0.5 s < T < 2 s whereas the surface-wave amplitudes for the determination of the surface-wave magnitude Ms have to be measured on standard long-period filtered (SRO-LP or WWSSN-LP simulated) records, typically in the period range 17 s < T < 23 s.

- For more guidance on magnitude determination, using also other phases and records/filters, consult section 3.2.1 and related annexes.

- Networks and arrays should additionally measure and report slownesses and azimuths for P waves.

- For improved determination of epicentre distance, the measurement and reporting of travel-time differences such as S–P, SS-P etc. are very important, and for improved hypocenter determination additionally the proper identification and reporting of depth phases such as pP, sP, sS and of core reflections (PcP, ScP etc.).

- Picking and reporting of onset-times, amplitudes and periods of other significant phases, including those not identified, are encouraged by IASPEI within the technical and personnel facilities available at observatories and analysis centers as being a useful contribution to global research. These extended possibilities for parameter reporting are now well supported by the recently adopted IASPEI Seismic Format (ISF), which is much more flexible and comprehensive than the traditional Telegraphic Format (see 10.2 as well as IS 10.1 and 10.2).

- For reporting of seismic phases (including onsets not identified) one should exclusively use the new IASPEI phase names. For the definition of seismic phases and their ray paths see IS 2.1.

Acknowledgments

Recommended overview readings (see References under Miscellaneous in Volume 2)

Kennett (2002)
Kulhanek (1990 and 2002)
Payo (1986)
Richards (2002)

Scherbaum (2001 and 2002)
Simon (1981)
Willmore (1979)